technische unive dortmund

Institut für Umformtechnik und Leichtbau

FAKULTÄT MASCHINENBAU

Master of Manufacturing Technology

Institut für Umformtechnik und Leichtbau

Prof. Dr.-Ing. Dr. h.c. Matthias Kleiner

Prof. Dr.-Ing. Dr.-Ing. E.h. A. Erman Tekkaya

“ M a s t e r ´ s T h e s i s ”

Determination of Residual Stresses in Cold Extruded Parts by Contour Method

by

Oguzhan AYDIN

Matriculation no.: 207389

Supervisors:

1. Prof. Dr.-Ing. Dr.-Ing. E.h. A. Erman Tekkaya

2. M.Sc. Felix Kolpak

3. Prof. Dr.-Ing. habil. K.-D. Bouzakis

4. Assoc.Prof. Dr. Caner Simsir

Issued on:dd Month yyyy

Submitted on:dd Month yyyy

Abstract

Residual stresses are self-equilibrating stresses scattered throughout whole solid body in the absence of any external load. Under eutectoid temperature without recrystallization, these stresses inherently increase up to considerable high values for engineering materials during cold forming processes. Forward cold extrusion is one of these forming processes to manufacture engineering components in which the effect of residual stresses might be significant on mechanical properties and lifetime of a product. For this reason, residual stresses must be known for the quality of a part. Contour method is relatively a new experimental method developed to measure residual stresses in a component. Contour method provides an invaluable opportunity to the researches to determine two-dimensional residual stress map all over cross section in a part. In cold-extruded rods, axial residual stress which is in extrusion direction might be the most effective component of all stress tensor at several mechanical properties such as fatigue strength and durability. Axial residual stress relaxes fully after perpendicular flat cut in a part. In this work, these axial residual stresses of the asymmetric and full cylindrical parts manufactured by cold extrusion with three different extrusion ratios and the effects of extrusion ratio on axial residual stresses were investigated using contour method. The maps of whole cross sections are obtained for all three extrusion ratios and compared to the findings by other methods in the existing works in literature. For contour method, wire electro-discharge machining (WEDM) was employed to cut very smoothly specimens whose materials are a type of case hardening steel in this work. The potential error sources and their contribution to the final results such as surface roughness, cutting conditions are studied in the frame of this work. Finally, finite element analysis (FEA) of full extrusion process using commercial codes in order to validate experimental result was implemented as well as sensitivity analysis of extrusion with the varied selected parameters of the process.

Table of Contents

Abstract **III**

Table of Contents **iv**

Nomenclature **vi**

1 Introduction **1**

2 State of the Art **3**

2.1 Residual Stresses 3

2.2 Residual Stress Measurement Methods 5

2.2.1 Contour Method 5

2.2.2 Other Experimental Measurement Methods 11

2.3 Cold Extrusion and Residual Stresses in cold extrusion 26

2.4 Wire Electro-Discharge Machining 28

3 Goal of the Work **32**

4 Cold Extrusion and Manufacturing of Parts **34**

5 Wire Electro-Discharge Machining **42**

5.1 Clamping Apparatus Design 43

5.2 Resolidification 44

6 Data Processing **46**

6.1 Surface scanning 46

6.2 Surface alignment 49

6.3 Truncating and surface fit 50

6.4 Application of data to finite element model 53

7 Result and Discussion **56**

7.1 Contour Method Results 56

7.2 FE Analyses Results 64

7.3 Experimental Results versus FE Results 68

7.4 Sensitivity Analysis of Cold Forward Extrusion 71

8 Summary and Outlook **76**

Works Cited **79**

Appendix A **LXXXIX**

Nomenclature

In this section, abbreviations and symbols with their indices are given with their basic short descriptions.

Formula Symbols

Variable	Unit	Description
E	MPa	Young's modulus
F	N	Force
v	-	Poisson's ratio
π		Pi value
D	µm	Lattice distance
D_0	µm	Stress free lattice distance
k_f	MPa	Yield stress
a	µm	Crack length
$R_{p0,2}$	MPa	Yield strength at 0.2%
t	mm	Thickness
φ	-	True strain
μ	-	Attenuation coefficient
ρ	$kg \cdot m^{-3}$	Density
σ	MPa	Stress
τ	MPa	Shear stress
R_a	µm	Average surface roughness
R_z	µm	Height between peak and valley

Variable	Unit	Description
h, k, l	-	Miller indices
θ	Degree	Bragg's angle
φ	Degree	Azimuth angle
ψ	Degree	Pole angle
I	cd	Intensity
K, K_{Irs}	-	Stress intensity factor
$\underline{r},\underline{t}$	-	Calibration coefficient

Indices

Index	**Description**
0	Initial value
max	Maximum
min	Minimum
A	The case before cutting
B	The case after cutting
C	The case of forcing back
xx	Physical quantity in x direction
yy	Physical quantity in y direction
xy	Physical quantity in xy plane

Abbreviation	Description
CAD	Computer Aided Design
DHD	Deep Hole Drilling
FEM	Finite Element Method
FEA	Finite Element Analysis
FE	Finite Element
MoS_2	Molybdenum Disulfide
SR	Strain Relief
2D	Two-dimensional
3D	Three-dimensional
CMM	Coordinate Measuring Machine
EDM	Electrical Discharge Machining
RS	Residual Stress(es)
SIF	Strain Intensity Factor
WP	Water Pressure
WEDM	Wire Electro-discharge Machining
W-EDM	Wire Electro-discharge Machining
XRD	X-Ray Diffraction

1 Introduction

Cold-extruded products have been finding many applications in different industries. Lifetime of these products has importance for quality and environment. Residual stresses generated mostly by manufacturing processes influence heavily service lives of the products. Residual stresses desired to be known for lifetime of products can be measured through a number of experimental methods and one of these is contour method explained by Prime (2001). Very similar to other destructive techniques, the method is based on stress relaxation after a straight and flat cut through cross section.

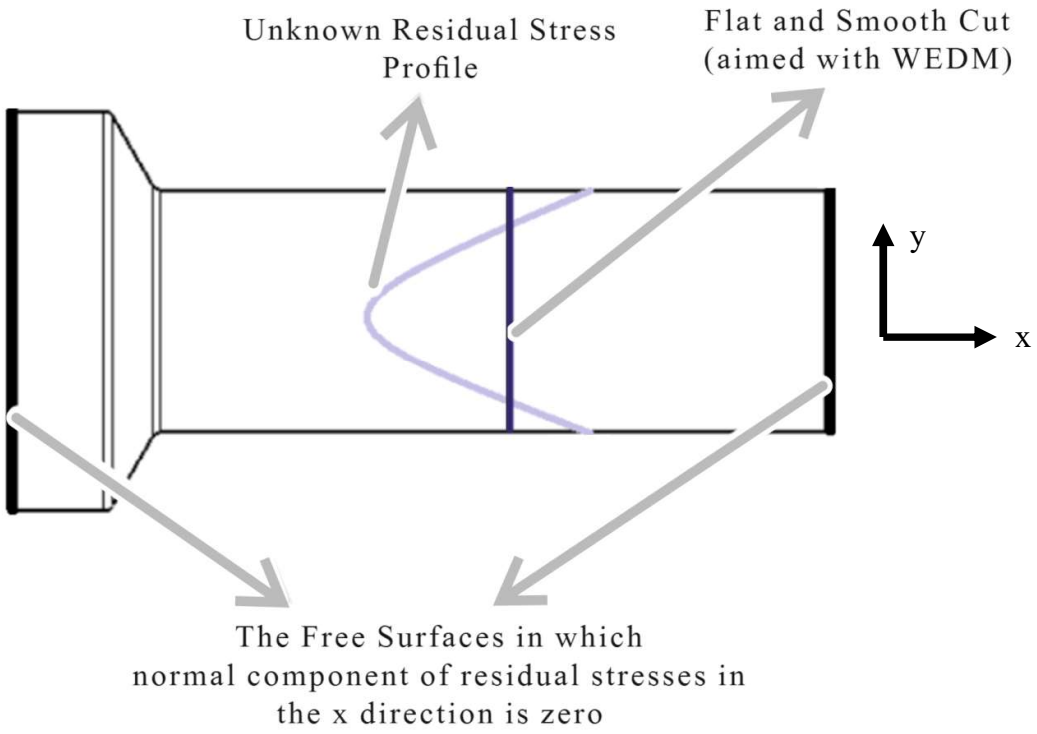

Figure 1.1: Illustration of unknown stress profile to be determined via contour method.

The method allows researcher and engineers to obtain two-dimensional residual stress map of normal stress component which is perpendicular to cutting plane. In theory, the perpendicular component of residual stress tensor to outer surface of a workpiece is zero. In other words, the outer surfaces of a workpiece are free edges or surfaces. In the **Figure 1.1**, free surfaces in which axial stress, σ_{xx}, is zero are drawn in bold.

Cutting is a consequential step for contour method while the flatness of the cuts play momentous role in for the success of method and residual stresses (RS) induced by cold extrusion process must not be affected by cutting process to accomplish accurate determination of RS. Conventional cutting processes include high forces, stresses and contacts between workpiece and tool which distort original residual stress distribution and can cause much more newly developed residual stresses in a component. Wire electro-discharge machining (Wire-EDM or WEDM) is such a cutting process which does not exert any cutting force and friction on workpiece. In this process, material removal is succeeded by heating and even evaporating the material by the help of electrical energy.

It would be useful to analyze both cut surfaces scanned by microscope to eliminate noise appearing during surface scanning, the effect of shear stresses, plasticity and some other effects caused by cutting which will be discussed in Chapter 2 and Chapter 5 in this work. Theoretical background of contour method that lies behind Bueckner`s superposition principle is explained in detail in Chapter 2 as well as discussion from literature sources are represented in that chapter.

Chapter 4 is devoted to the discussion of manufacturing of specimens and forward cold extrusion process. In this work, data processing consists of four main steps which are surface alignment, truncating, surface fitting (smooth) and curve fitting discussed in detailed way in Chapter 6.

In the last step of contour method, fit curve is applied as displacement boundary condition to finite element model. This last step was implemented in the commercial software MSC Marc Mentat and obtained results are discussed in Chapter 7. Finally, a summary of obtained results of residual stress measurement by contour method and finite element analysis (FEA) using commercial software Abaqus Standard and the future look together with possible future studies are given in the final chapter.

2 State of the Art

2.1 Residual Stresses

Residual stresses (RS) that are inherently constructed in the existence of misfits inside material are assorted commonly by the distances along which their impact is balanced. While level I stresses, σ^{I}, are identified as macro residual stresses equilibrating themselves over the width of at least several grains, σ^{II} and σ^{III} represent micro scale and nano scale RS, respectively.3rd level residual stresses are engendered by the misfits of intra-granular dislocations within a grain. For fatigue life of metal components, σ^{I} might be more the focus of interest Withers and Bhadeshia (2000). The **Figure 2.1** illustrates the variation in residual stresses along distance. The residual stress at a point yields to the **Equation 2.1**.

$$\sigma^{RS} = \sigma^{I} + \sigma^{II} + \sigma^{III} \tag{2.1}$$

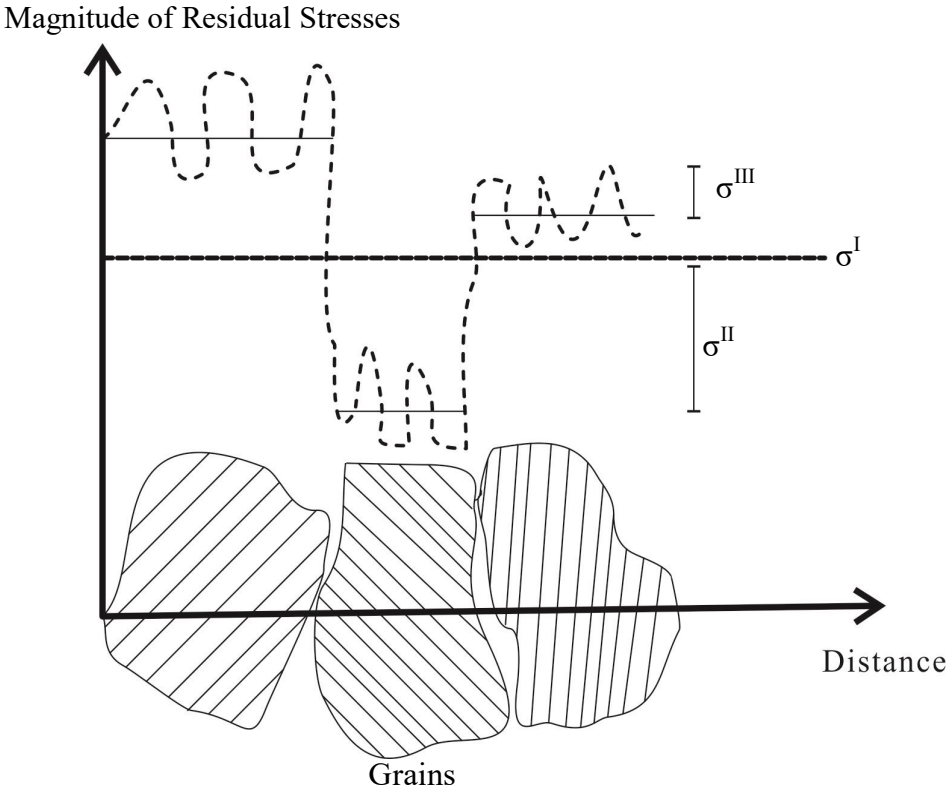

Figure 2.1: The demonstration of the types of residual stresses.

Some residual stress measurement methods can elicit information only about level I stresses such as crack compliance and contour method, while a researcher can investigate other types of RS with x-ray and neutron diffraction methods.

Almost all manufacturing processes forming, cutting, casting, assembly, additive manufacturing generates residual stresses (RS). In some processes, compressive RS in surface regions is produced deliberately to enhance resistance of material to fatigue, stress-corrosion cracking and pitting corrosion such as shot peening, blasting and laser shock peening and unwanted tensile RS is dangerously built in some other manufacturing operations such as welding, additive manufacturing.

Webster and Ezeilo (2001) stated that surface tensile residual stresses might engender crack initiation and crack growth while compressive RS might restrain detrimental effects. Spiedel (1975) investigated the reasons of stress-corrosion cracking (SCC) in high strength aluminium alloy and approximately 40 percent of failures are attributed to residual stresses generated during heat treatment and manufacturing processes, particularly, forging rather than service stresses. In the same study, it is noted that bulk materials are more susceptible to SCC while the ability of cracks is not sufficient to advance in extrusion direction or forging due to stretched grains in this direction in each time and crack growth occurs predominantly in transverse direction. Rhouma et al. (2001) studied the effects of some surface treatment processes generating surface compressive residual stresses and outlined that surfaces with these stresses produced by the application of surface treatment process maintain improved resistance to pitting corrosion and stress corrosion cracking. Beavers et al. (2000) descried stress corrosion cracking in the regions which is subject to more elevated tensile residual stress in pipes. Level I tensile RS is also found to be critical by Ghosh et al. (2011) during the tests conducted with specimens produced by varied manufacturing methods.

Residual stresses can be mitigated by performing heat treatment or adequate forming operations. Various heat treatment processes in which a component is heated to temperature above recrystallization temperature or slightly below recrystallization temperature are commonly applied to relieve RS such as normalizing, spheroidizing, annealing, tempering .etc. Convenient heat treatment process differs broadly according to

material type and needed material properties. Cooling rate typically becomes a decisive factor of final microstructure Callister and Rethwisch (2011).

Compression and stretching are two reputable methods reported extensively in literature to eliminate residual stresses. Koc et al. (2006) studied the reduction of RS in quenched aluminium blocks administering aforementioned methods. Significant drop in RS in blocks is achieved with both of methods. Prime and Hill (2002) reach comparable result with stretching method in stresses in both rolling and transverse directions of rolled aluminium plates.

During the lifespan of a component, service stresses combine with RS. Consequently, material failure below yield strength might be beheld. Nonetheless, compressive residual stresses are expected to increase resistance to fatigue life and stress corrosion Koc et al. (2006). Residual stresses are also proven to be responsible for the alteration in the yield points of materials Ekmekci et al. (2004).

2.2 Residual Stress Measurement Methods

2.2.1 Contour Method

Contour method based on elastic deformation due to residual stress redistribution after contour cut was introduced by Prime in 2001. In this method, the part will be cut and elastic deformation on the cut surfaces will be measured with the one of various methods to develop finite element model in order to obtain original stress distribution all over cross section of a part.

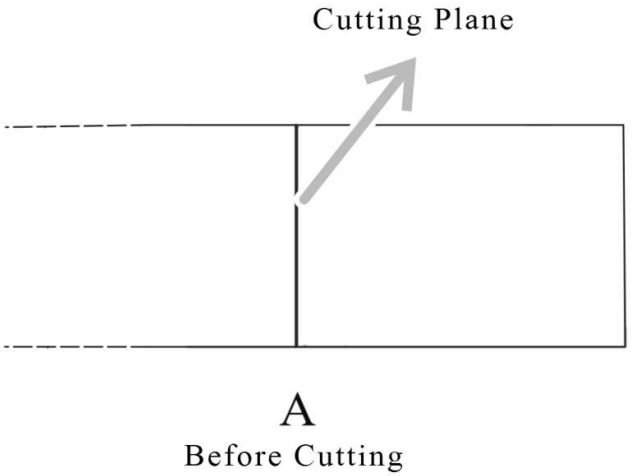

Figure 2.2: Perpendicular cutting plane to axial residual stresses Prime (2001).

Since axial stresses in the extrusion direction are aimed to be found in this study, cutting plane has to be perpendicular to that direction for fully relaxation of the stresses. After straight cut, a new free surface on which axial stress, σ_{xx}, will be zero emerges. Complete relaxation of shear stresses, τ_{xy} and τ_{xz}, is not expected. But, the assumptions include that only σ_{xx}, τ_{xy} and τ_{xz} contribute to the deformation since a flat cut is aimed in contour method. Averaging deformation of both cut surfaces eliminates shear stress effect on deformation while shear stresses are anti-symmetric on cut surfaces. As a result, conventional contour method calculates only normal stress, σ_{xx}. Superposition principle proposed by Bueckner (1958) enlightens theoretical background of contour method.

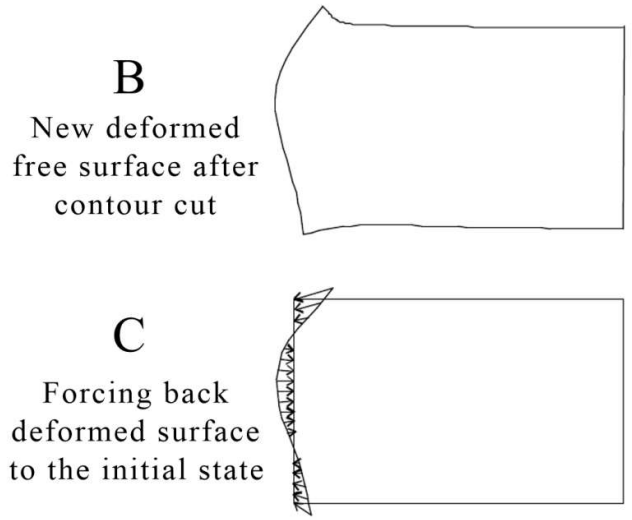

Figure 2.3: Illustration of Bueckner's Principle Prime (2001), Bueckner (1958).

Case B depicted in the **Figure 2.3** with the exaggerated view illustrates stress relaxed contour after straight cut. Pressing this surface elastically back to original position would yield initial residual stress tensor in accordance with Bueckner`s principle. This condition is also propounded with the **Equation 2.1** for contour method by Prime (2001). In the Equation 2.1, σ without a subscript refers to full stress tensor while the superscripts correspond to the cases, A, B and C.

$$\sigma^{A}=\sigma^{B}+\sigma^{C} \tag{2.2}$$

Conventional cutting methods are not compatible for contour method and do not satisfies the requirements for elastic relaxation. Tremendous cutting and frictional forces between workpiece and tool induce new residual stresses and cause the alteration of the original residual stress distribution in a component.

Different effects of wire-edm process on original residual stresses were widely discussed in literature Prime (2001), Prime (2009). Although wire-edm can present sensible cutting conditions for contour method within aimed accuracy limit, their contributions to the calculations of the final results have the same paramount importance since they are hurdles for the integrity of contour method. Prime (2001) suggests performing

superficial cutting on a free surface by wire-edm to experience the adequacy of the proposed cutting method.

After contour cut, residual stresses release and cause elastic deformation which must be measured with high accuracy and precision on the cut plane. While elastic deformation caused by residual stress redistribution might be in the range of a few micrometers in most cases, the required acute precision might necessitate studying and exploring for the residual stresses of any component to be measured.

Diverse variety of methods such as laser profilometer or a mechanical type of coordinate measuring machine (CMM) are utilized to obtain the knowledge of surface deformation for this method (Prime et al. 2004), Prime (2001). In this thesis, an optical scanning method is employed with AliconaInfinite Focus microscope for this goal. Prime et al. (2004) discusses that measuring tip of a mechanical CMM would cause deformation which would contribute to inaccuracy.

Surface scanning ends up with the thousands of data points whose number will be even greater with an optical CMM. The microscope provides the user with many thousands of data points with superior resolution which could be helpful for accuracy but together with the sacrification of time in data handling. Nonetheless, written programming codes would retain this stage in reasonable.

Besides abundance of data points, the insertion of plenty thousands of data points into a finite element model would be another unreasonable gruelling which necessitates the data processing. The commercial software MATLAB has been used to process data sets extracted from optical CMM and curve fitting in this study. In section 6, the procedure followed and function codes produced in this study with the aforementioned commercial software is discussed further.

Prime (2001) worked on the validation of contour method both numerically and experimentally. In his study, a bend test is carried out using carefully prepared specimens and the predicted results and the measured contour method results show reasonably agreement at even low strain. Addition to this study, Prime et al. (2001) obtained plausible agreement between neutron diffraction method and contour method in the residual stress analyses of 12 passes welded steel plate.

Tensile residual stresses would cause recessions whereas the release of compression stresses would cause prominence shaped deformations on a surface. Therefore, reverse sign of measured contour is inserted into FE model by Prime (2001).

DeWald and Hill (2001) studied the different surface fitting methods of deformed surface after cutting for accurate result. Later, Prime and Martineau (2002) investigated the residual stresses of impacted steel plate by tungsten carbide sphere by using contour method through thickness of the plate and compared the results obtained by numerical simulation.

Then, Prime et al. (2003) applied contour method to 37 mm thick butt weld and weld of two different materials (316 stainless steel and 1100 Al) in which application of other methods such as neutron diffraction and x-ray diffraction would be difficult or inaccurate due to the microstructural differences and thickness of the materials since these methods are sensitive to microstructural changes and limited to specimen size. Another study for correlation of contour method is performed by Zhang et al. (2004). They compared contour method results of welded specimen with neutron and synchrotron x-ray diffraction techniques and reached very gratifying agreement between contour method and diffraction methods.

In conventional destructive methods, strain due to relaxation of residual stresses is measured by the help of strain gages which are pasted on free surfaces on which strain is measured. These free edges become considerably away from cutting location while cutting is going on (Prime 2009). These other strain relief (SR) methods are discussed in next subsections in more detailed way.

It is demonstrated that clamping strategy is great of importance for accurate results during cutting process by wire-edm. In the previous studies, symmetrically clamping resulted in better results than asymmetrically clamping Traore et al (2014), Prime (2001).

Prime (2009) discussed that relaxation of residual stresses during cutting process leads to rotary motions which do not comply with flat cut assumption. Addition to this, cut surfaces might move toward each other or move away after stress relaxation named as

bulge effect. Tensile relaxed stresses may lead to the vicissitude of cut width whereas compression types may end up with the recut of contour surfaces.

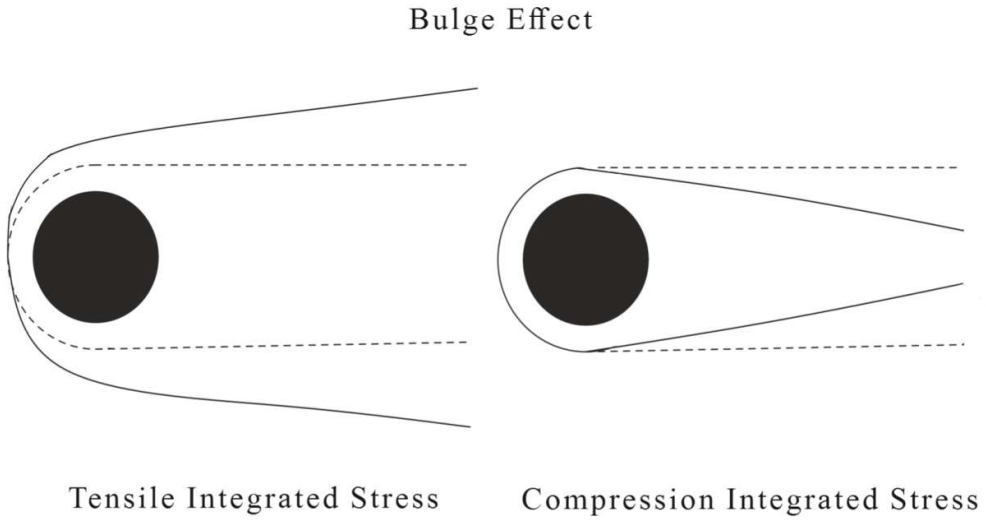

Figure 2.4: Bulge effect developed during cutting.

Besides, it is observed that by the researchers that the bottom of cut location serves as stress concentration location and crack tip as illustrated in the **Figure 2.4**. Bulge effect augments the potentiality of plasticity around crack tip. As a result of these, considerable deviation in measurement might occur because of plasticity Prime (2009). Plastic deformation might take place according to the basic fracture mechanic formula given by the **Equation 2.3**.

$$\sigma = \frac{K}{\sqrt{\pi a}} \tag{2.3}$$

Shin (2005) and Sun et al. (2017) stated the that location of clamping mitigate the effect of plasticity and obtained improved result with the clamping which is nearby cutting plane. For these reasons, special designed clamping apparatus would be a necessity. Particularly, two rotary motions of samples which will be cut by wire-edm must be restricted by clamping apparatus. This matter is further discussed in chapter 5.

The reproducibility of measurements of residual stresses might be consequential to a researcher. Hill and Olson (2014) investigated quenched and stress relieved aluminium alloy to study this phenomena in contour method. For each of materials, 5 specimens are prepared under the same condition to espy the repeatability of contour method. In

their work, the increase in standard deviation reaches approximately only 20 MPa at the near edges.

Conventional contour method also restricts the location of cutting operation by wire-edm. This limited the application of contour method to asymmetrical parts at the earlier ages of the method. Mahmoudi and Saedi (2015) applied contour method performing asymmetrical cut in quenched stainless steel blocks and determined residual stresses using both of two asymmetric halves of the part at the same time. Achieved residual stresses from asymmetric halves were averaged and the result was confirmed with numerical analysis. This is put forth by the **Equation 2.4**.

$$\frac{\sigma_{left}+\sigma_{right}}{2}=\sigma_{average} \tag{2.4}$$

In this equation, σ_{left} and σ_{right} refer to the stresses in both sides of the cut achieved in the FE analysis. Both halves of the cut must be modelled with the reverse of the mean of the opposite two contours.

An overview of residual stress measurement methods is provided in the following sub-chapters to gain basic understanding of the conditions under which the application of contour method might be reasonably plausible.

2.2.2 Other Experimental Measurement Methods

In the literature, experimental measurement methods of residual stress are classified into two basic groups:

- ✓ Destructive methods and
- ✓ Non-destructive methods.

2.2.2.1 Destructive methods

Destructive methods are the methods in which some amount of material is removed during experiments and consequently the specimens might not be used any more afterwards. Amount of removed material can be very different according to method and specimen. Contour method can be categorized in this group as well the as other strain relief (SR) techniques. Contour method is discussed in the beginning of the Chapter 2.

- ✓ Hole drilling,
- ✓ Crack compliance,
- ✓ Ring core and
- ✓ Deep hole drilling (DHD).

Short comparisons of hole drilling method, crack compliance, ring core method and deep hole drilling method with contour method are given in next subchapters. The possible limitations and advantages over contour method are described.

Hole Drilling

Hole drilling method is one of most used strain relief approach for residual stress measurement. The method includes measurement of strains in different direction to be employed to compute stresses. Measured strain by the help of strain rosettes which generally include two or three strain gages placed according to recommendations around the hole that will be drilled by a drill in certain number of steps in order to measure residual stress along hole depth. Similarly, the method is based on elasticity theory which assumes stress relaxation takes place only elastically.

In hole drilling method, a workpiece must be classified into thin or thick for computation procedure. For thin workpieces, maximum thicknesses are defined in the standards with to the type of strain rosette employed. Strain measurement is implemented by strain gage rosettes attached on the flat surfaces. That is, increasing hole depth will increase the distance between strain gage rosettes and the bottom of hole which causes inaccuracy of measured strain increase. As a result of this, hole drilling method is sufficient only to measure near-surface residual stresses. Therefore, a hole can be drilled only until a maximum value for residual stress determination. Hole diameter also limits its recommended maximum hole depth which can be high up to 1.0 mm. In this method, σ_x, σ_y, τ_{xy} can be calculated by using measured elastic strains through mathematical equations for a thin material with the maximum thickness of 0.2 times the diameter of strain gage rosette for the common type rosette ASTM E837 (2014).

$$\sigma_x = \frac{E\underline{k}}{\underline{r}\,(1+\nu)} + \frac{E\underline{l}}{\underline{t}} \tag{2.5}$$

$$\sigma_y = \frac{E\underline{k}}{\underline{r}(1+\nu)} - \frac{E\underline{l}}{\underline{t}} \tag{2.5}$$

$$\tau_{xy} = -\frac{E\underline{n}}{\underline{t}} \tag{2.6}$$

In these equations, $\underline{k}$, $\underline{l}$ and $\underline{n}$ are calculated by principle strain values, ε_1, ε_2, ε_3 measured by strain rosette whilst $\underline{r}$ and $\underline{t}$ refer to the coefficients chosen from the tables with respect to hole depth and diameter ASTM E837 (2014). Near surface residual stresses might be the main interest of an engineer due to the fact that crack initiation can take place in outer surface. Hole drilling method can considered as a semi-destructive method while drill hole might be ineffective in quality and appearance of a product during lifespan. Depth of a drill hole can be kept shallow if desired not to waste the products. Maximum inaccuracy of this method is stated to be as much as 10 percent ASTM E837 (2014). Ring core which is an another method to evaluate RS is discussed in next subchapter and the comparison to hole drilling method and the illustrations of both method are provided by the **Figure 2.5**.

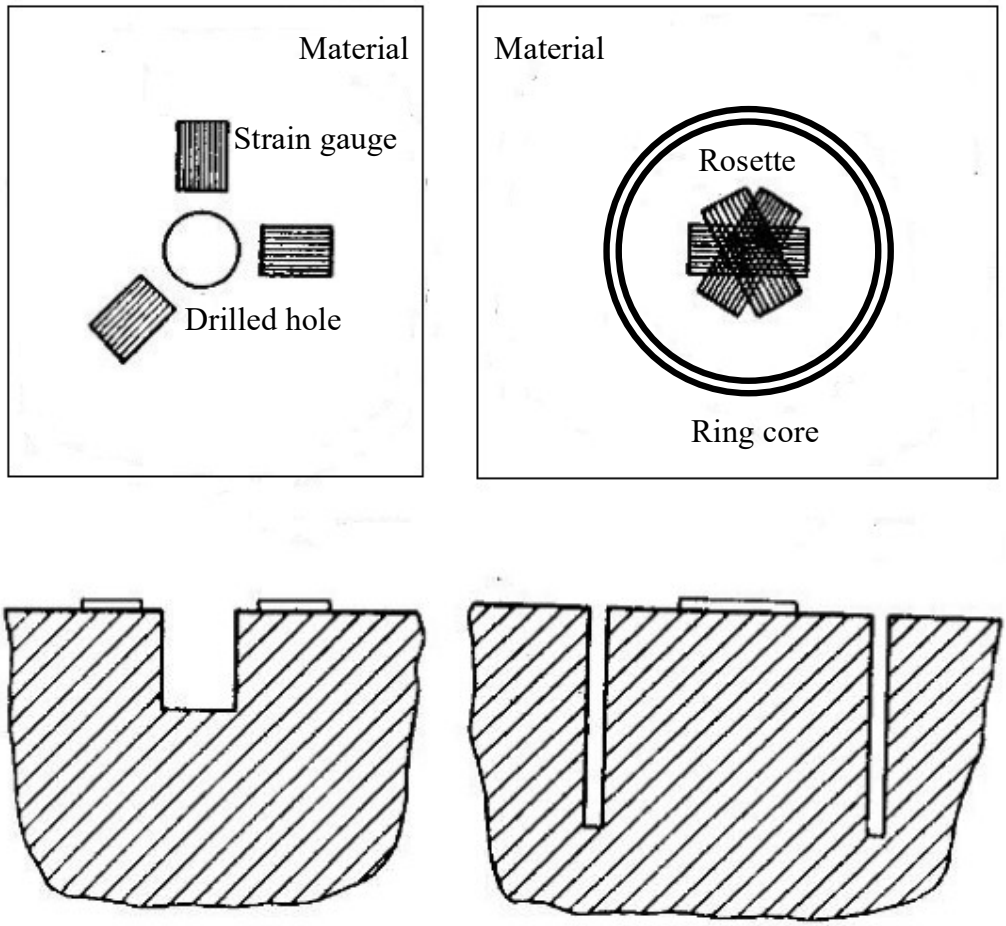

Figure 2.5: The comparison of hole drilling and ring core method Schajer (2001).

Ring Core Method

In ring core method, strain gauge rosette similarly to hole drilling technique is employed to measure the in-plane strains after incrementally the creation of a circular narrow groove which is wraparound the strain gauge rosette for residual stress (RS) measurement. After removing the amount of material, stresses relax on the cut surfaces. Strains are measured by a rosette pasted previously. Various types of cutters are employed for cutting operation such as ring saw. RS might be measured by the use of the method in the depths up to 5 mm while the diameter of groove could vary. The contribution of eccentricity of circular groove and rosette to the error might be less in this method compared with hole drilling method. The calculation of stresses is realized by the help of the calibration coefficient whose determination necessitates performing further experiment or developing a FE model. Calibration coefficients which will be

used in the calculation of stresses include some assumptions and inaccuracy. Integral method approach is often applied for inverse calculation. The one issue to note is that in one direction RS is negligible during calculation. RS up to yield point can be measured by ring core method Schajer (2001), Civin and Vlk (2009). Ring core method might still be used less than hole drilling method for residual stress measurement. This fact may be due to the reason that hole drilling method is simpler to apply.

Crack Compliance

Crack compliance also often called slitting method is a destructive method for measurement of residual stresses. Strain relief in any component with residual stresses in it is realized by developing a slot step by step on workpiece instead of a drill hole unlike hole drilling method. In order to create a slot, saws, electrical discharge machining (EDM) or electrochemical methods are employed. EDM process and electrochemical processes would cause less error induced by plasticity. Strain or displacement is measured after each increment of cutting by means of the equipments such as strain gauge, micrometer or moiré interferometer. The strains averaged in each step are obtained as a function of depth pronounced as compliance function or compliances Prime (1999).

Schindler (1995) utilized stress intensity factor from measured strains by a strain gauge and basic principles of fracture mechanics to compute residual stresses. The **Equation 2.7** is employed for this aim.

$$K_{Irs}(a)=\frac{E'}{Z(a)}\frac{d\varepsilon_m}{da} \tag{2.7}$$

ε_m is measured and averaged strain differences at each increment from a random measurement point, m. Z(a) named influence function depends on the distance between the location of m and crack tip Schindler et al. (1997). Sensitivity and influence function accrue together with this distance. The calculated SIF is employed to determine residual stresses using the inverse of the **Equation 2.8**. The symbols E' and a' correspond to generalized Young Modulus and actual crack length, respectively Schindler et al. (1994), Schindler (1995)-.

$$K_{Irs}(a) = \int_0^a h(y,a)\ \sigma_x(y)\, dy \tag{2.8}$$

The weight function, *h(y, a),* varies with geometry, crack length and type Petrosky and Achenbach (1978), Bueckner (1970). Average stress in each increment can be determined individually with the help of the Equation 2.8.

Cheng et al. (1993) applied crack compliance method to investigate 166 mm thick plate and wire-edm was exploited to create slot in their work. As it is observed from the works that crack compliance method could be employed thicker material than hole drilling method and diffraction methods. Sensitivity to distinguish low level RS could be better than hole drilling method Cheng et al. (1991).

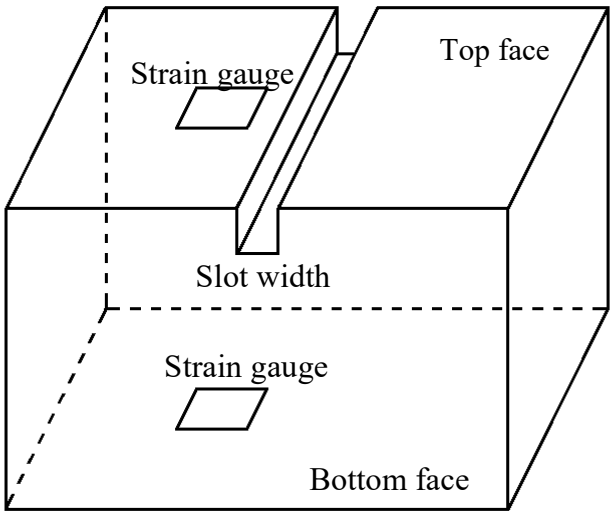

Figure 2.6: The schematic view of crack compliance method.

Deep hole drilling method

Deep hole drilling method abbreviated frequently as DHD is another method based on strain relief. The method allows its users to measure residual stresses through thickness. In literature, measurements up to 500 mm thick parts are reported with this method Mahmoudi et al. (2008). DHD method includes the drilling of a reference hole mostly through thickness. The diameter of reference hole can vary between 1.5-6 mm. For this purpose, a gun drill is frequently employed. Afterwards diameter of drilled hole must be measured accurately at discrete depths and angles by the help of an air-gage. Following to this step, the reference hole is extracted cutting coaxially and circularly around reference hole. The extraction of reference hole is previously carried out

by electrochemical methods but this is replaced by wire-edm to reduce eccentricity of reference hole and circular cut. Finally, the diameter and of reference hole remeasured at the same locations and the angles like previously performed as well as the height of extracted cylindrical column is measured during wire-edm process. The four basic steps of DHD method is demonstrated by the **Figure 2.7**. The number of measured depths and angles might be 2 and 4, respectively Smith et al. (2000). The difference between the initial hole diameter and deformed hole diameter is utilized to compute strain and stress Mahmoudi et al (2008).

Concentricity of reference hole and circle cut by wire-edm and measurement with air-gage might introduce considerable amount of error. Although reasonable accuracies of the method are stated in literature, inaccuracy might sometimes reach beyond the expected amount while the measurement of diameter requires fair accuracy in this method.

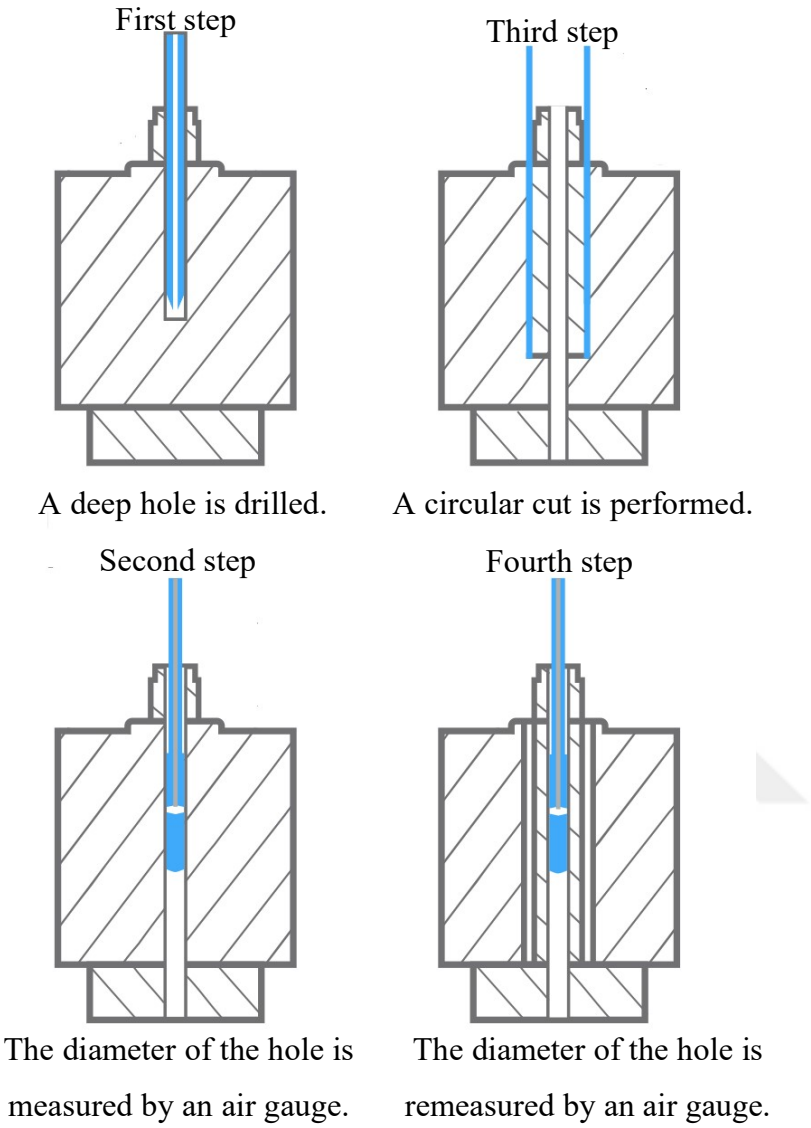

Figure 2.7: The steps of deep hole drilling method Veqter Ltd. and Hill Engineering.

2.2.2.2 Non-destructive methods

Non-destructive methods are the methods specimen are not damaged during experiment and can be reused after this. Well-known non-destructive methods might be

- ✓ X-Ray diffraction,
- ✓ High energy x-ray diffraction,
- ✓ Neutron diffraction and
- ✓ Ultrasonic methods.

Among these methods, X-ray diffraction and neutron diffraction method are compared with contour method as well as ultrasonic methods. Main drawbacks and advantages of those methods are described to provide a comparison to contour method.

X-Ray Diffraction

The discussion of x-ray diffraction method in literature to evaluate residual stresses dates back to 1930 to our knowledge after the discovery of X-rays by Wilhelm Röntgen in 1912. Reflection of X-rays was calculated for the first time in literature by W.H. Bragg and W.L. Bragg. An equation which is also known as a basis for x-ray diffraction method and named Bragg`s law after their study arises. The Bragg`s law given in the **Equation 2.9** uncovers the relationship between wavelength, lattice distance and Bragg`s angle.

$$\lambda = 2\, D_{hkl} \sin \theta_{hkl} \tag{2.9}$$

The lattice distance, D_{hkl}, could be computed with the known wavelength of the used beam and Bragg's angle, θ. X-ray beam generated by a X-ray tube disperses onto a sample. The intensity and the location of peaks of diffracted beams reflected from the specimen are measured by means of diffractometers as illustrated in **the Figure 2.8**. Here, *2θ* angle which will be used in the Bragg`s equation depends on the diffracted plane. The method also necessitates the accurate knowledge of free stress lattice distance symbolized frequently with D_0. The stress-free lattice distance will be altered in the presence of residual stresses which renders strain calculation possible. Consequently, the location of diffraction peak will differ slightly due to this reason. As shown in the **Figure 2.9**, different *2θ* angles are obtained from varied grains in which residual stresses vary Lin et al. (2016).

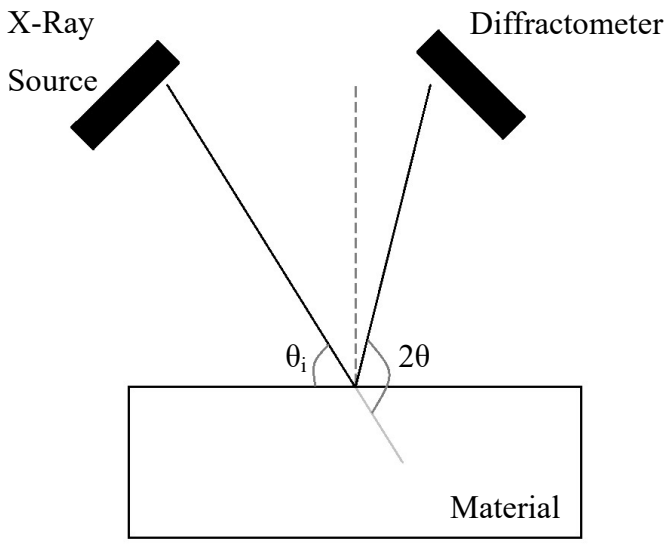

Figure 2.8: The demonstration of XRD method.

$$\Delta\theta = -\tan\theta_0\left(\frac{\Delta D}{D_0}\right) \tag{2.10}$$

The difference in Bragg`s angle caused by the change in lattice distance, $\Delta D$, can be calculated by help of the **Equation 2.10**. Here, $\theta_0$ is Bragg`s angle diffracted from a stress free or reference lattice distance Lin et al. (2016).

Strain, $\varepsilon_{\varphi,\psi}$, might be calculated by the formula, $(D_{\varphi,\psi} - D_0)/ D_0$ whilst $D_{\varphi,\psi}$ corresponds to the aforementioned stressed lattice distance in the direction of φ and ψ which represent azimuth and pole angles, respectively. The ψ angle is the angle between the normal of lattice plane and specimen surface normal. In various φ and ψ angles, measurements are repeated to evaluate residual stress depending on the method and to increase accuracy Noyan and Cohen (1987).

In order to take measurements from various directions, specimen or X-Ray source is often tilted in different methods. In the **Figure 2.10**, it is seen that the location of diffraction peak alters with respect to tilt angles.

Measurement of residual stresses with X-Ray method in highly textured and components with multiple phases includes difficulties. In addition to this, simple X-Ray can measure the depth only up to approximately 10 micrometers while in the case of hard X-Rays penetration depth is much higher.

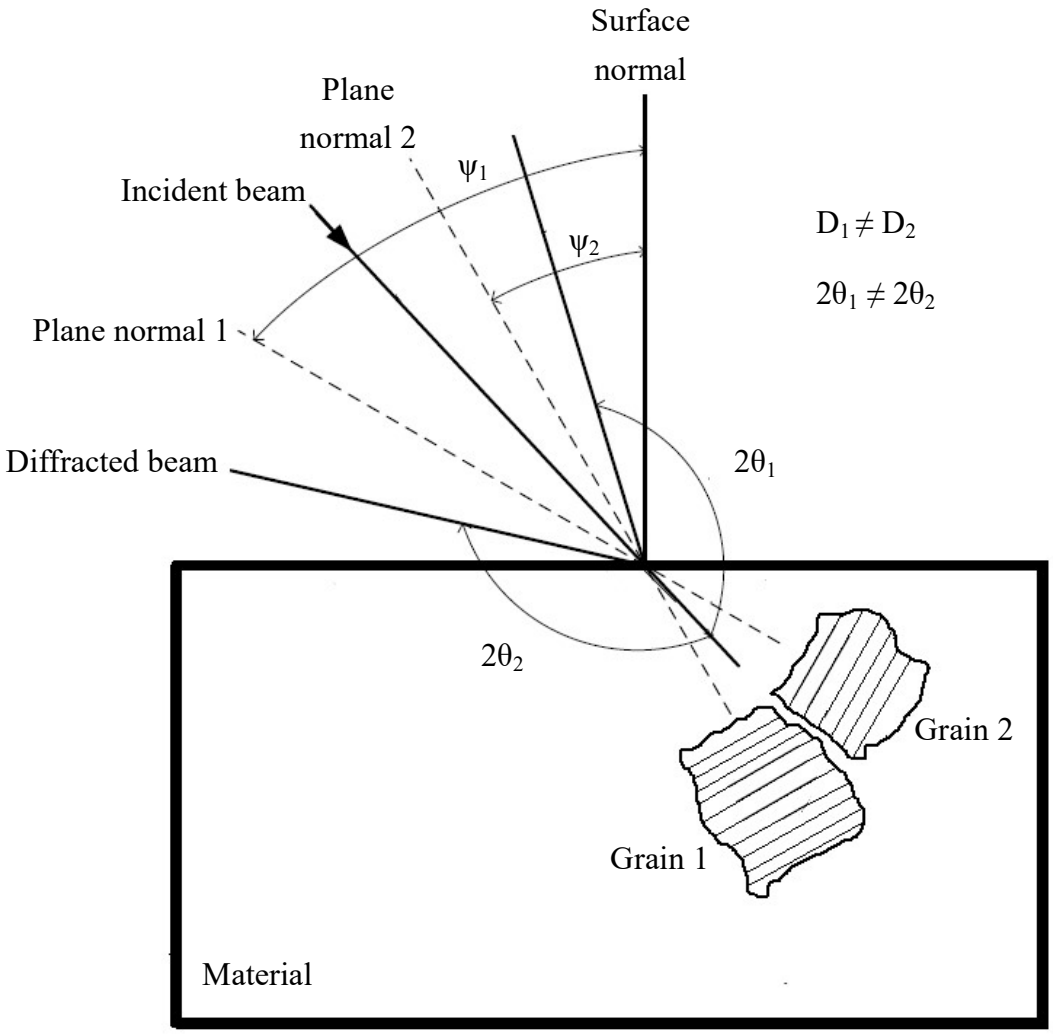

Figure 2.9: The θ and ψ angles Lin et al. (2016)

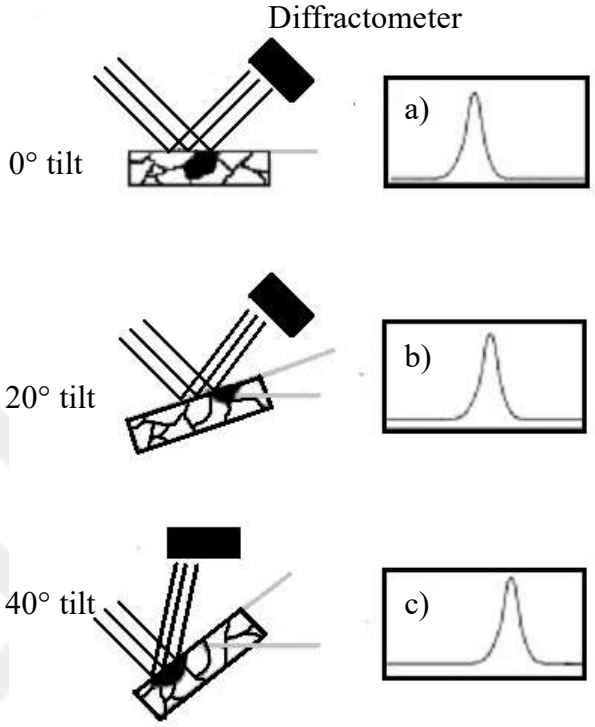

Figure 2.10: Measurements at different titls h and m Analytical Services.

Another limitation of X-Ray diffraction method is that extremely rough surfaces could be problematic with XRD method. When XRD is used so as to determine internal residual stresses, it would be a destructive method after outer part of any component is destroyed by etching process in this case to prepare samples.

High energy X-Ray diffraction is carried out with the use of special designed part called synchrotron to produce higher energy electrons. These high energy electrons generate x-rays with high intensity which could penetrate deeper section. Owing to this surpassing property of synchrotron devices, diffraction method becomes usable for the determination of residual stresses in bulk materials.

Penetration depth of X-Rays varies according to material. Hard X-rays could penetrate mostly 3 or 5 centimetres in steel and 9 or 12 centimetres in aluminium alloys Kandil et al. (2002). Moreover, the volume of a component would reasonably affect the measuring time.

Neutron Diffraction

Neutron diffraction method shares the same basic principles as x-ray diffraction method (XRD). X-ray source and beams of XRD are replaced by a neuron source and high energy neutrons in this method. Thanks to this fact, parts with high penetration depth of interest can be investigated. Penetration depth in this method varies with material types like in XRD while attenuation coefficient depends on material density and atomic number. Intensity of beam can be given as in the Equation.

$$I = I_0 e^{(\mu t)} \tag{2.11}$$

Another advantage of neutron diffraction method might be utilized to separate micro residual stresses from macro residual stresses using poor spatial resolution over x-ray diffraction. In this case, macro stresses can be averaged and eliminated while micro stresses are left. Neutron diffraction method is also very often used to validate other methods. The method also shares very similar disadvantages with XRD when the method is compared with contour method Hauk (1997). The accuracy in neutron diffraction method is discussed to be about $\Delta D/D=10^{-4}$, which will correspond to ± 21 MPa deviation for steel products Hauk (1997). The determination of full stress tensor would be realized with the measurements in 6 directions. However, more measurements might be useful to study further measured stresses in tensor. As stated in literature, neutron diffraction method allows its users to compute D versus $\sin^2\psi$ data up to the point where $\sin^2\psi$ is equal to one while this value might reach 0.9 in x-ray diffraction method. In the remaining interval, measured D might be disparate. The lack of data in this range might be great of importance for cold worked material.

Ultrasonic methods

Ultrasonic methods which are based on the acoustoelastic effect use ultrasound waves to measure non-destructively residual stresses. In accordance with the acoustoelasticity, the magnitude and direction of stress lead to change in the velocity of sound waves measured subsequently by transducers. Among ultrasonic methods, refracted longitudinal waves are addressed to be the more useful and reliable by different authors Rossini et al. (2012). The presence of texture in material under study affects notably reso-

lution and certainty like in the other non-destructive methods. Besides this, the measurement of speed often called time of flight measurements might include difficulties and uncertainty while the change in the wave velocity is small Kandil et al (2002), Karabutov et al (2008). As penetration depth of waves depends on frequency and wavelength, applied depth of ultrasonic methods reaches 1-2 millimetres Belahcene and Lu (2002). One benefit of the method to note is that it would impose less financial burden on its users than diffraction methods Rossini et al. (2012), Kandil et al. (2002). Furthermore, the availability of portable instruments for refracted longitudinal wave method is widely stated in literature.

The methods necessitate the use of the acoustoelastic coefficients whose determination requires prior experiments to actual measurement. However, measuring residual stresses in this way might be relatively rapid although pre-experiments could be a bit of time-consuming Rossini et al. (2012).

Table 2.1: Measurement of residual stresses in thick sections.

	Deep hole drilling	**Crack compliance**	**High energy XRD**	**Neutron diffraction**	**Contour method**
Removal of material	Yes	Yes	No	No	Yes
The use of calibration coefficients	No	Yes	No	No	No
Cost or inaccessibility	Moderate	Low	High	High	Moderate
Measurable depth	Large components are possible	Large components are possible	25-50 mm in Fe	25-50 mm in Fe	Large components are possible
Main difficulties	Eccentricity of cut, Measurement	Inverse calculation, Plasticity	Multi-phase, Texture, Accessibility	Multi-phase, Texture, Accessibility	Clamping, Cutting, Plasticity

Difficulties always exist for measurements of residual stress. Furthermore, residual stresses in thick sections are even more complex to identify. For instance, thickness might be broader than one centimetre. The **Table 2.1** provides insight into comparison

of mostly used methods for evaluation of residual stresses inner region of thick components. Contour method might be considerable amongst the methods.

2.3 Cold Extrusion and Residual Stresses in cold extrusion

In a full forwarded cold extrusion process, a raw material pushed by a ram proceeds through a die gaining the desired shape in its cross section. Initially, workpiece is surrounded by container while a friction force between this container and material is produced as well as between die and material during forming operation. Typical materials might be various types of steel, aluminium, lead and magnesium alloys. The products of closed-die extrusion like rod extrusion could be produced at higher strains compared by open-die type Lange (1985).

Tekkaya and Gerhardt (1985) investigated numerically residual stresses of the cold worked rods due to inhomogenous plastic flow during the process. In the core of the components, they found compressive axial stresses that are balanced with tensile stresses formed at outer regions. These outcomes obtained from the FE analyses are strengthened by the experiments with the same alloy, C15 steel, in their study. Pyzalla and Reimers (1999) reached a very similar stress state with the experiments of XRD, high energy XRD and neutron diffraction with the true strain 0.5. The authors also repeated the experiments with the strains 1.2 and 1.6. Pyzalla et al. (1999) analyzes the residual stress state of extruded rods in the axial direction by the use of the experimental technique alike high energy XRD called white high energy XRD and achieves the findings correlating the abovementioned results together with the near surface compression stresses that might be caused by the friction between die and workpiece. Residual stresses are discovered to be in the same profile in both extrusion and drawing operations by Rudkins et al. (1994). They noted that magnitudes of RS are greater in extrusion compared to drawing although the situation becomes vice versa at small strains. Tekkaya and Gerhardt (1985) also discovered that ejection process reduces axial RS reasonably. The acknowledgement of the drop in the magnitudes and gradients of stresses are also stated by Zucko et al. (1997). The authors also highlight that surface compressive stresses detected in their study at high strains influence favourably resistance to corrosion.

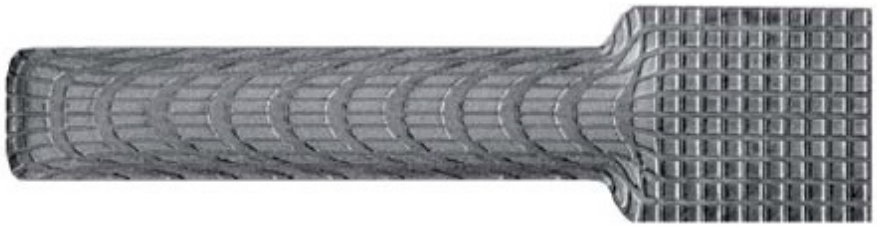

Figure 2.11: The flow of the specimen with the grids Ossenkemper (2018)

Pyzalla et al. (1999) noted that grains in middle imposed on stretching while near surface ones are mostly compressed in a full forwarded cold extrusion. Similar observation can be deduced from the microstructure in the transverse direction as well as experimental work performed by Ossenkemper (2018). The grids on a C15 extruded steel rod prove how material flow develops during process, evidently.

The components produced by drawing and extrusion might be highly fiber textured and anisotropic Atienza et al. (2005).Besides isotropic hardening, kinematic hardening with Bauschinger effect inevitably occurs. Thus, a researcher might expect greater yield strength in tensile than in compression in the extrusion direction in the extruded rods. This case might turn out to be reverse in perpendicular directions.

Defects of extrusion might occur mainly due tremendous forces. Cracks might be spotted as a result of elevated temperature and stresses. Fatigue strength of punch might be another factor an engineer should take into consideration for mass production Lee and Chen (2000). Material undergoes extensive deformation in a cold extrusion. When formability of billet is exceeded, a defect commonly known as central bursting may be witnessed. Plancak (1990) noted that material requires higher formability degree in die corners and centre of die exit. Joun et. al (2011) stated that die angle, friction and reduction area might be responsible for central bursting. Different material damage models to predict central bursting are studied in literature Joun et. al (2011), Soyarslan et. al (2008). Another defect occurs in the form of galling which deteriorates surface roughness and quality of the products Heinrichs and Jacobson (2011).

Die angle are found to effective in punch forces in aluminium extrusion by Chaudhari et. al (2012). Onuh et al. (2003) obtained similar result in cold extrusion with aluminium and lead alloys and stated that die angle at 90 degrees minimizes the required

punch forces. Chaudhari et al. (2012) also discussed that land area causes the required extrusion force to increase.

A lubricant might affect significantly material flow during process, surface quality and roughness Various lubricant types are investigated in literature. Syahrullail et al. (2011) suggests more environmentally friendly biodegradable lubricant which is palm stearin. Hafis et al. (2013) studied lubricant quantity and its effects on process and stated that lubricant quantity carries importance for process efficiency. Molybdenum disulfide (MoS_2) employed also as lubricant in this thesis is widely used for cold extrusion process Bay (1994). During extrusion process, friction coefficient might be high when contact forces rise Wagener and Wolf (1994).

2.4 Wire Electro-Discharge Machining

Wire electro-discharge machining (WEDM or wire-edm) often also called wire electrical discharge machining is an advanced machining technique for electrically conductive materials. Wire-edm is not directly research aim of this thesis. However, the success of contour method is fairly contingent on cutting and clamping conditions. Therefore, the study of the influence of cutting and clamping is still a high level of obligation as well as cutting parameters.

Wire-edm is very suitable process to generate some complex shapes and tight tolerances. The method provides high accuracy and precision. In this machining method, material removal happens by the help of electrical energy. As illustrated schematically in the **Figure 2.12**, supplied voltage is applied to a workpiece and wire generally chosen as conductive soft or hard brass or Zinc coated brass and conductive workpiece.

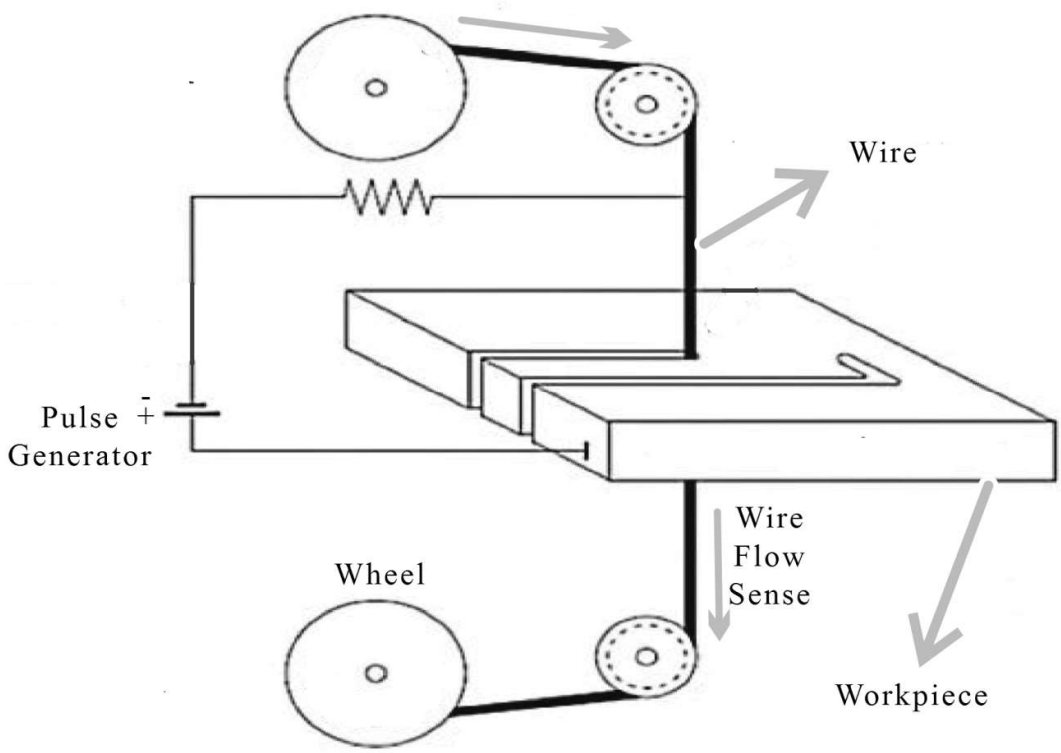

Figure 2.12: A schematic view of wire-edm Goyal (2017).

A discharge plasma forms and electrons moves from one electrode and strike against another electrode which cause the temperature to increase in the electrodes so that even some amount of materials evaporates and some other amounts melts. Evaporated matter and some portion of molten matter swept away by dielectric fluid are removed from both electrodes that are workpiece and wire. Some fragment of molten material may resolidify on the workpiece. This resolidified portion forms white layer which might be defined as possible error source on the cut surface.

Shabgard et al. (2011) stated that white layer thickness and surface roughness rise with the increase in pulse-on time. Pulse-on time might also diminish the efficiency of di-electric fluid which might contingently be error source. Hascalik and Caydas (2004) noted in their study that white layer has an untempered martensitic structure and this portion cools rapidly. Consequently, hardness of cut surface decreases with depth. The authors also demonstrated that thickness of white layer is significantly affected by the amount of energy transferred. Microcracks and high tensile residual stresses present in

white layer. White layer in EDM process is investigated by Ekmekci (2004). Similar to wire-edm, high pulse-on time causes white layer thickness to increase in accordance with the study. White layer is further discussed in the Chapter 5.

Surface roughness is found to deteriorate with increasing voltage and pulse-on time Hascalik and Caydas (2004). Tomura and Kunieda (2009) studied numerically and experimentally the effects of electromagnetic force on wire movement during process and they stated that it might cause the oscillation of wire. As the absence of cutting forces in wire-edm process is valuable for contour method, those existing forces such as electromagnetic and electrostatic may influence negatively flat cut.

In addition to these, high cutting energy might also cause cut width to increase. Prime and Kastengren (2011) discuss that bulge errors decrease with the drop in cut width and cutting procedure has the assumption of zero kerf width.

Maher et al. (2016) observe that the effects of wire speed and tension is minor on white layer thickness and pulse-off time might mitigate white layer thickness. Another process parameter in wire-EDM which might increase cut width and white layer thickness is voltage since it boosts spark energy. Hereby, voltage might inherently broaden cut width as pulse-on time.

Tosun et al. (2003) studied experimentally variation of crater sizes and discovered that crater size tends to increase with the voltage while flushing pressure lowers crater depth and diameter. In the study, wire speed is found to be less effective to crater size while pulse-on time and voltage are the most significant factors.

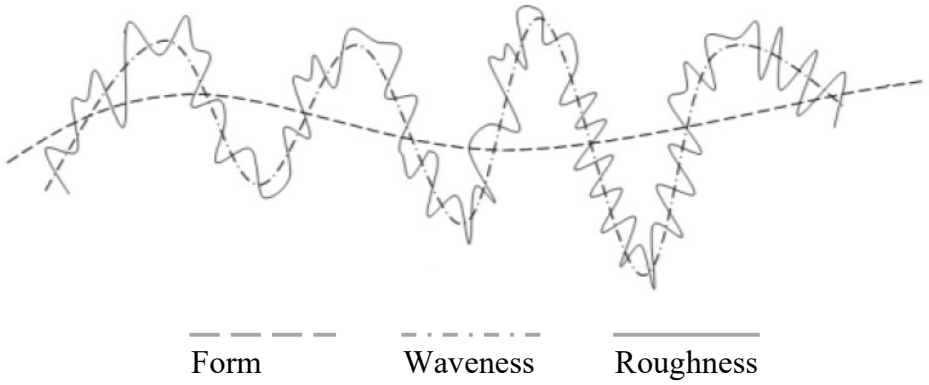

Figure 2.13: The illustration of surface topography Whitehouse (2011).

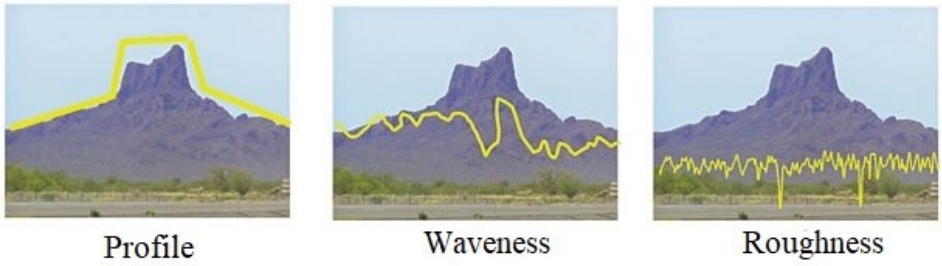

Figure 2.14: Profile, waviness and roughness Cohen (2012), Michigan Metrology.

After cutting process, contour topography except roughness, waveness is composed of and surface form to which elastic deformation is expected to contribute. **Figure 2.13** and **Figure 2.14** exhibit general surface topography from the studies in literature**.** Averaging contour of two opposite surfaces would diminish the error engendered by waveness and roughness. These issues are taken into consideration during the implementation of the experiments and further discussed in the Chapter 5 and 6.

3 Goal of the Work

As already stated, contour method developed in the very beginning of 21st century can be considered as a young method to investigate RS and the interest of the researchers in it has been growing in the last years. Moreover, measurement of residual stresses by contour method might present some advantages over other residual stress measurement techniques in certain cases. Although hole drilling and ring core are able to predict the components, σ_{xx}, τ_{xy} and τ_{xz} of stress tensor where drilling is carried out, these methods can provide knowledge of residual stresses only up to certain depths. Residual stresses might be important not only in a certain location but also in all over the body for huge number of products. Addition to this, two dimensional stress map of cross section can be obtained by contour method. To investigate residual stresses in the whole cross section of bulk materials, high energy x-ray diffraction method (XRD) or neutron diffraction method can be used. However, these methods could bring into consideration their own error sources and limitations such as cost and the requirements for sophisticated laboratory equipments that cannot be found in every manufacturing hall as summarized in the **Table 2.1**. Even though neutron diffraction and high energy XRD could be implemented to determine micro residual stresses, the separation of macro stresses from micro stresses could often be confusing in these diffraction methods in the final.

Some previous works indicate that contour method can give satisfactory results within certain accuracy limit Zhang et al. (2004), Prime (2001). Because of all these reasons, contour method might gain more popularity in future. The method might become more useful to measure residual stresses in the cold forming products, as well.

In literature, contour method is widely studied with hollow cylindrical parts and their welding processes. Besides these studies, Pollard et al. (2016) studied residual stresses of hot-extruded titanium alloy after post-processing via contour method. Furthermore, Prime et al. (2003) investigated an aluminium alloy forged to relieve stresses with multiple cuts after quenching process that generates undesirable tensile RS for fatigue life. Similar specimens to Prime et al. (2003) are also used by Hill and Olson (2014) to test the reproducibility of contour method. However, any work keywords on the applica-

tion of contour method to asymmetrical and full cylindrical parts manufactured by cold extrusion are not detected after browsing with the keywords on Google Scholar, ScienceDirect, Los Alamos website for contour method...etc. This work aims to study residual stresses of the parts manufactured by cold extrusion process with varied extrusion ratios via contour method that could be a sensible alternative in many cases for the products in the various industries if the application of the method can be expandable into these areas.

4 Cold Extrusion and Manufacturing of Parts

For this study, the chosen material is 16MnCr5 steel which is the one of widely used materials for cold extrusion. It is a case hardening steel whose chemical composition and allowable deviation as percentage are given in the **Table 4.1** below.

Table 4.1: The weight composition of 16MnCr5 Alloy DIN EN 10084 (2008).

	Material 16MnCr5					
Alloying Element	*C*	*Si* *Max.*	*Mn*	*P* *Max.*	*S*	*Cr*
Percentage by mass	0.14-0.19	0.4	1.00-1.30	0.025	≤0.035	0.80-1.10
Permissible deviation	±0.02	±0.03	±0.05	±0.005	±0.005	±0.05

All the raw materials used are coated with Zinc-Phosphate coating and lubricated with Molydenum disulfide (MoS_2) which is suggested for extrusion process. Bay (1994) discussed this coating process, chemistry behind the lubrication in cold extrusion process and lubrication for such a steel alloy and its process in detailed way.

Initial raw materials have a cylindrical shape whose diameter and height are 25 mm and 25 mm, respectively. Raw materials were produced by cold drawn after continuous casting. A heat treatment process was applied to regain ductility for further cold forming process. Microstructures of four raw specimens were investigated under Nikon Eclipse LV150 optical microscope in this work. For this goal, two specimens were cut horizontally and other two specimens were cut vertically using Struers Rough Cutting Instrument. Rubbing of horizontally cut specimens performed with Struers Automatic Sanding and Polishing Instrument for 5 minutes for every grindstone value. The values of grindstones were gradually increased from 320 to 1000. Vertically cut specimens

were rubbed manually. Finally, a mixture of acetone and nitric acid was applied to four faces which will be viewed under microscope with the different magnifications varied from 50X to 1000X.

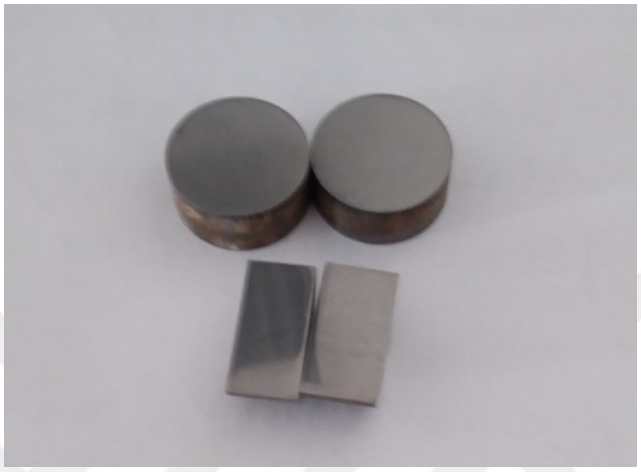

Figure 4.1: The prepared samples for optical microscope (horizontally cuts are above).

Horizontally cut specimens will provide microstructure from the cold drawn direction while others provide from the transverse direction to the process. It would always be possible to see the effects of heat treatment process viewing microstructural images represented in the **Figure 4.2**.

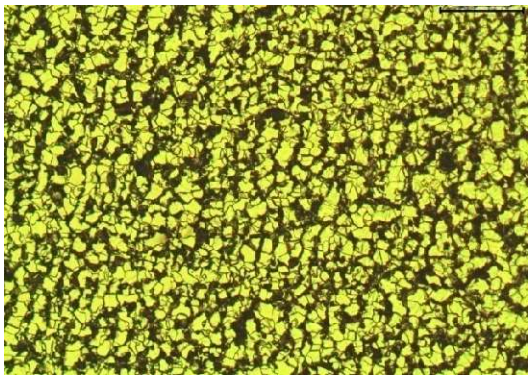

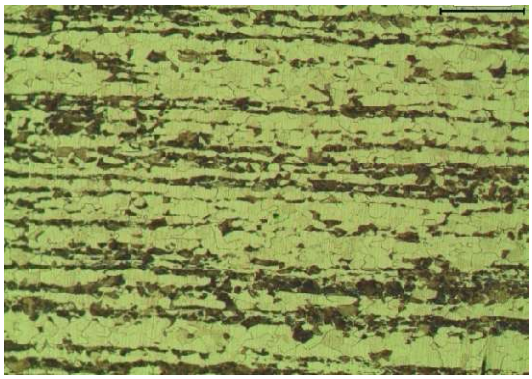

Figure 4.2 a): The view from ext. direction **Figure 4.2 b):** from trans. direction.

First two numbers in the designation of the alloy, 16MnCr5, defines the carbon composition in accordance with DIN standards. The alloy can be classified as a hypoeutectoid alloy while the carbon rate, 0.16 percent is lower than the eutectoid composition. The existence of two phases comes into sight. One of these is proeutectoid α-phase

(ferrite) with body-centred cubic (BCC) structure and has a look of a light colour whereas the view of the other phase which is pearlite that consists of a lamellar structure of ferrite and cementite (Fe_3C) is in dark. In pearlitic structure, thickness ratio of ferrite to cementite might be approximately 8. More uniformly distributed grains of light phase and dark phase appear at the similar sizes although some grains at diversified sizes exist. In transverse direction to the extrusion direction, α-phase and cementite appear in lamellar structure.

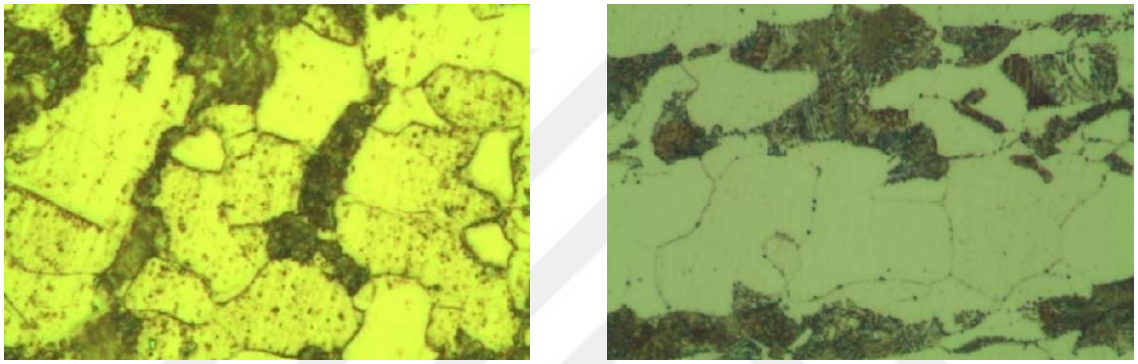

Figure 4.3: The microstructure views with 1000X magnification

The lamellar structure of pearlite could be clearly observed under a scanning electron microscopy (SEM) but Nikon Eclipse optical microscope provides magnification only up to 1000X. The lamellar structure of pearlite may be roughly seen in the **Figure 4.3** that represents the 1000X magnification images. Even though normalizing procedure does not deaden fully residual stresses generated by cold drawing, it eliminates reasonably remaining stresses. This heat treatment process for 16MnCr5 might be performed in the vicinity of air over 800 °C Harichard et al. (2012). Yield strength might be expected to be about 400 MPa. But the allowable deviations in chemical composition might end up with the shifts in stress-strain diagrams of the samples from divergent manufacturers.

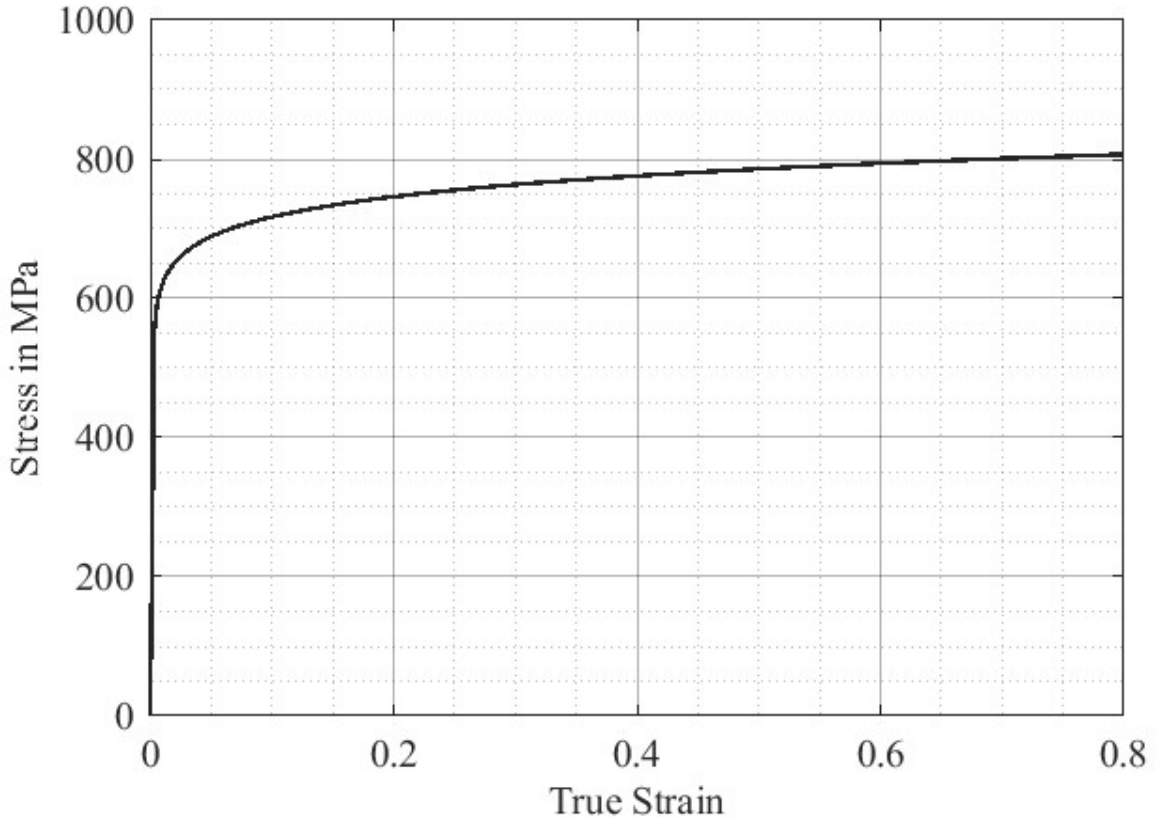

Figure 4.4: Stress-strain diagram Caner and Duran (2018)

Applied force causes atoms to slide over each other which is called slip mechanism. Slip mechanism results in plastic deformation by the help of existence of dislocations. After sliding, atoms bond with new neighbour atoms. In general belief, these compressive residual stresses would enhance mechanical properties of material while tensile stresses would decrease fatigue strength, wear resistance etc.

This study was planned to include the investigation of effects of extrusion ratios on residual stresses in cold-extruded cylindrical parts. Therefore, three dies used vary in extrusion ratio although the cone angles which are 120 degrees and initial raw material are the same in each time. Cone angle might be expected to be effective at tool life more rather than product life Lange (1985). The technical drawings of the dies will be presented in the Appendices. Two parts were manufactured with each extrusion die. In total, the production of six parts with three different extrusion ratios was implemented. Some specimens whose diameters vary are shown as well as an initial material on the **Figure 4.4**.

Figure 4.5: The cold-extruded specimens with the diverse diameters and a billet.

The **Table 4.2** exhibits further details about the final diameters, extrusion ratios and corresponding true strain to each extrusion ratio. A D-frame Eccentric MAWI Crank Press with a maximum force capacity of 3000 kN has been used for manufacturing. This type of mechanical presses uses electromechanical motor as driving unit. P unch speed varies with respect to a sinusoidal function. Therefore, speed of punch increases at the very beginning and reaches a maximum value. Punch force might exhibit very steep step-up with the punch displacement until a maximum force, probably till 2-4 millimetres. Afterwards, punch force might slightly decrease due to the drop in total contact area between die and billet while process is proceeding. The ejector`s maximum stroke is approximately 80 mm, respectively. Friction coefficient might be about 0.04-0.08 Lange (1985). The completion of one cycle with the ejection process prolongs only a few seconds in total. Significant reduction in residual stresses with the occurrence of the ejection process might happen as demonstrated in literature by Tek-

kaya and Gerhardt (1985). All extrusion processes are carried out at room temperature and under the same conditions.

Figure 4.6: The illustration of one of the extrusion dies.

Extrusion force might be elevated while processing the lowest thickness reduction. As a result of this, service life of 1.4 strain die might be the least while contact forces between die and billet tremendously high. The **Figure 4.6** illustrates one of the dies employed during the manufacturing of the samples in this study.

Table 4.2: Extrusion ratios and true strains of the parts.

Initial diameter of workpiece *(mm)*	**Final diameter of workpiece** *(mm)*	**Extrusion ratio**	**True Strain**
25	12.41	2.01	1.4
25	15.16	1.65	1
25	17.62	1.42	0.7

Hardness is defined as the resistance of material to being permanently deformed. This mechanical property is often employed to predict ultimate tensile strength. Besides this, Vickers hardness could be utilized to predict yield strength of the components after cold working Tekkaya (2000). Vickers hardness measurements with the diamond pyramid tip are performed for each extrusion ratio in certain numbers. Measurements are implemented discreetly in the centres of circular cross section. For this aim, Zwick / Roell ZHV 10 with 1.961 N load and 20X magnification is employed. Measured average diagonal length of imprints and Vickers harness values of true strain are represented in the **Table 4.3**.

Table 4.3: Vickers hardness's and diagonal lengths of indentations of three specimens.

Extrusion Ratio	**True Strain**	**Diagonal Length** (µm)	**Vickers Hardness**
2.01	1.4	37.08	336.5
1.65	1	36.23	283.8
1.42	0.7	33.22	270.4

Finite Element Analysis of Cold Forward Extrusion

In the framework of this study, the FE analyses in commercial code Abaqus standard are performed to validate the results obtained from contour method as well as the analyses in the code Simufact to study a standard cold forward extrusion under various conditions such as in different friction coefficients, die angles and temperatures. In addition to press time, following ejection process is included in all analyses.

Only axisymmetric analysis would be sufficient since cross sections of the cylindrical rods studied in this thesis are symmetric. In Abaqus Standard, static general axisymmetric analysis and Full Newton solution scheme are enabled during the analyses at the three different extrusion ratios. A standard axisymmetric stress element, CAX4HR, and transient type analysis are selected. This type of element has 4 nodes uses reduced integration scheme Abaqus manual (2016). Young modulus and Poisson's ratio of both die and billet are taken 210 GPa and 0.3, respectively.

In both Abaqus Standard and Simufact, billet is meshed with 0.2 size elements while die has coarser size mesh. The coarser mesh of die is reduced to a finer mesh in the regions near contact zones with die. Coulomb friction coefficient is applied in the most of analyses and taken as 0.04 or 0.042 during the analyses. In mixed friction model in Simufact, friction factor is taken as 0.3. Similarly, 4-node bilinear elements also are enabled during the sensivity analyses in the commercial software Simufact. Temperature dependent data existing in Simufact for 16MnCr5 alloy is utilized to study temperature on axial RS. The results of the analyses performed in Abaqus Standard are compared with the experimental findings. All result from the analyses are presented and discussed in the Chapter 7.

5 Wire Electro-Discharge Machining

As already explicated in the subchapter 2.4, cutting and clamping whose implementations are discussed in this chapter are cornerstones for the integrity of contour method. The exigence of low power cutting settings in order to mitigate cutting errors comes in view. Therefore, the cutting process is performed with low energy per unit time to accomplish necessities of the assumptions and single cut is applied in every cut.

Kerf width which might be the one of the main potential sources as discussed earlier is the total width of wire diameter and the gaps between wire electrode and workpiece. The **Figure 5.2** demonstrates kerf width.

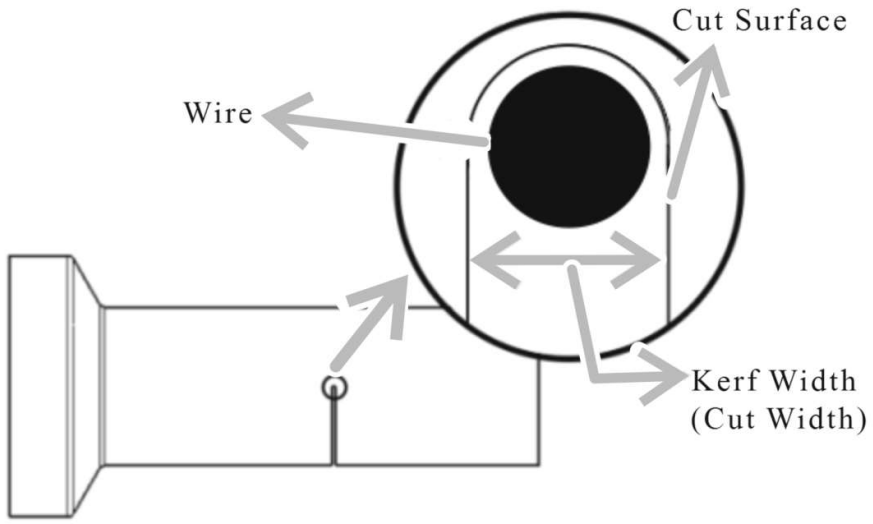

Figure 5.2: 2D demonstration of cut progression.

Deionised pure water is generally chosen as dielectric fluid. For dielectric fluid, high pressure setting is adjusted which will boost the impact of dielectric fluid on removing molten material and heat.

Alteration of cutting time occurs with respect to thicknesses of workpieces that are diameters of rods in this study. Cutting middle size specimen prolongs approximately 40 minutes. High cutting time can be considered as a disadvantage for contour method, but only a few specimens are cut and this process does not affect directly pro-

duction time. Although cutting with lower power will increase further cutting time, cutting even with lower power might be a future study. .

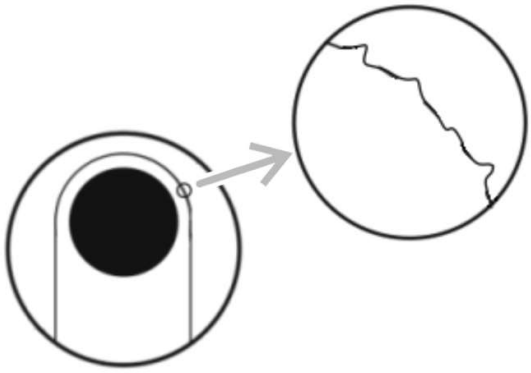

Figure 5.3: The formation of roughness.

Roughness of contour surfaces might be noteworthy issue to discuss for accuracy, while a few micrometers might significantly alter the stresses. R_a value is known as average surface roughness while R_z is the vertical difference between the lowest point and highest point. Surface roughness measurements are realized using a profilometer with a couple of contour surfaces. Surface roughness, R_a, deviates between 0.9 and 1.9 micrometers which would cause significant deviation in the results. However, calculation of average contour might substantially mitigate surface roughness effects.

5.1 Clamping Apparatus Design

Contour method includes the assumption that the cut carried out by wire-edm process is perfectly flat and smooth. Movement and rotation of the specimens during cutting process can violate this assumption and even small changes in the positions of the specimens would result in considerable amount of error in measurement result. Later, surface scanning, with which surface contour will be acquired will be performed assuming that cutting process itself does not make contribution to variation of the cut surface contour. More concisely, one can say that cutting process results in neither bulges nor recesses on the cut surfaces in accordance with the assumption. These variations occur only due to the relaxation of the residual stresses that exist within the product after the production.

Although cutting by wire-edm process is performed at very low power, which highly decreases kerf width and white layer that are discussed topics in the next section, these would not be enough for reasonable accuracy of the results.

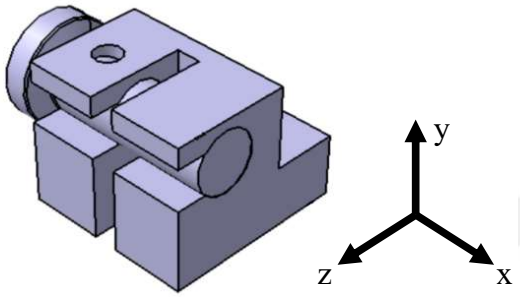

Figure 5.4: The representation of clamping procedure.

The authors like already discussed in the Chapter 2 in more detail state that rotary motions must be avoided along two axes, as well. Designed clamping apparatus restricts two rotary motions around y-axis and z-axis to keep cutting plane motionless and cutting smooth as well as the movements along these axes are not allowed. Clamping locations are intended to be close to cutting plane for this aim. Translation movement along x-axis is not expected at the time of cutting. Two clamping apparatuses were designed and manufactured for this aim. Technical drawing of both clamping apparatus with their dimensions will be presented in the Appendices.

5.2 Resolidification

Even though white layer whose formation was described in the beginning of chapter is very thin lamina in only a few micrometer range on both surfaces of the cut, the presence of white layer might be obstacle for stress relaxation and error source. Low power cutting settings are also aimed to diminish the thickness of white layer or completely mitigate this lamina. Deionised pure water pressure (WP) whose goal is to take away molten material is adjusted to higher values for contour cut.

For the investigation of white layer, two surfaces processed by wire-edm from individual specimens cut further perpendicularly to wire stand through length of half part.

Tests are carried out with 2500X magnification and the pressure below 2.10^{-5} mbar using ZEISS MERLIN scanning electron microscope. As the **Figure 5.5** demonstrates, no distinct white layer is observed on contour surfaces. As a consequence, a researcher might conclude that the distortion of surface due to resolidification and its contribution are likely minor.

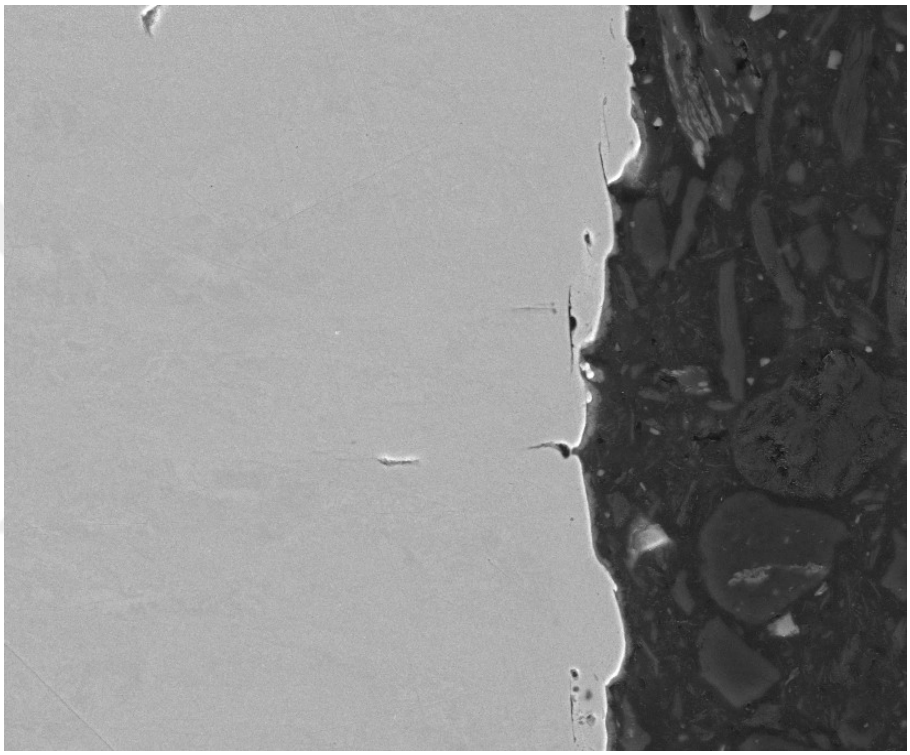

Figure 5.5: The illustration of cut surface of another sample under SEM.

6 Data Processing

Direct use of measured data from CMMs in finite element (FE) model is not possible. Moreover, measured data might inevitably include some noise in it. In addition to this, all data points are randomly distributed in a data set that is formed in such way that inserting it into finite element model would be arduous and time consuming. All of these reasons render data processing compulsory before the use of it in finite element analysis (FEA). Each surface consists of many data points. Therefore, data sets also are impossible to handle manually. After the implementation of surface scanning discussed in section 6.1, data alignment, truncating and smoothing are implemented step by step in Matlab.

Since cross sectional area of the specimens is cylindrical and symmetric, surface alignment for contour method only for this study would be simpler. Best fit plane is set by AliconaInfinite, in most cases. Howbeit, the inclusion of distorted data and plastic deformation might affect significantly the position of reference plane. In these cases, procedure to set the least squares plane should be carried out to reset this reference plane. Best fit plane would be set in a way that the distance of all data points to the plane is minimized. For this reason, y and z values are kept fixed in our case as well as the sum of data points in the x direction is calculated according to the set Cartesian coordinates in the Figure 5.6.

After data processing, the deformation along radius is fit into polynomial curve. When the polynomial curve is obtained, it would be very easy to insert this curve in finite element analysis step of contour method.

6.1 Surface scanning

In the Chapter 2, some literature resources about surface scanning realized with optical coordinate measuring machines for contour method were already mentioned. In contrast to those in literature, AliconaInfinite has some its own specific properties and measurement procedure. Gain and contrast are adjusted to 1.00. The selected objective lens might be the most effective factor that will determine resolution and number of

data points. In this study, scanning is performed with 5X objective lens. Another factor that will change resolution and measurement time is scanned surface area. Surface scanning of one face of the specimen with the biggest diameter includes over 1,000,000 data points. Scanning process took slightly more time for this specimen although resolution value is better for small specimens due to scanned areas. While resolution value is better for small specimens, number of data points is high for these specimens. Best repeatability which might be the most important property for contour measurement is given as 0.12 μm for the machine. The machine performs 3D measurements with the focus variation method with which large surface areas up to 10000 mm^2 can be measured on a reference plane while confocal microscopes can measure narrower profile of a surface locally. All data can be extracted as text files that can be comfortably used in any other software.

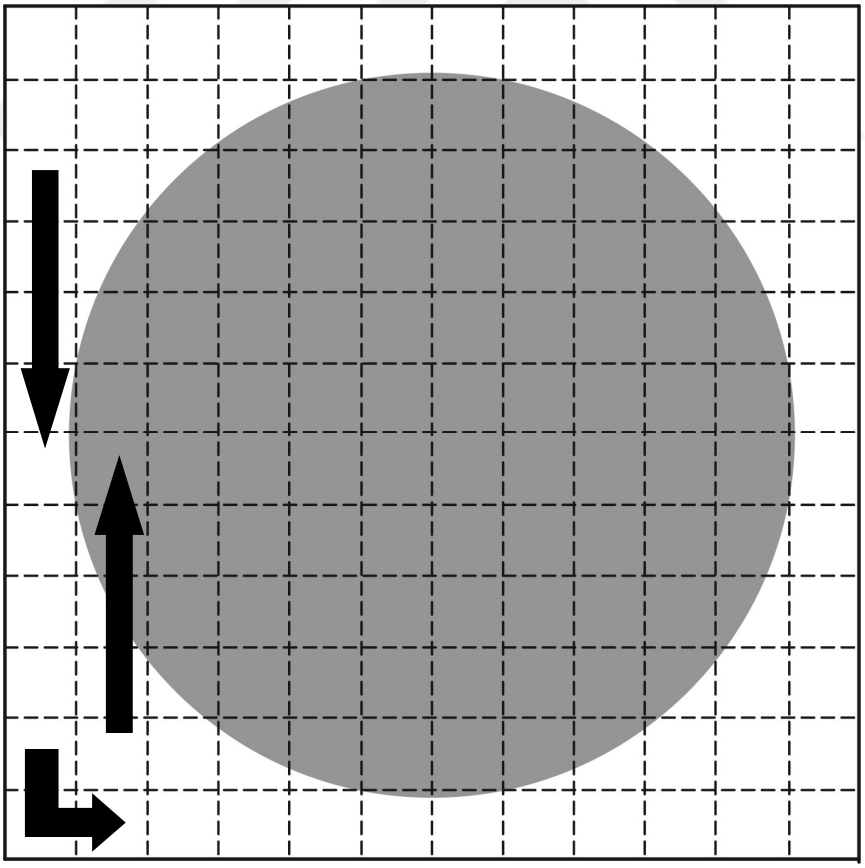

Figure 6.1: The occurrence of scanning process.

AliconaInfinite divides total area into equal sized grids, which will be scanned one by one afterwards. After scanning one grid, the tip passes near one by the help of the planar movement of the table. The size of grids drops with the increasing lens magnification. In that case, resolution will be enhanced while scanning time rises. The arrows in the **Figure 6.1** demonstrate a possible scanning direction. The **Figure 6.2** presents general view of the optical measuring machine and the photos taken while the measurements are going on are depicted in the **Figure 6.3**.

Figure 6.2: The view of AliconaInfinite from the front (Alicona Catalogue).

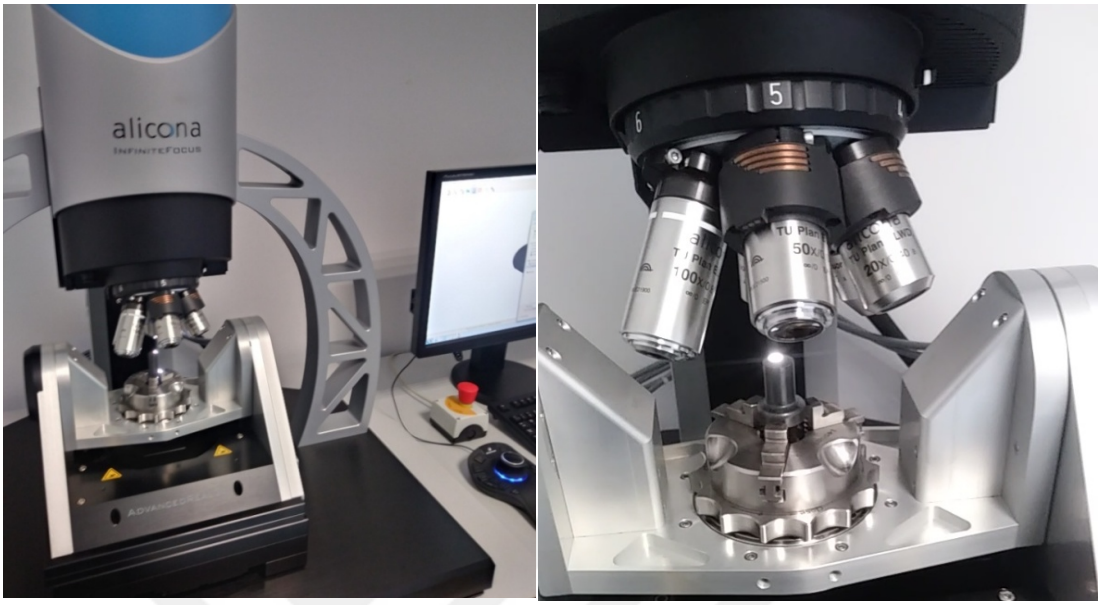

Figure 6.3: The illustration while surface scanning takes place.

6.2 Surface alignment

The **Figure 6.4** represents the scattering of data from the optical CMM on y-z plane. The data centres of cut surfaces are disparate. Before proceeding with data processing, the centres of data and the origin of Cartesian coordinates must be superposed for the sake of simplicity. Mean and median values whose locations in cut surfaces are close to each other are specified by the help of the commercial software, Matlab. Mean value is the average of all data whereas the value in the middle refers to median. Here, first function file in Matlab is run. Reverse sign of mean values of y and z coordinates are added to coordinate values of each data. After this operation, new data set is collected around the origin of coordinate system.

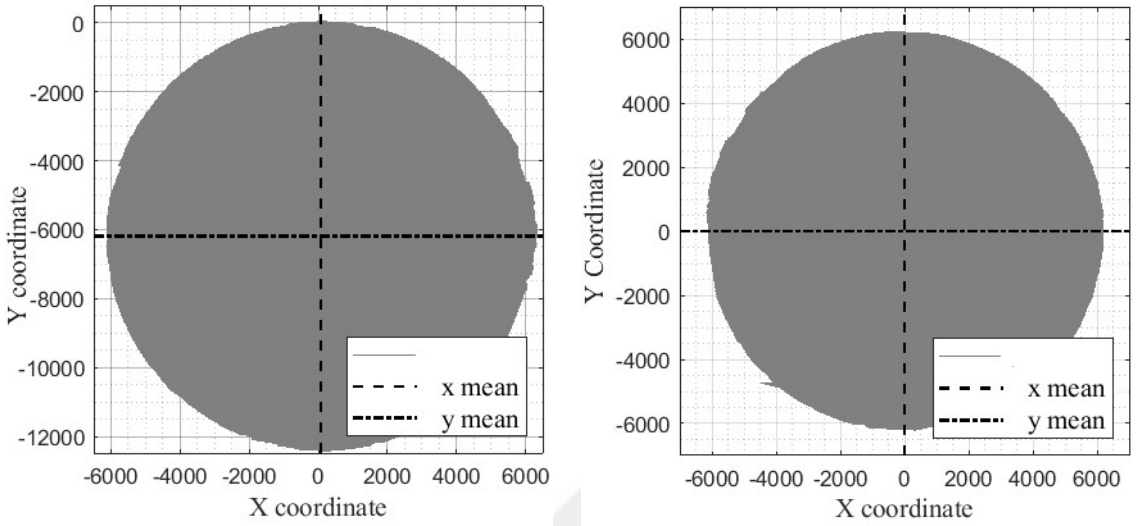

Figure 6.4 a): Before surface alignment, **Figure 6.4 b):** After surface alignment.

6.3 Truncating and surface fit

Many researchers state that near edge data is unreliable for contour method due to plasticity and bulge effect. Plasticity discussed in Chapter 2 in detailed way does not allow obtaining any knowledge of elastic deformation in its region. Tensile integrated bulge contributes to crack propagation and breakage, as well. Bulge effect and stress concentration become detrimental at the final end of cutting. The **Figure 6.5** demonstrates the breakage which is observed after an unsuccessful cutting process. Besides that, data from surface scanning might include some noise data. For all of these reasons, it is inevitable that truncating which includes elimination of the distorted data must be carried out for a reasonable measurement before processing data further and the application to finite element model. Approximately, 1.0 mm near edge data is eliminated from the smallest diameter specimens while roundly 1.2 mm data is removed from other specimens.

Final End of Cut
(The breakage region can be seen.)

Figure 6.5: The appearance of breakage.

A function file named as “step1.m” was prepared to run in Matlab. The file opens the surface aligned data by the previous function file, “step0.m” and eliminates near edge data with respect to the distance of data point to the origin and some distorted data. Addition to “step1.m” file, “step2” and “step3” files were prepared for data processing in Matlab. These two function files smooth surface data. The radius of circular cross section is divided into intervals as illustrated in the **Figure 6.7**.

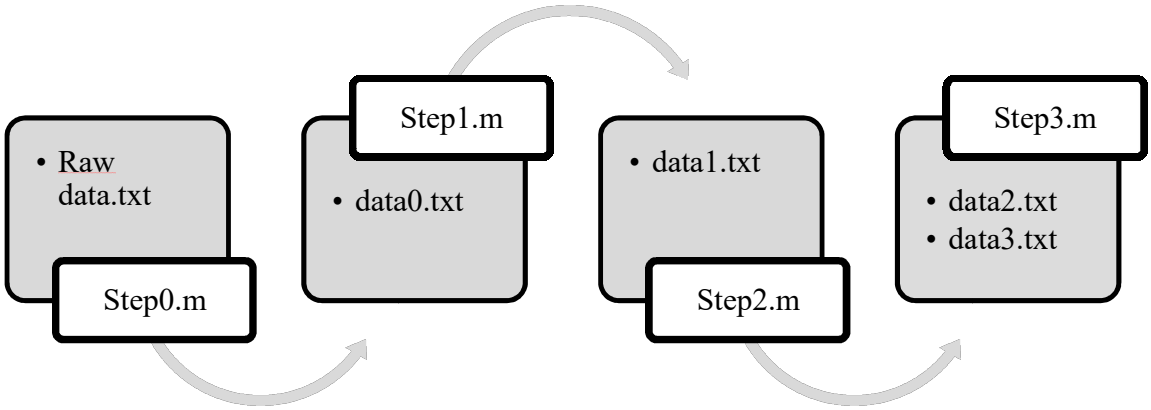

Figure 6.6: The illustration of the working cycle of .m files.

All function codes utilize the output .txt file or files from the previous function file to realize processes and save the processed data for upcoming function code in the directory folder. All written function files, “step=.m”, “step1.m”, “step2” and “step3”, were presented in the Appendix.

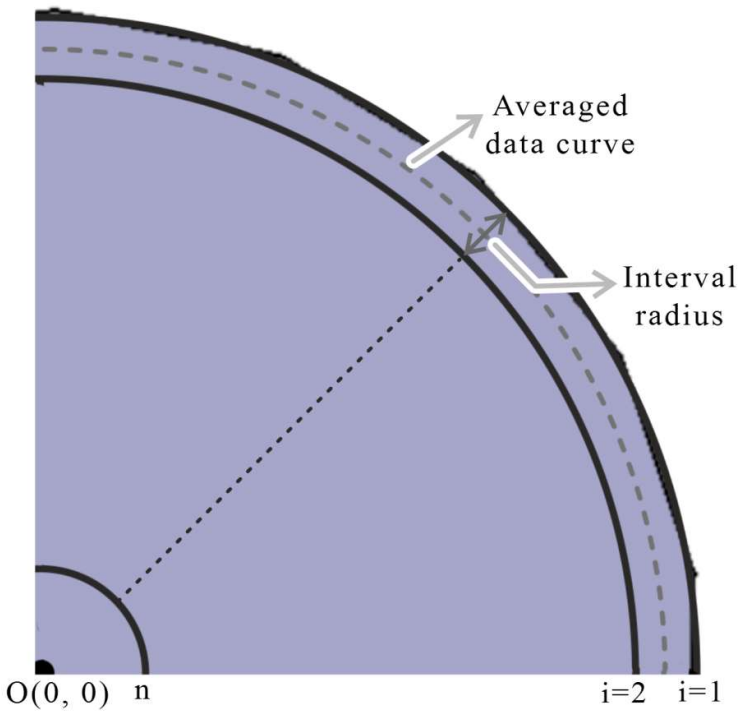

Figure 6.7: The partition of surface area.

Samples used in this thesis are full cylindrical rods. Because of this reason, variation of axial residual stresses in the extrusion direction is expected to happen along radius from the centre of cylindrical rod to outer edge and in the same manner in all directions. Thus, it would be meaningful to prepare FE model as only 2D axisymmetric model as well as whole surface is reduced to a simple 2D curve from centre of circular cross section to outer edge. In this purpose, the cross-sectional area is divided into n interval. This is followed by the computation of average data in each interval with the corresponding average distance to the centre. Average contour is computed as presented in the intervals of certain distance.

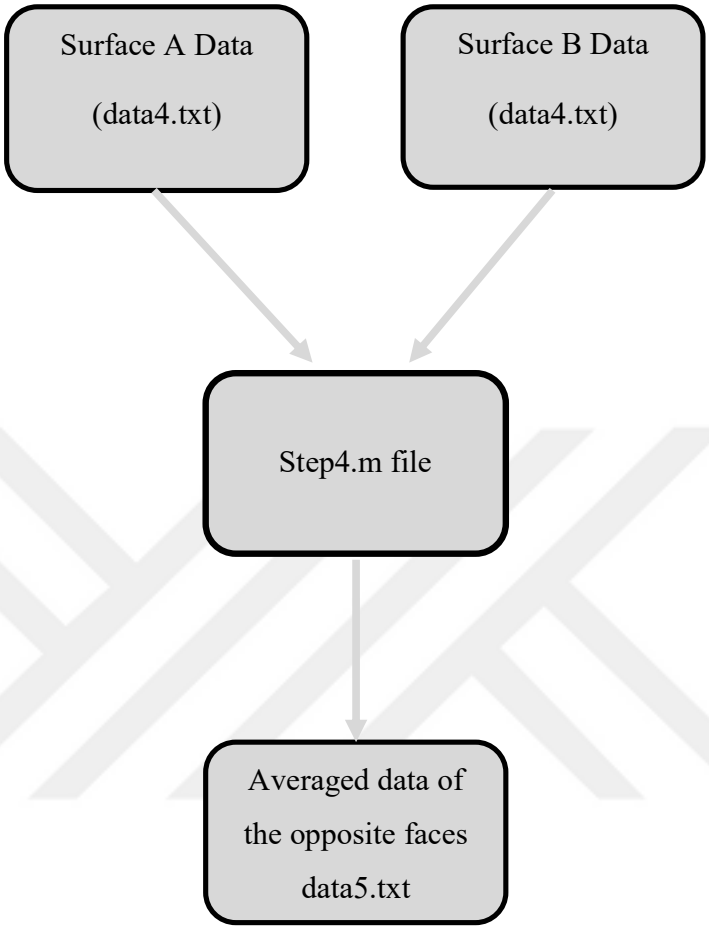

Figure 6.8: Averaging of data sets of two surfaces.

Like already explicated in the Chapter 2, shear stresses, τ_{xy} and τ_{xz}, and the cutting effects necessitate the use of the mean of the surface deformations. After the implementation of the work on data set, the mean deformation of two opposite surfaces is calculated and the outcome must be inserted into FE model as displacement boundary condition described in the following subchapter. The last function code can be found in the Appendices.

6.4 Application of data to finite element model

For contour method, finite element (FE) model could be developed in separate two ways. First, relaxed surface can be forced back to its initial position after the fit curve is embedded in cut surface in a drawn model. Second method which is to apply curve fit as displacement boundary condition to the initial smooth and flat surface in FE

model is reverse of first method. The latter would give the same result and be better for simplicity. Because the implementation of fit surface in FE model would be difficult since fit surface consists of many data points and the dimensions of two halves are too much greater than elastic deformation which is in the range of micrometres. Curve fitting was implemented by using the same commercial software, as well. The appearance of a 4^{th} polynomial curve could be in the **Equation 6.1**

$$x = p_1 z^4 + p_2 z^3 + p_3 z^2 + p_4 z + p_5 \tag{6.1}$$

In order to obtain polynomial like in the Equation 6.1 instead of using commercial software, the one could employ polynomial regression using final data. Due to the nonlinear equation, the use of linear algebra would be necessary.

$$\begin{bmatrix} n & \sum_{i=1}^{n} z & \sum_{i=1}^{n} z^2 & \sum_{i=1}^{n} z^3 & \sum_{i=1}^{n} z^4 \\ \sum_{i=1}^{n} z & \sum_{i=1}^{n} z^2 & \sum_{i=1}^{n} z^3 & \sum_{i=1}^{n} z^4 & \sum_{i=}^{n} z^5 \\ \sum_{i=1}^{n} z^2 & \sum_{i=1}^{n} z^3 & \sum_{i=1}^{n} z^4 & \sum_{i=1}^{n} z^5 & \sum_{i=1}^{n} z^6 \\ \sum_{i=1}^{n} z^3 & \sum_{i=1}^{n} z^4 & \sum_{i=1}^{n} z^5 & \sum_{i=1}^{n} z^6 & \sum_{i=1}^{n} z^7 \\ \sum_{i=1}^{n} z^4 & \sum_{i=1}^{n} z^5 & \sum_{i=1}^{n} z^6 & \sum_{i=1}^{n} z^7 & \sum_{i=1}^{n} z^8 \end{bmatrix} \begin{bmatrix} p_5 \\ p_4 \\ p_3 \\ p_2 \\ p_1 \end{bmatrix} = \begin{bmatrix} \sum_{i=1}^{n} x_i \\ \sum_{i=1}^{n} x_i z \\ \sum_{i=1}^{n} x_i z^2 \\ \sum_{i=1}^{n} x_i z^3 \\ \sum_{i=1}^{n} x_i z^4 \end{bmatrix} \tag{6.2}$$

The **Equation 6.2** could be written to determine 5 coefficients of a 4^{th} degree polynomial. In this equation, n refers to number of processed data while z corresponds to radius. For solution, the inverse of first matrix could be crossed with the matrix on the right side. Very similar algebraic equations could be formed for 5^{th} and 6^{th} degrees polynomials. In these cases, matrices dimensions vary according to the number of coefficients. For example, a 6 by 6 matrix would appear where a 5^{th} degree polynomial with the six unknown coefficients is constructed.

Finally, the best fit curve is applied as displacement boundary condition to the flat surfaces while the other ends of halves are fixed in that direction in FE analyses. The situation is schematically illustrated in the **Figure 6.9**. Like previously stated in Chapter 2, both of two halves must individually be modelled in FEM software with respect to their dimensions since the specimens are anti-symmetric with respect to cut plane. The stresses along the radius in the direction of x-axis are taken from the analyses. These stresses coming from two halves are different and need to be averaged through the **Equation 2.3** in accordance with contour method. . For the analyses, element type

10 proposed and assigned to the finite elements. All of the results is presented and discussed further in the next chapter.

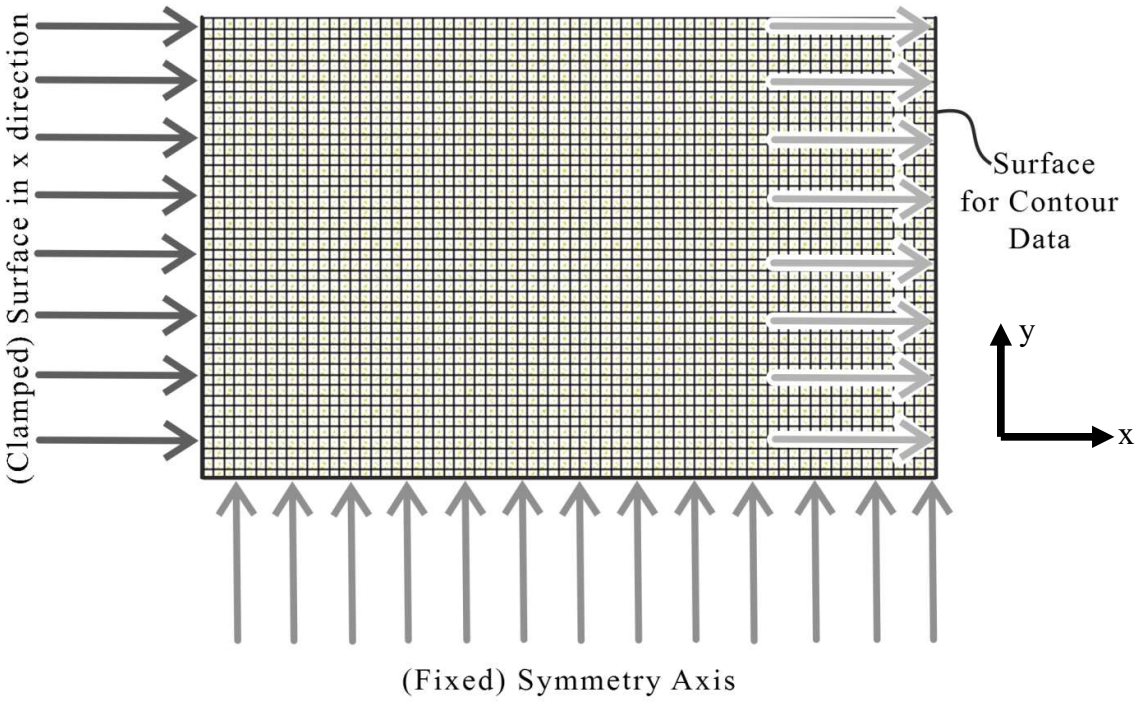

Figure 6.9: The boundary conditions of linear elastic model.

7 Result and Discussion

7.1 Contour Method Results

As a result of all experiments and studies, aimed axial residual stresses is determined and discussed in this chapter. Each extrusion ratio like already mentioned in the Chapter 4 has two specimens which are compared by each other and the works in literature. In accordance with the results, the conclusions are presented.

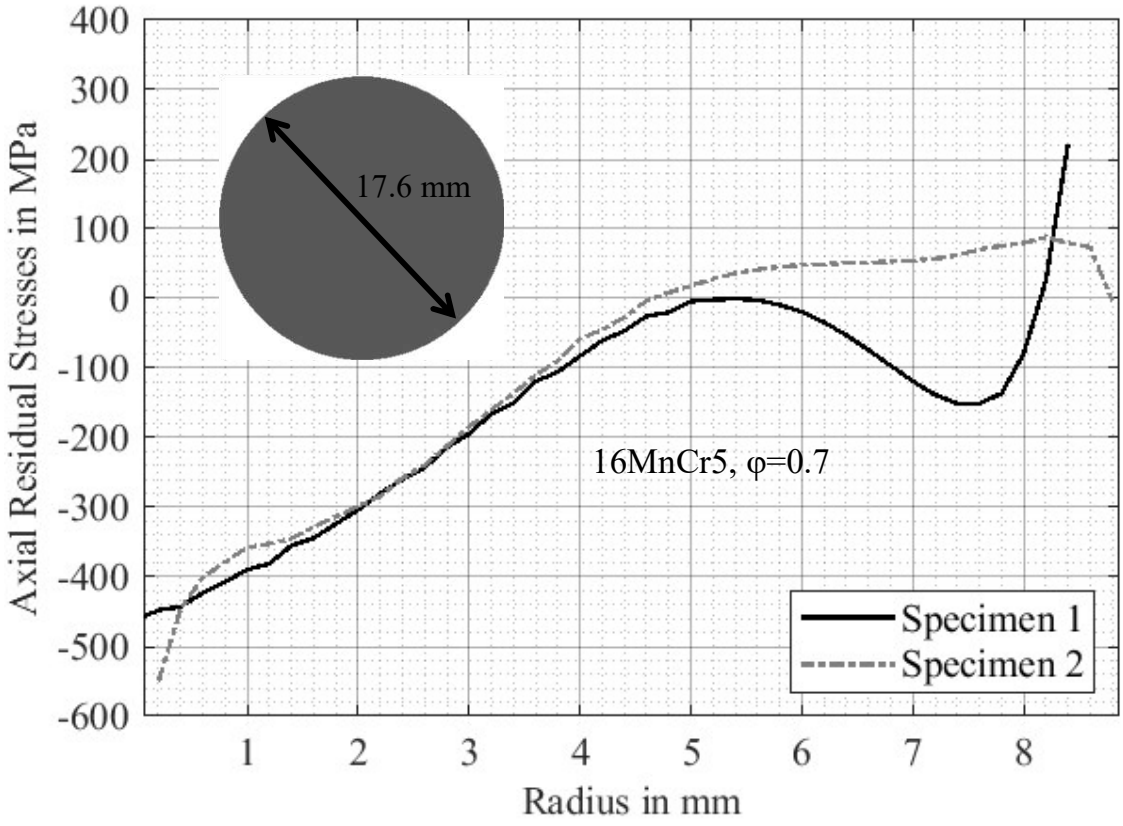

Figure 7.1: Residual stresses in the parts produced with 0.7 strain.

The **Figure 7.1** demonstrates the findings during the investigation of the highest thickness specimens. The compliance of two specimens might be acceptable at the inner regions while residual stresses (RS) at the regions close to surface are not seen in a harmony. In this study, compressive stresses identified in the core while tensile residual stresses reaches approximately a hundred MPa. However, tensile stresses might not

be reliable. Liable causes for this are highlighted in the next chapter. Specimen 2 also exhibits poor amount of near surface compressive RS which might be interpreted as plausible due to the friction. Compressive stresses have peaks of nearly 450 MPa and 530 MPa in the specimen 2 and the specimen 3, respectively.

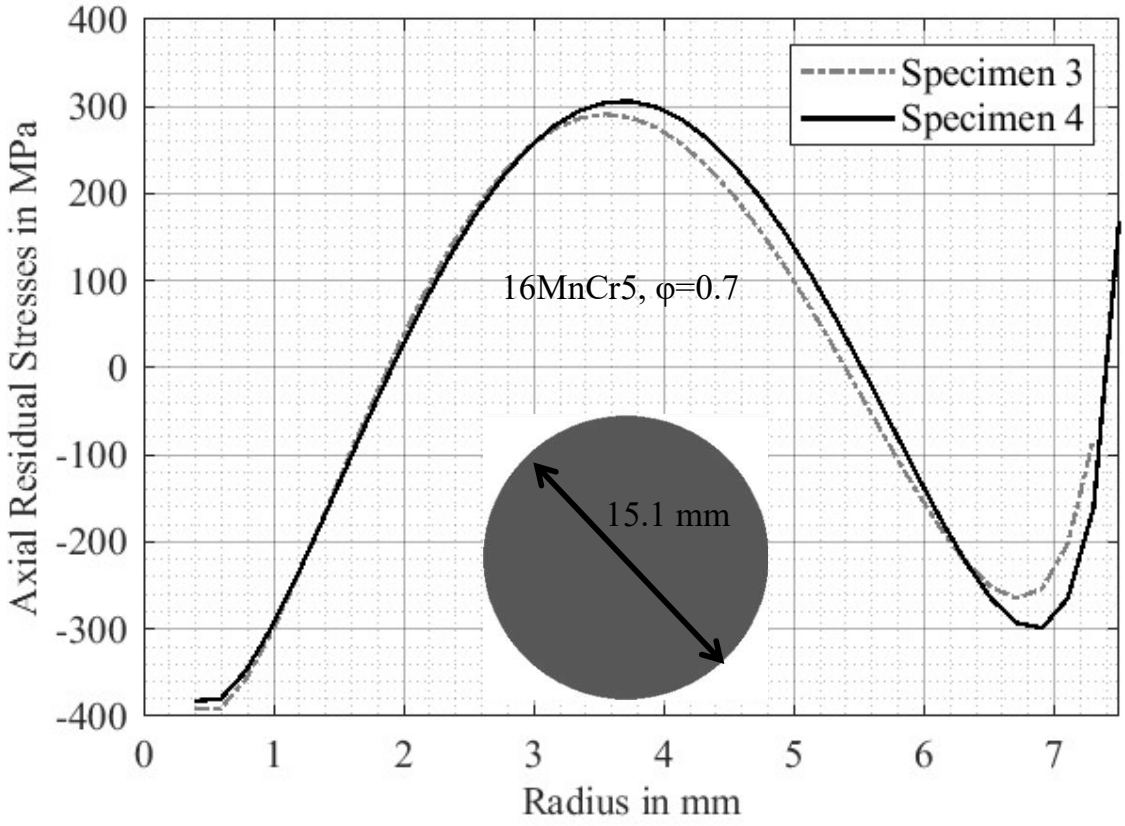

Figure 7.2: Residual stresses in the parts produced with 1.0 strain.

On the contrary to the findings with true strain 0.7, the obtained results experience very sensible agreement when middle-sized samples are investigated as presented in the **Figure 7.2**. The existence of compressive residual stresses is observed in the kernel the same as the studies in literature while tensile RS spreads over nearly 4.5 millimetres in the middle radius. Stress gradients are very steep compared to first two specimens. The differences between the maximum compressive and tensile stresses are less than 10 MPa in these samples while the maximum tensile stress is about 300 MPa. The one remarkable issue to note is the observation of compressive residual stresses at the region which is close to the surface. But this might be very reasonable when someone considers inhomogeneity of plastic flow. The plastic flow occurs more inhomoge-

neously when it is compared with the lower strain. Here, the amount of residual stresses is less which might also be acceptable, though. Only near surface residual stresses might exhibit noticeable deviations.

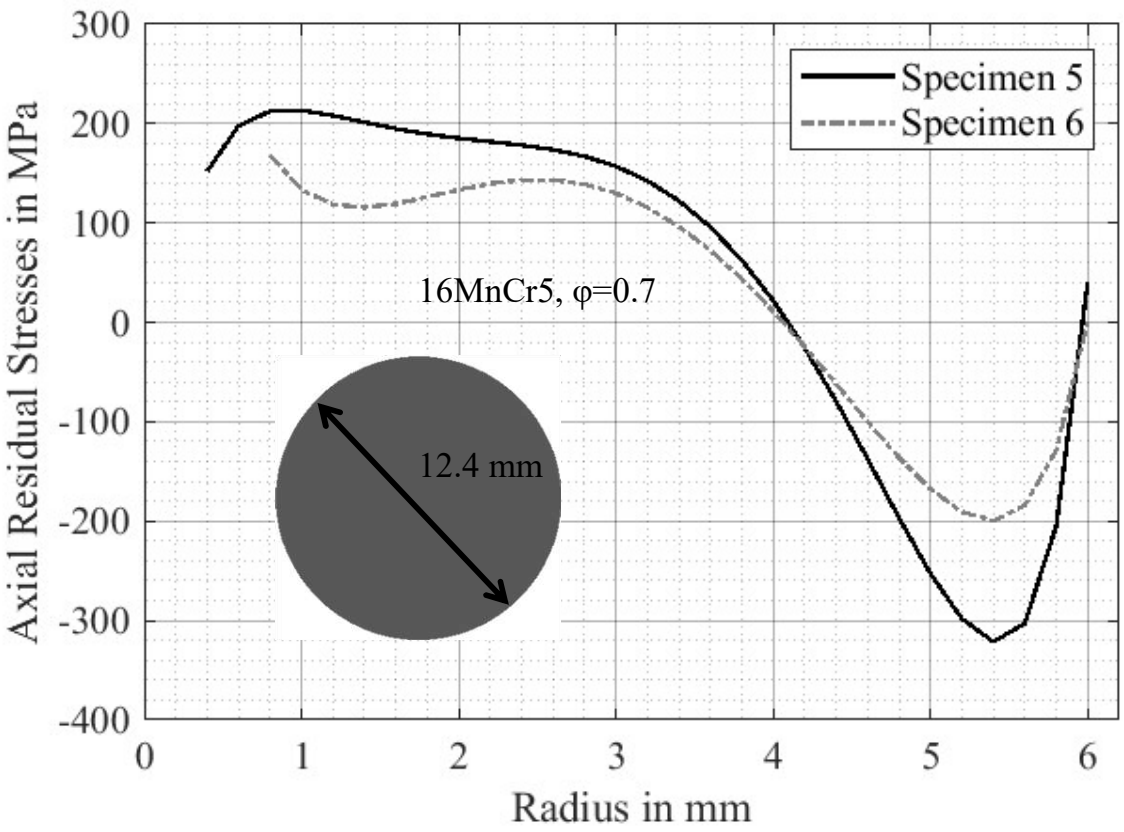

Figure 7.3: Residual stresses in the parts produced with 1.4 strain.

The **Figure 7.3** demonstrates the results from the samples produced with 1.4 true strains whose residual stresses similarly alter rapidly, as well. Surprisingly, tensile residual stresses have been discerned in near core regions. Compressive residual stresses have been found to be in subsurface below surface. The agreement between two specimens is not very gratifying although the predicted stress profiles comply with one another, well. Stresses in the very middle of specimens are not always possible to determine because of scanning process. This matter with its reasons will be stated in the next chapter. Very similarly to the specimens manufactured with 1.0 true strain, compressive residual stresses which are close to surface exist in these specimens, as well. The maximum tensile and compressive residual stresses are approximately 215 MPa

and 320 MPa in the specimen 5, respectively. The results from specimen 6 might be more unreliable due to the distortions during cutting process.

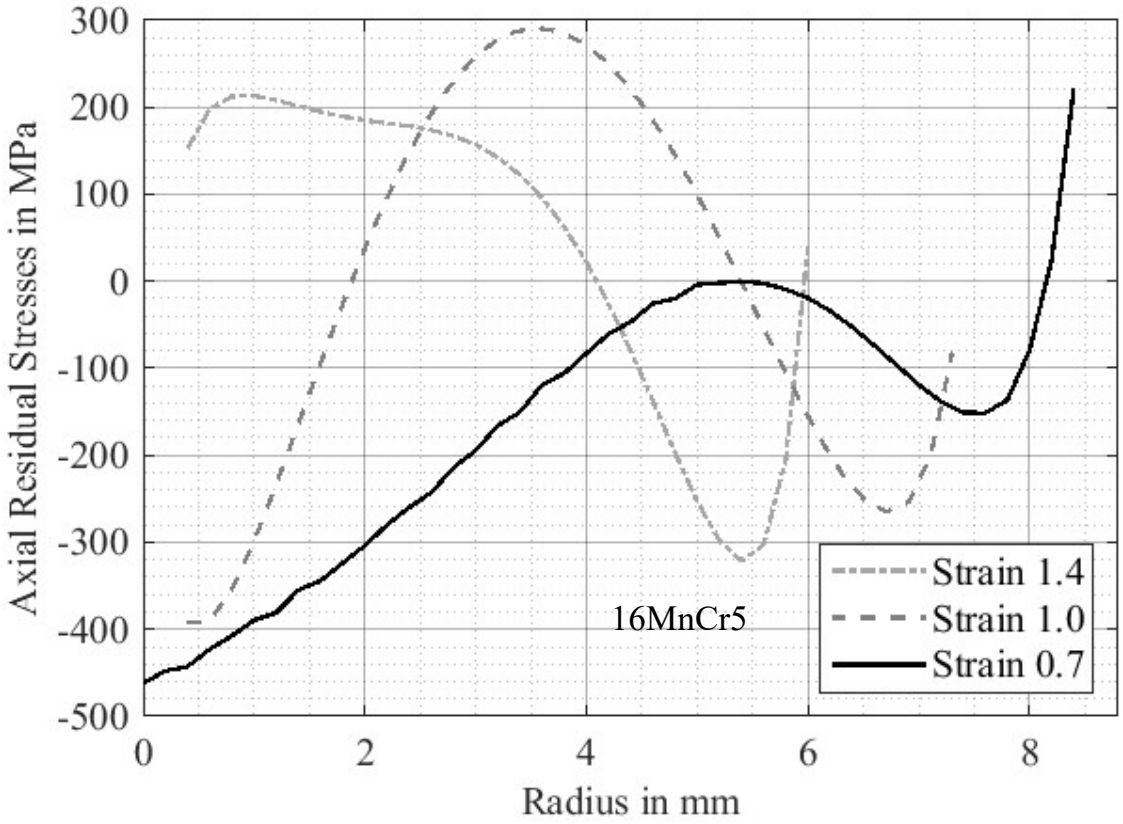

Figure 7.4: Residual stresses in different strains.

The **Figure 7.4** illustrates the distribution of residual stresses with respect to radius obtained from three extrusion ratios. As expected, all of strain values include some compressive residual stresses in the kernel. However, the distribution of compressive stresses takes place up to the distance that is even less than half millimeter. Compressive residual stresses spread widely at inner region at 1.4 true strain. Tensile RS stresses come into view in the middle zones at both true strain 1.0 and true strain 0.7. The existence of conspicuous stress gradients at these strains might have tremendously important role for their fatigue strength. More uniform alteration in RS in the thickest specimens has been observed during the study. In the outer zones at the strains 0.7 and 1.0, residual stresses appear in very similar shapes. Plastic flow of material during forming operation might have predominant impact at residual stresses in macro level. The obtained curve of residual stresses with true strain 1.0 is very similar to the flow

pattern presented by Ossenkemper (2018). To conclude, residual stresses are strongly contingent on the amount of strain.

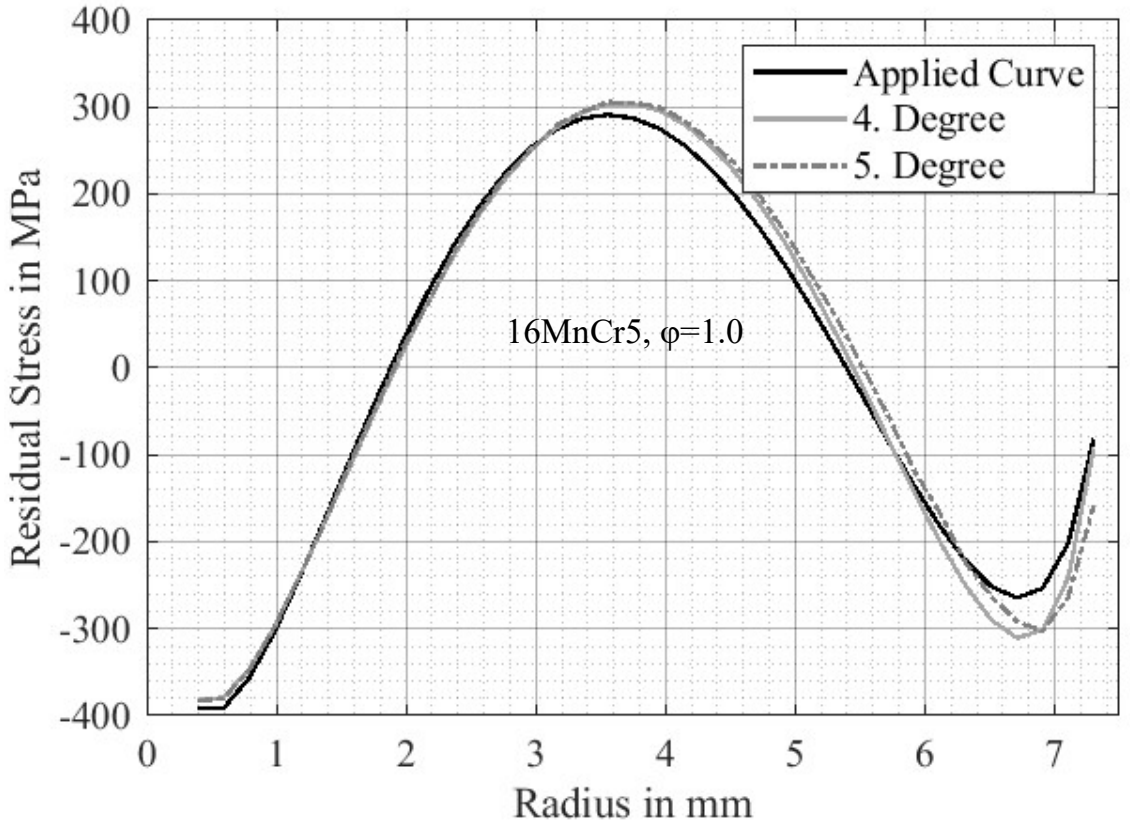

Figure 7.5: The application of varied curves

The residual stresses from applied different curves are investigated in this study. The results may vary in accordance with fit curves. However, a curve which fits to data well must be studied for correct determination of residual stresses. Howbeit, knowledge of residual stresses might not be sufficiently accurate for engineering design. Therefore, enough number of data points must be processed for this aim as well as truncating operation must be compressed only to tight area as much as possible. The minimized error might be expected from adequately performed curve fitting operation as described in Chapter 6 in this thesis.

The **Figure 7.5** exhibits residual stresses obtained from specimen 3 with the application of a 4^{th} degree, a 5^{th} degree and the used curve in the actual analysis. The difference between the curves increases up to 50 MPa in near-edge part where the measured

data with optical measurement is cropped due to the occurrence of the bulge effect and plasticity as stated in Chapter 2 in this thesis. In other regions, stress deviations reach a maximum which is less than 9 MPa.

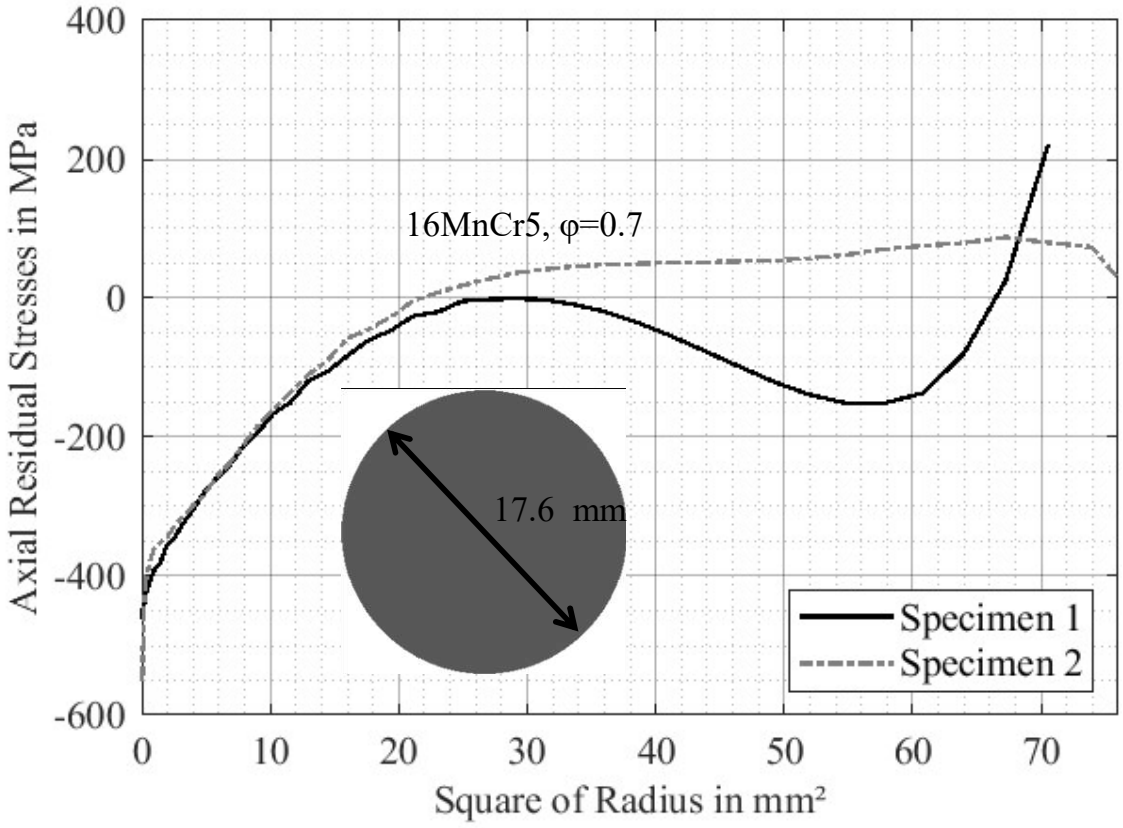

Figure 7.6: Residual stresses versus square of radius at 0.7 strain.

The Figure 7.6, **Figure 7.7** and **Figure 7.8** show the variations of residual stresses with respect to square of radius. The representation of results in this manner may be useful for the comparison with the sources in literature.

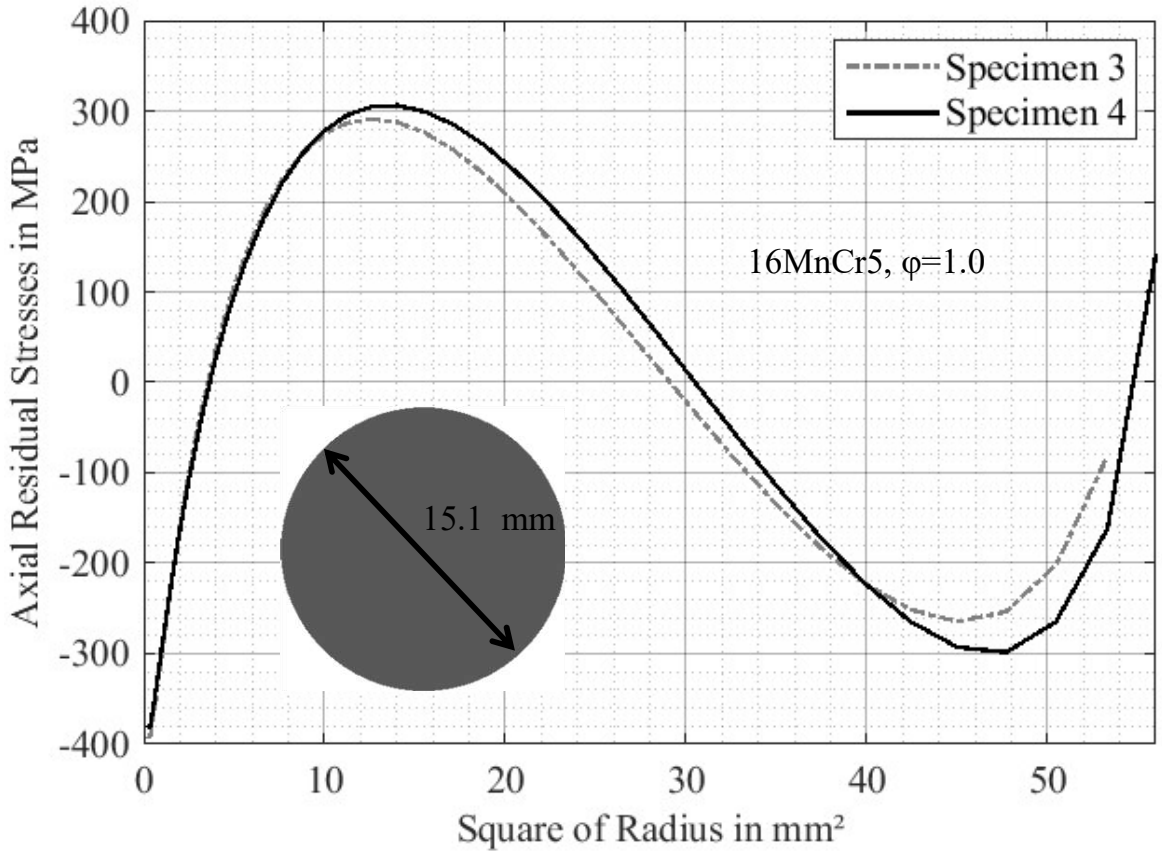

Figure 7.7: Residual stresses versus square of radius at 1.0 strain.

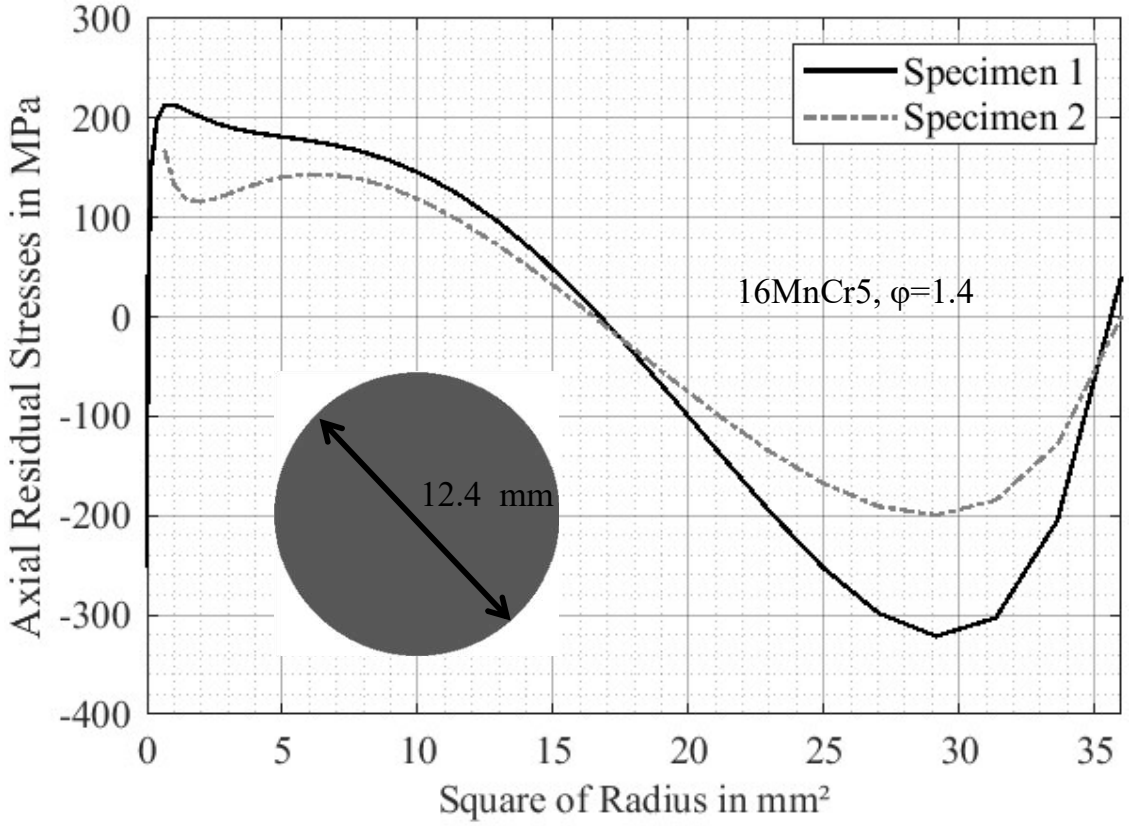

Figure 7.8: Residual stresses versus square of radius at 1.0 strain.

7.2 FE Analyses Results

As already stated previously, finite element analyses are carried out using commercial software Abaqus Standard for all extrusion ratios in order to correlate experimental results. Die has to be modelled as linear elastic material to view the effects of ejection process on residual stresses as stated in literature Tekkaya and Gerhardt (1985).

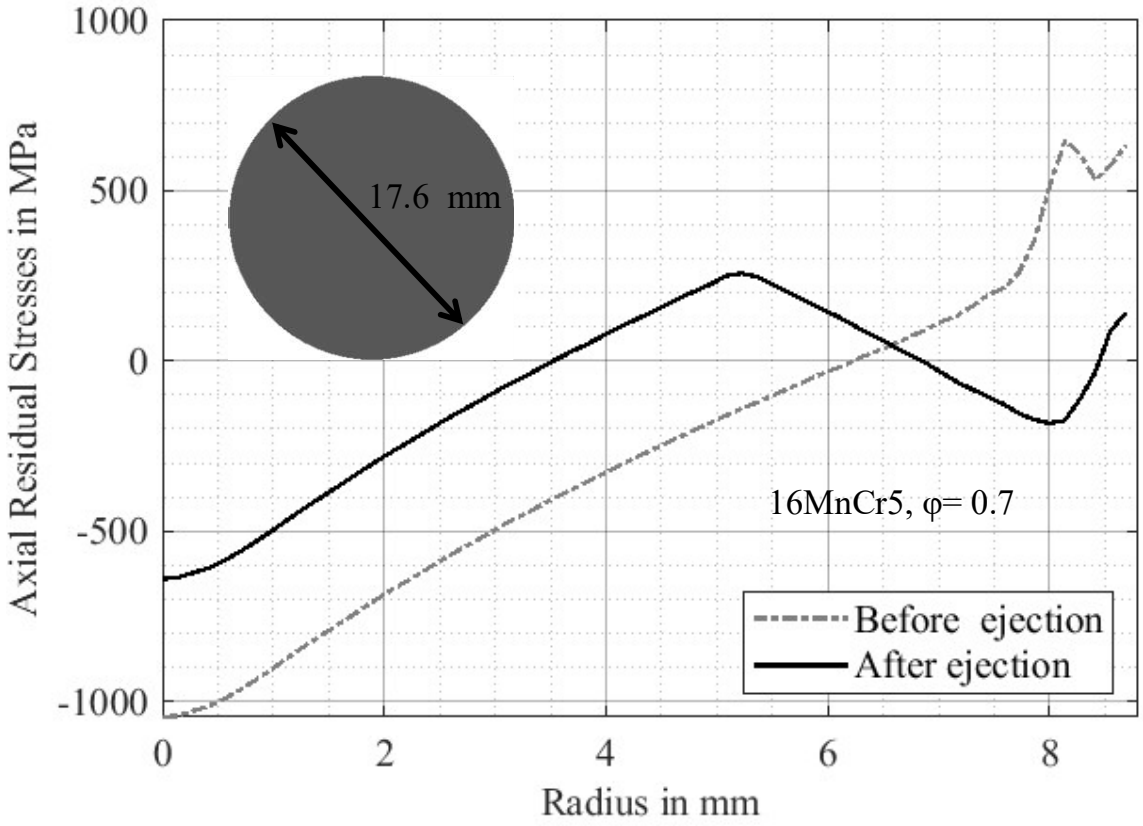

Figure 7.9: The alteration of axial residual stresses with ejection process at strain 0.7.

In this study, the reduction in axial residual stresses is experienced at all three strain rates as demonstrated in the **Figure 7.9**, **Figure 7.10** and **Figure 7.11**. The Figure 7.9 clarifies the alteration in the axial residual stresses at true strain 0.7.Observed compressive RS in the core of rods exceeds 1 GPa while compressive stresses drops significantly and even turn into tensile stresses in some regions. Moreover, tensile residual stresses near outer surface which might threaten fatigue life seriously appear before ejection process. However, surface tensile stresses reduce greatly with ejection in accordance with the finite element study. The Figure 7.10 exhibits the change residual stresses at 1.0 true strain with ejection. Before the ejection process, closely identical

stress profile to the one in the lower true strain is monitored. In the same manner as lower true strain, compressive RS diminishes remarkably in the core region.

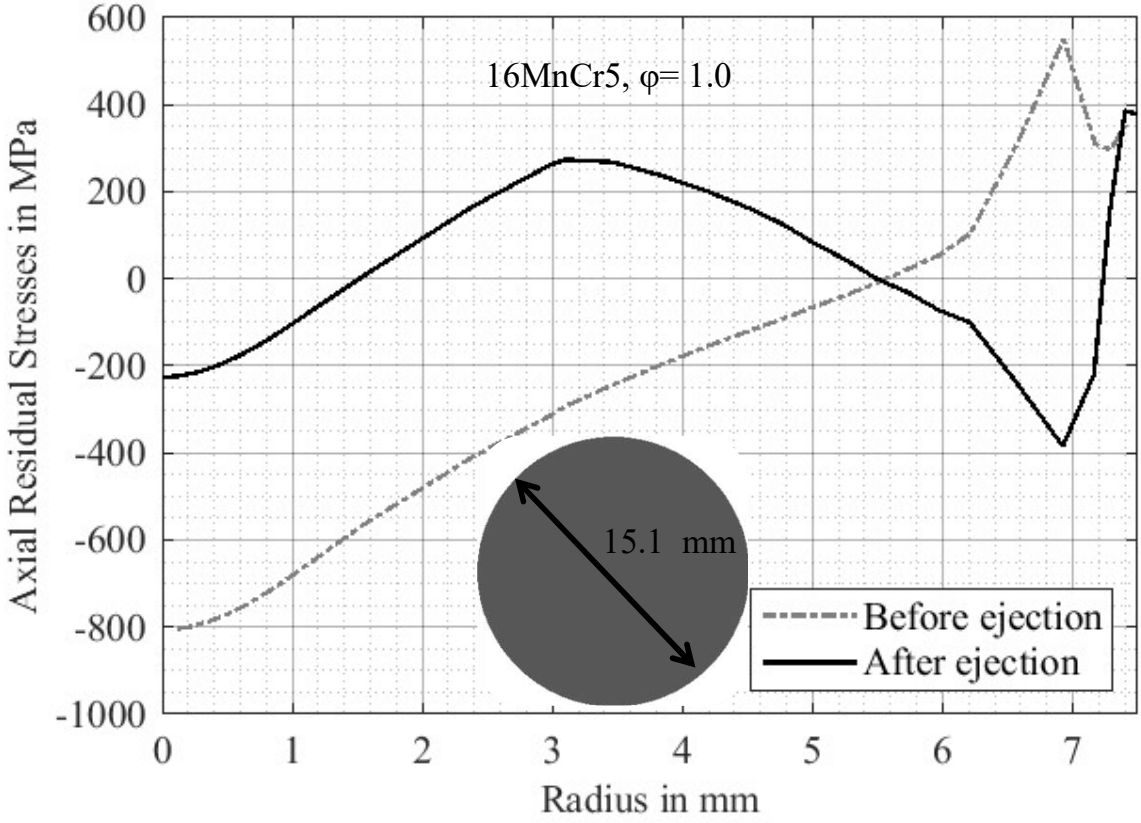

Figure 7.10: The alteration of axial residual stresses with ejection process at strain 1.0.

However, the notable amount of tensile stresses near surface still remains although these stresses are being lowered during the ejection process. It must be noted that immense tensile RS in the subsurface is converted into compressive stresses whose magnitude is slightly less than 400 MPa.

Figure 7.11 depicts the axial residual stresses at 1.4 true strain. Experienced residual stress profile before ejection at this strain resembles the others. Exceptionally, surface compressive stresses form during the punch movement. Surprisingly, compressive RS in the core of a bar turns into small tensile stresses. Addition to this, cylindrical rod experiences low stress gradient in the interior regions. Nonetheless, critical surface tensile residual stresses form except subsurface compressive residual stresses. Tensile residual stresses reach up to over 400 MPa in accordance with the FE analysis. Furthermore, steep stress gradients emerge in the outer zones as embodied in the Figure

7.11. The **Figure 7.12** exhibits the colourful maps of extruded rods at three different strains investigated in the scope of this study. In the Figure 7.12, the stresses which exceed 500 MPa as magnitude are exemplified by grey and black colours.

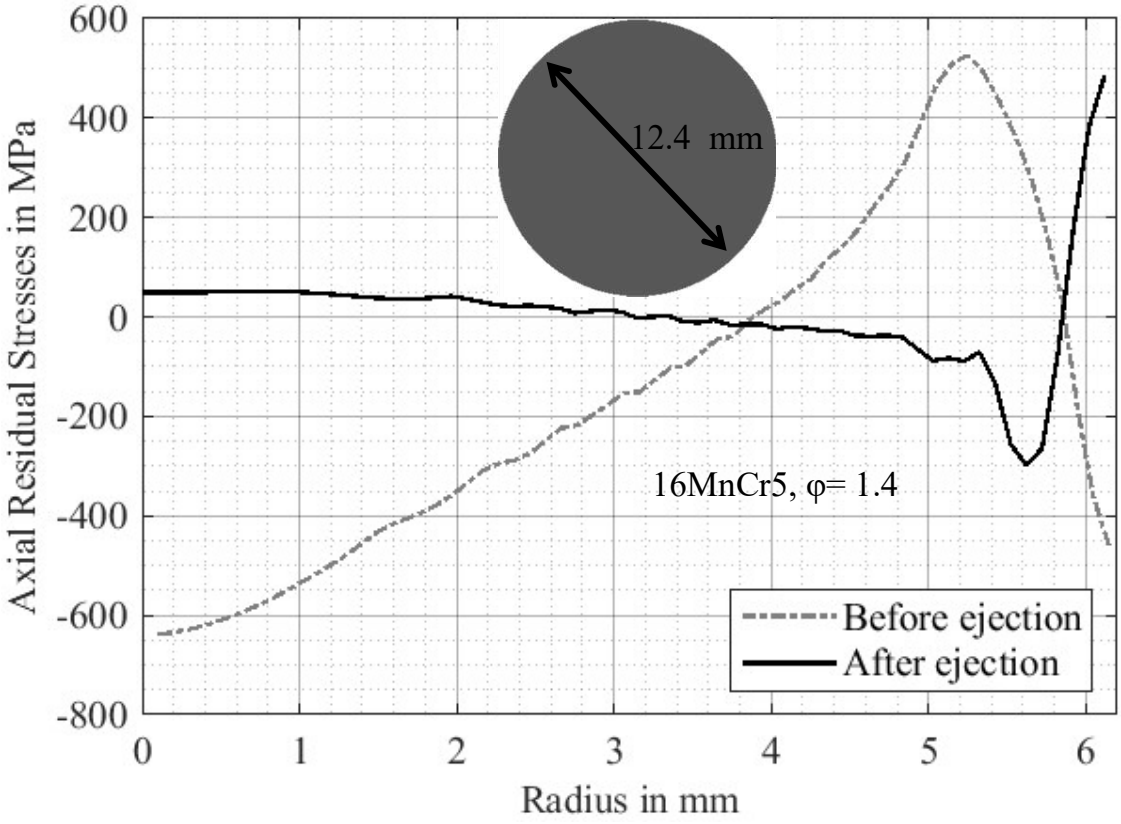

Figure 7.11: The alteration of axial residual stresses with ejection process at strain 1.4.

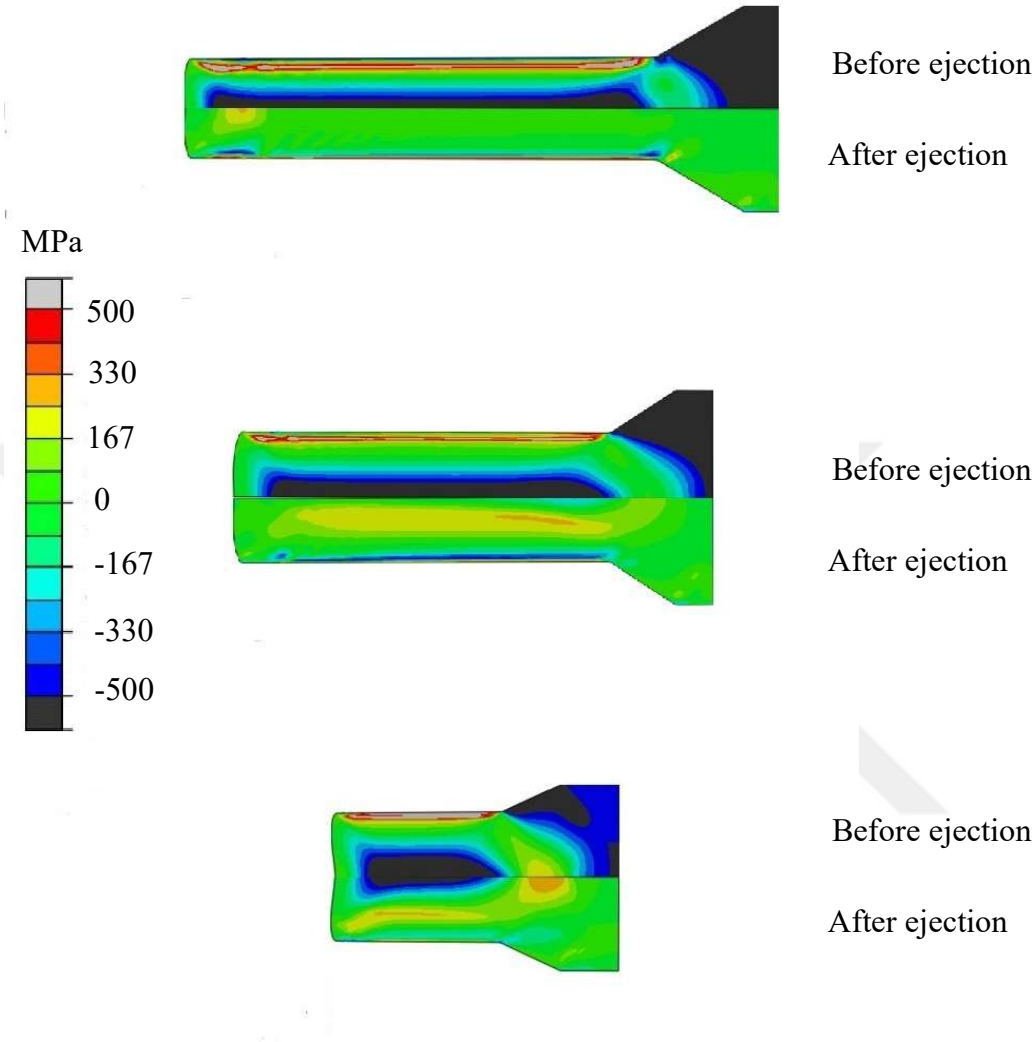

16MnCr5, φ= 1.4, 1.0 and 0.7 orderly

Figure 7.12: The illustration of the colourful map of axial residual stress.

7.3 Experimental Results versus FE Results

The comparison of experimental findings with to finite element analyses is represented in this subchapter. The **Figure 7.13**, **Figure 7.14** and **Figure 7.15** demonstrate the experimental and numerical results observed in this study.

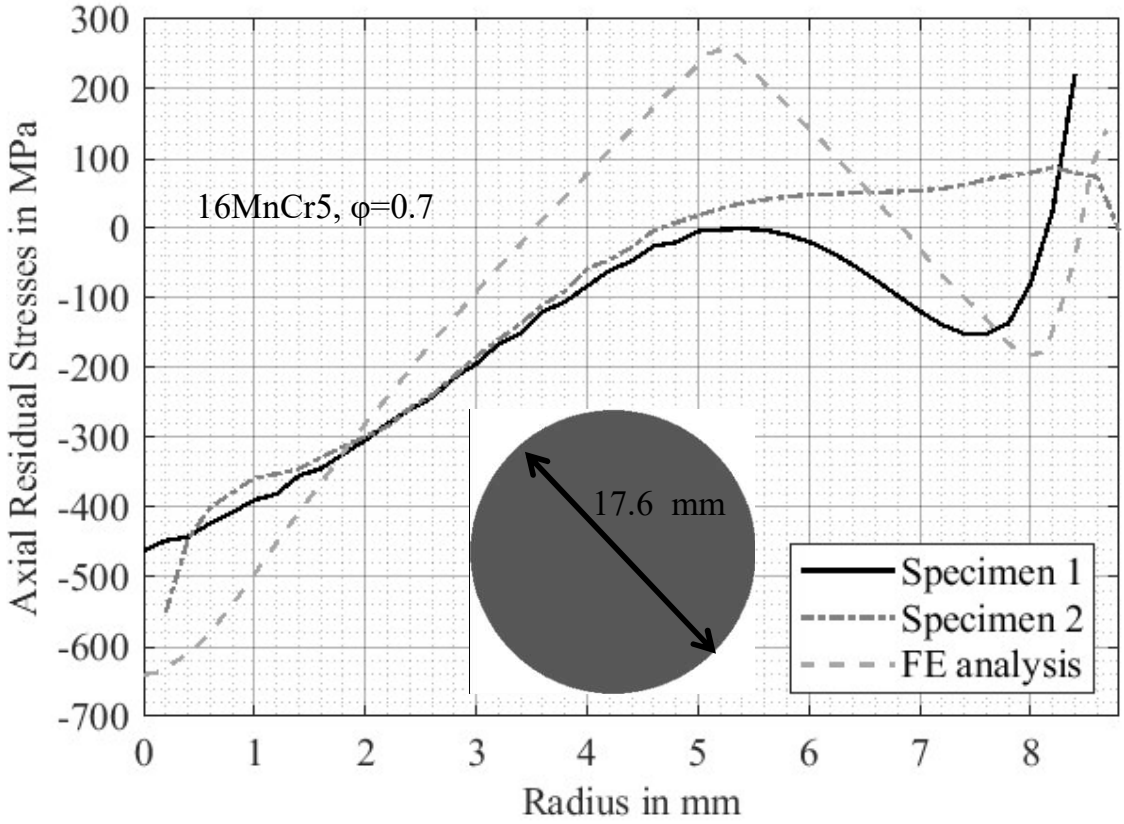

Figure 7.13: The comparison of the experimental and numerical results at strain 0.7.

Even though the residual stress profile obtained from the specimen 1 and the FEA stress profile resemble one another, the magnitudes of the stresses do not comply well as illustrated in the Figure 7.13. Except this, the magnitudes of RS in both compression and tension in the FE analysis are considerable greater. The peak tensile stress is approximately 250 MPa according to the numerical evaluation of RS at this strain. However, the existences of the kernel and subsurface compressive residual stresses are confirmed by both FE analysis and specimen 1 studies. Additionally, these two analyses also approve surface tensile residual stresses.

The Figure 7.14 exhibits the axial RS at true strain, 1.0. The consistence of numerical and contour method results are strikingly improved when compared to the findings of lower true strain. Even the magnitudes of RS comply with one another in some regions. The internal compressive residual stresses are also discovered numerically and experimentally at this true strain.

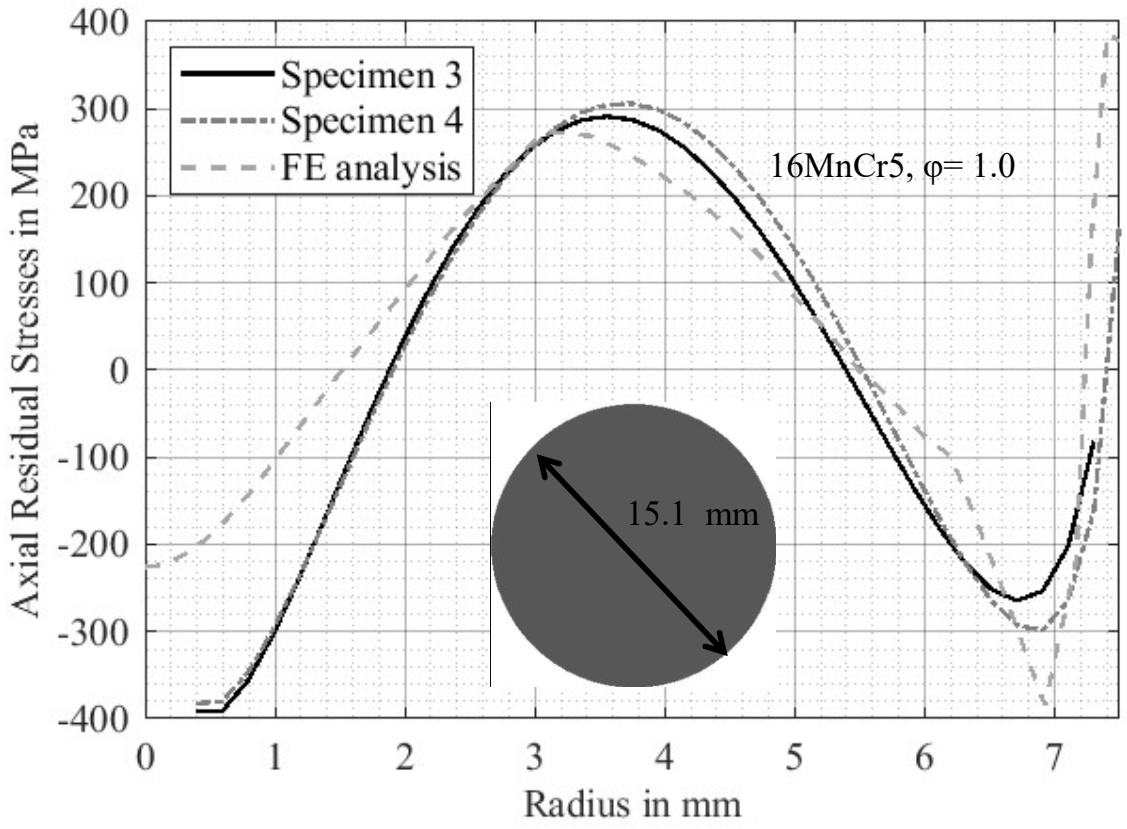

Figure 7.14: The comparison of the experimental and numerical results at strain 1.0.

FE analysis and experimental results approve that the tensile residual stresses exist in the middle zone between the core and surface. Moreover, tensile RS are also detected at the outer surface of specimens. Besides the core of cylindrical bar, residual stresses in compression are formed in subsurface regions.

The comparison of the contour method results with the finite element analyses is depicted in the Figure 7.15. Contrary to the lower strains and bar diameters, the tensile residual stresses form in the core regions although the amount of these tensile RS sometimes is insignificant. The difference between FE analysis and contour method result in the magnitude of tensile residual stresses is approximately 100 MPa in the

core. Residual stresses in compression are explored only in subsurface regions at this strain. However, the magnitudes of the stresses alter with respect to three analyses results. In accordance with the result of the numerical analysis, the amount of surface tensile residual stresses is significant. Additionally, the stress gradients in the subsurface and surface regions seem to be prominent, particularly according to the finite element analysis.

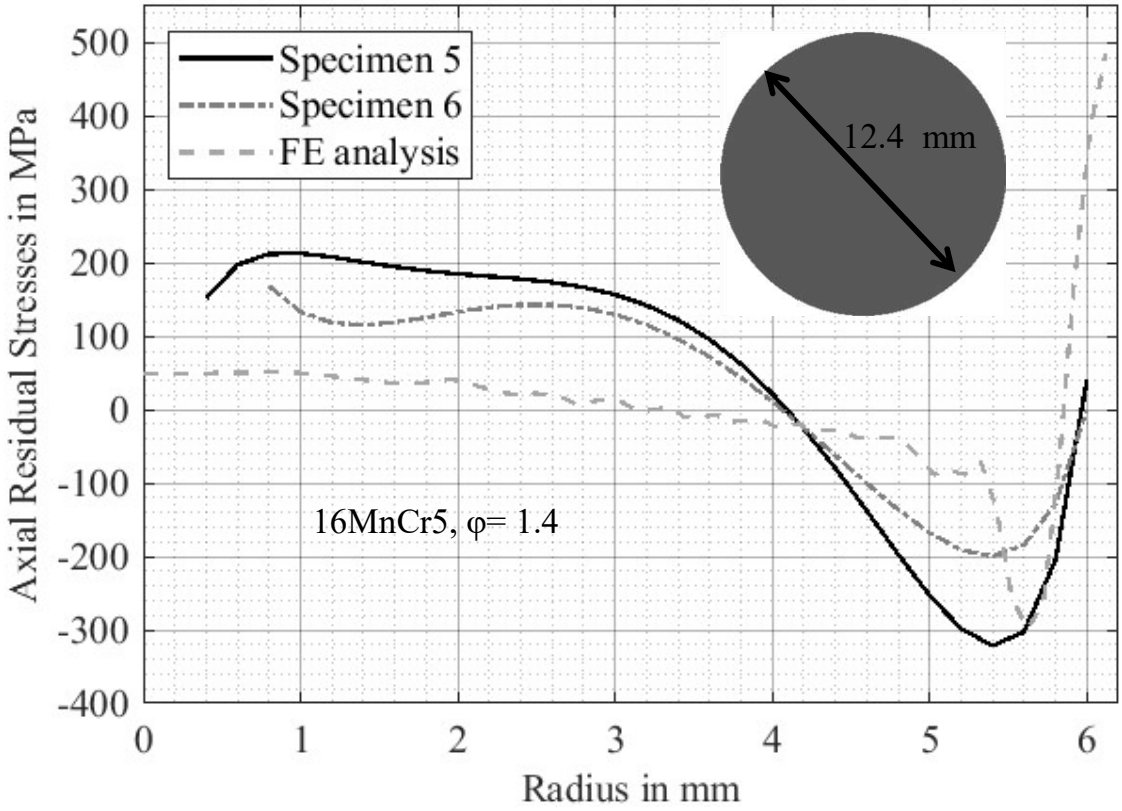

Figure 7.15: The comparison of the experimental and numerical results at strain 1.4.

7.4 Sensitivity Analysis of Cold Forward Extrusion

As already stated in the Chapter 4, the sensitivity analysis of cold forward extrusion is conducted using commercial software SimufactForming. The **Figure 7.16** exhibits the assessment of axial residual stress under the varied circumstances of friction. In cases of Coulomb friction and mixed Coulomb shear friction, axial residual stresses are roughly identical.

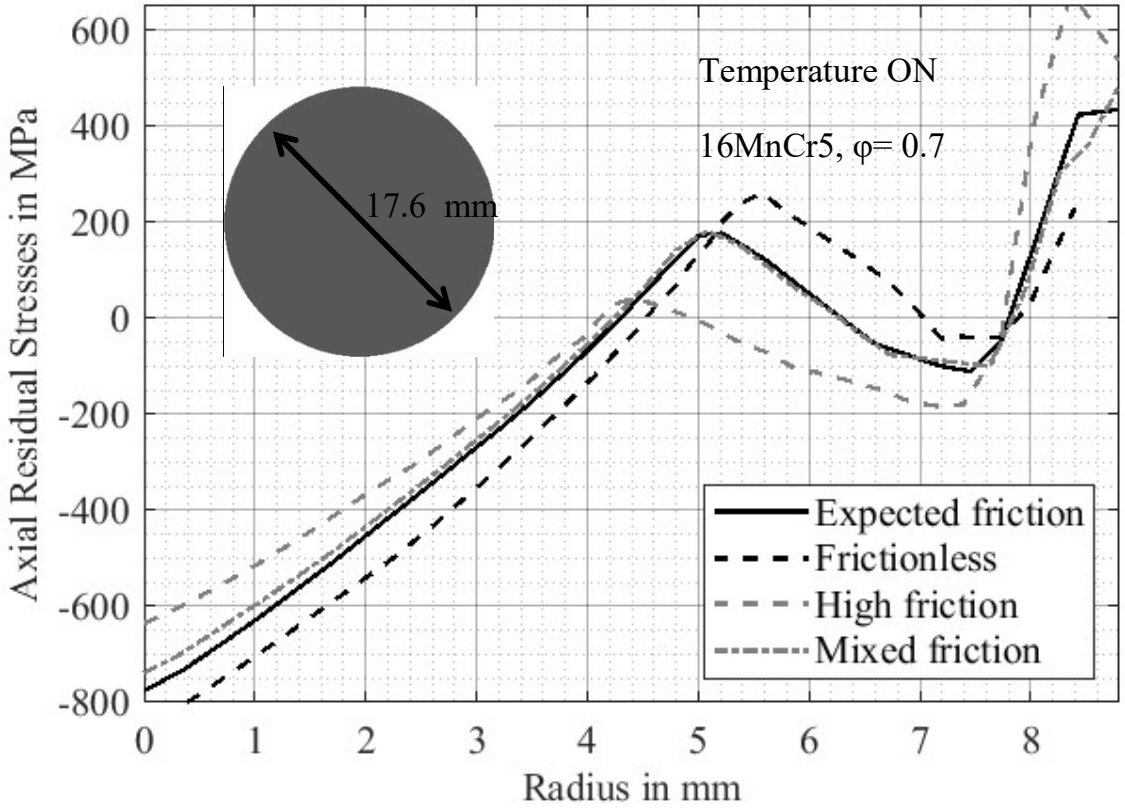

Figure 7.16: The analyses with various friction conditions.

In frictionless cold forward extrusion analysis, the excessive peak residual stresses in both compression and tension emerge. Even though under the condition of high friction axial RS is alleviated in the interior zones in accordance with the FE analyses, near surface tensile residual stresses which are primarily important and crack growth for fatigue life rise considerably.

The **Figure 7.17** represents the axial RS obtained with two different cone angles at true strain 1.0. The significant shifts appear between two die angles and the result of

60 degree die angle is more unrealistic. But the same residual stress profiles come into view.

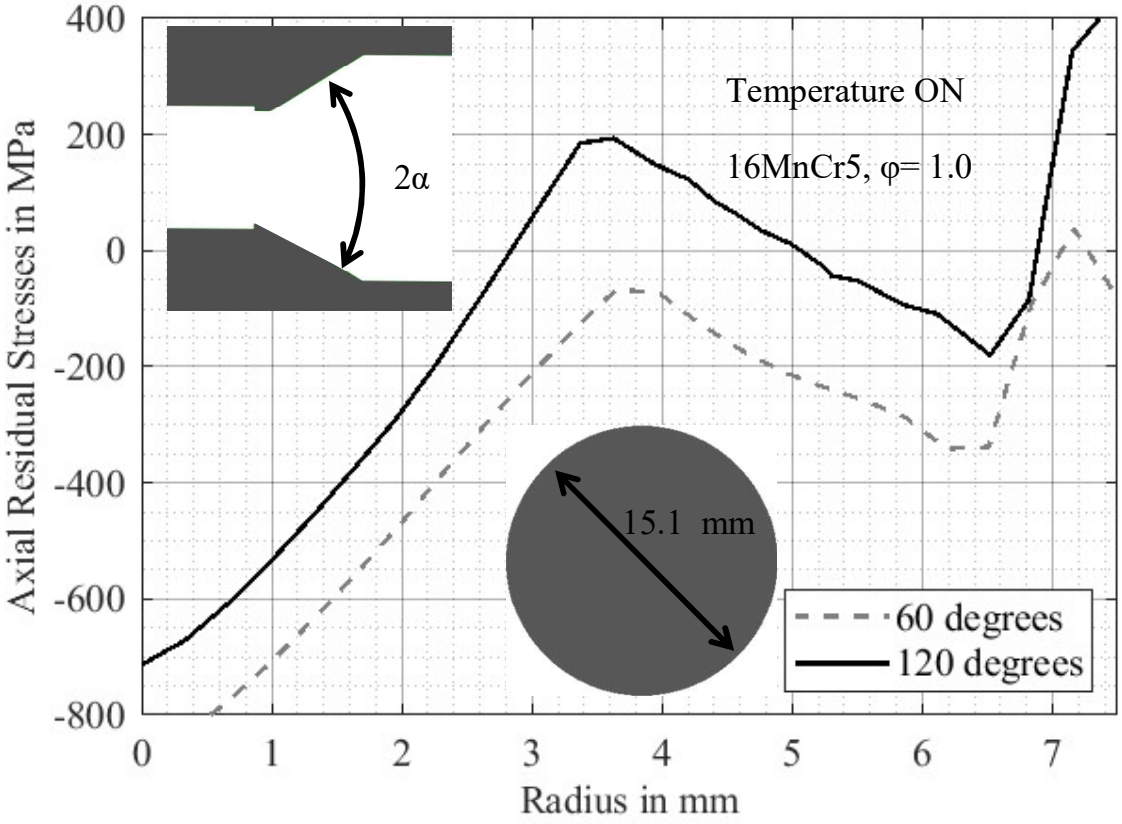

Figure 7.17: The variation in axial RS with two different die angles at strain 1.0.

As depicted in the **Figure 7.18**, cold forward extrusion analyses with the same die angles are also conducted at strain 0.7. The difference of axial residual stresses is insignificant at this strain. Exceptionally, surface tensile residual stresses are supreme when the die with 120 degrees cone angle is adopted. Internal compressive residual stresses subsist under both circumstances. Subsurface compressive residual stresses whose magnitudes attain to about 100 MPa.

The **Figure 7.19** illustrates the findings of cold forward extrusion at true strain 0.7 with the 120 degrees cone angle when temperature dependent data is enabled and disabled. In case of the utilization of temperature dependent data, the magnitudes of compressive RS and surface tensile RS grow. Axial tensile residual stresses reach over 400 MPa. The deviation in the compressive residual stresses aggregates in the core.

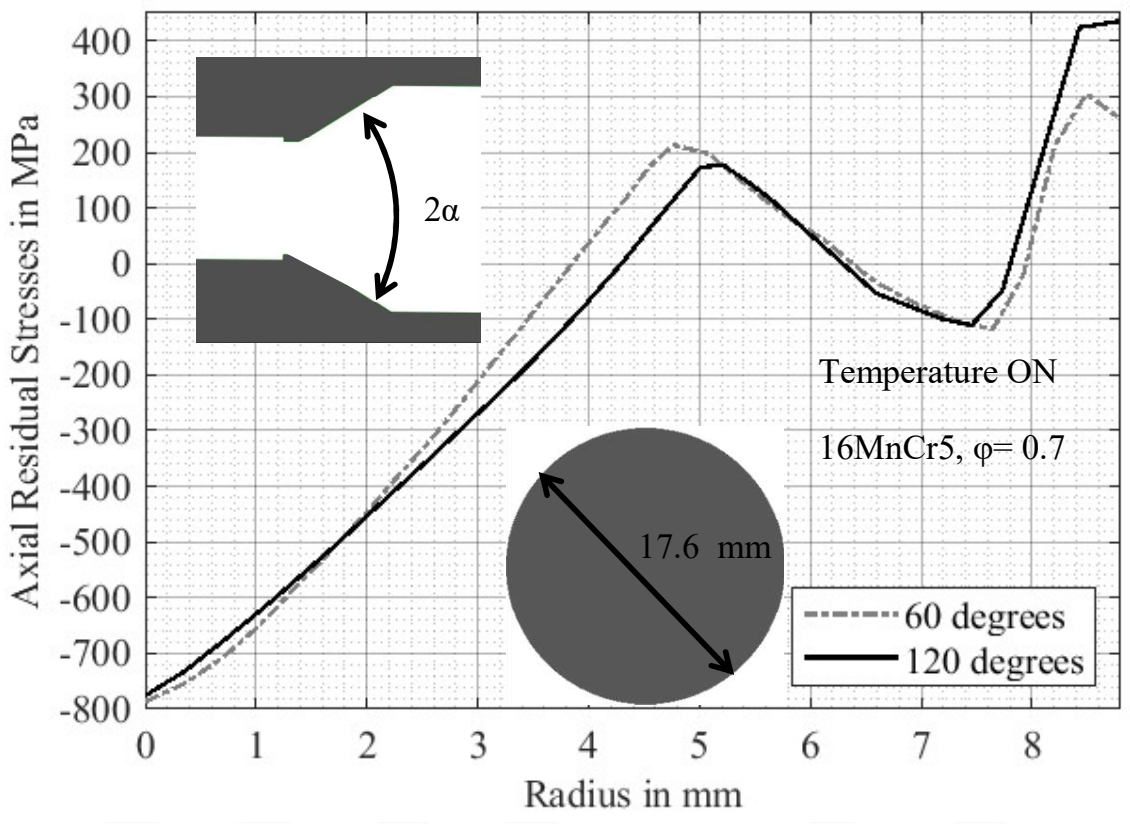

Figure 7.18: The variation in axial RS with two different die angles at strain 0.7.

The **Figure 7.20** exhibits the comparison of axial RS with the same two die angles when the temperature dependent data in commercial code is disabled. 120 cone angle aggrandizes surface tensile residual stresses as discerned in the preceding analyses.. The disparity in the magnitudes of compressive residual stresses amounts to maximum in the core.

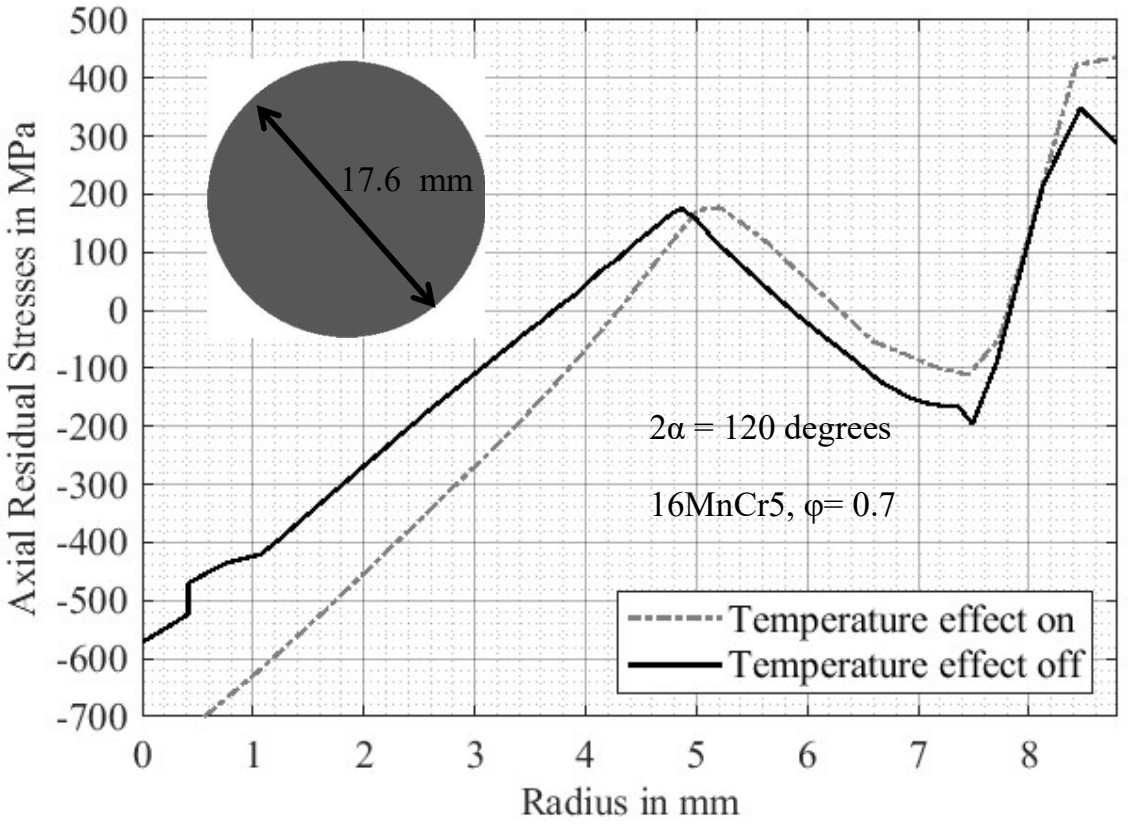

Figure 7.19: The variation in axial RS with the temperature dependent data.

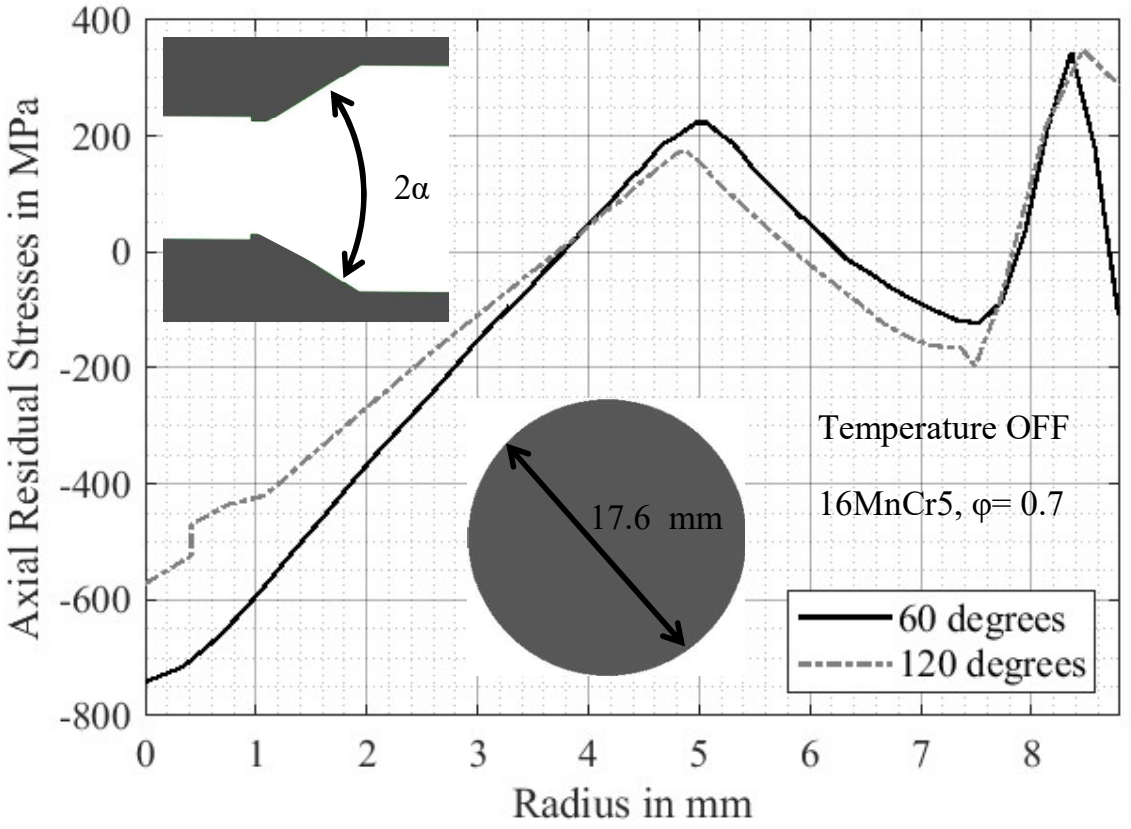

Figure 7.20: RS with two different die angles without temperature dependent data

8 Summary and Outlook

In this thesis, residual stresses of asymmetrical 16MnCr5 steel rods manufactured by cold extrusion with three different extrusion ratios are investigated via contour method. The results obtained from experimental work sometimes exhibits plausible agreement although the deviations in residual stresses become significantly high in some cases.

Similar to the works in literature, compressive residual stresses have been mostly observed in the interior Tekkaya (1985), Pyzalla and Reimers (1999) even though tensile stresses penetrate inner region at elevated strain. The change of axial residual stresses in 0.7 strain occurs more linearly while salient stress gradients have been seen in both 1.0 and 1.4 strains which might be very critical for fatigue life Waryoba and Mshana (1993), Milosevic et al. (2017). Besides this, micro residual stresses might accumulate more significantly at 1.4 true strain.

Application of contour method to asymmetric parts is previously conducted by authors Mahmoudi and Saedi (2015) and Sun et al. (2017). Unsurprisingly, the asymmetrical ends of long components do not include any extra problem or effort for determination of RS. Since FE model of contour method is solved linearly elastic and deformation occurs only in elastic range, relaxation of stresses have been observed up to the depths equal to radius as illustrated in the **Figure 8.1**. As a result, contour method could be applied when ratio between radius and length does not exceed one.

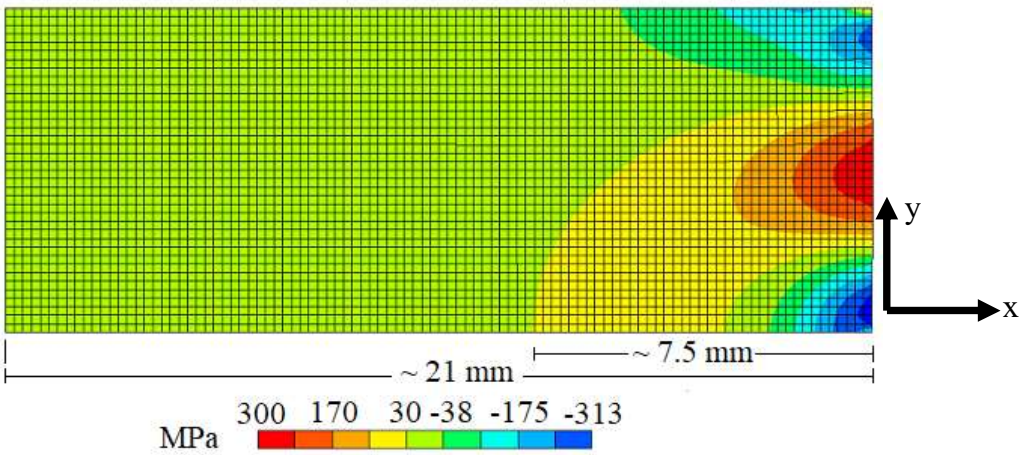

Figure 8.1: Linear elastic analysis.

Round surfaces might become more problematic and tedious while components with circular cross section tend to rotate more easily compared to a rectangular billet during cutting by wire-edm by the effect of even moderate forces. Water pressure or already relaxed stresses as discussed in Chapter 2 may cause a little amount of rotation which will be sometimes sufficient to distort the accuracy of measured data sets.

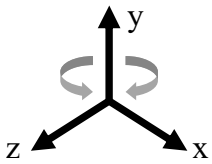

Figure 8.2: Tendency for rotation.

Therefore, it must be noted that the part must be clamped neither loosely nor superfluously tightly. In case of firmly clamping, a part during cutting operation might elongate elastically into cutting zone.

Defining reference (zero) plane on cut surfaces to measure deformation in axial direction may sometimes knotty especially when the rotation of workpieces takes place at the time of cutting. In addition to this fact, the occurrence of plasticity is inevitable during the experiments because circular cross section of cylindrical rods is narrowing down in a rapid manner while cutting is proceeding. Near edge data is eliminated since the effect of plasticity is observed in final cut edge. Near edge tensile residual stresses in cold extruded parts can be more effective to fatigue life.

Although several tryouts cutting are experienced in the framework of this work, cutting parameters can be further studied in future. In particular, flushing efficiency of water might be consequential to remove utterly molten metal for contour method. Pulse-on time, pulse-off time and water pressure might be primary factors while wire used could be thicker in case dielectric fluid may penetrate and sweep away molten material in easier way. A future finite element study may be taken into consideration for the goal of contour method while an experimental study of formation of resolidified layer may include hurdles as well as aforementioned cutting parameters.

In addition to near edge residual stresses, determination of residual stresses in the centre can introduce difficulties such as insufficient number of data points. The area of last intervals is the least where radius is less than 0.25-0.5 millimetres. Less number of data may affect detrimentally averaging procedure that would mitigate the effects of shear stresses, cutting and roughness.

To conclude, contour method could be applied to anti-symmetric large cold worked components even though the magnitudes of residual stresses sometimes become quite questionable. However other methods would induce their own error sources to measurement. Besides this fact, hole drilling, ring core and XRD methods are not suitable for bulk materials and the tools for high energy XRD and neutron diffraction are not always applicable to their potential users. These non-destructive methods of residual stress measurement have their own limitation such as penetration depth of beams. Suspicious results of contour method might be because of cutting conditions which can be improved in the future. It must be expressed that engineer and technician should have the knowledge of contour method. Particularly, clamping and cutting strategy must be experienced. As studied in literature, the evaluation of multi axial residual stresses might be applied to the rods as a prospective study Pagliaro et al. (2008).

Works Cited

Atienza, J.M., Ruiz-Hervias, J., Martinez-Perez, M.L., Mompean, M.J., Garcia-Hernandez, M., Elices, M., 2005. Residual stresses in cold drawn pearlitic rods. Scriptia Materialia 52 (2005), pp. 1223-1228.

Bay, N., 1994. The state of the art in cold forging lubrication. Journal of Materials Processing Technology 46 (1994), pp. 19-40.

Belahcene, F., Lu, J., 2002. Determination of residual stress using critically refracted waves and immersion mode. Journal of Strain Analysis 37 (1), pp. 13-20.

Beavers, J.A., Johnson, J.T., Sutherby, L.T. 2000. Material factors influencing the initiation of near-neutral pH SCC on underground pipelines. 2000 International Pipeline Conference 2 (2000), pp. 979-988.

Bueckner, H.F., 1958. The propagation of cracks and the energy of elastic deformation. Transactions of the American Society of Mechanical Engineers 80 (1958), pp. 1225-1230.

Bueckner, H. F. 1970. Novel principle for the computation of stress intensity factors. Zeitschrift für Angewandte Mathematik & Mechanik 50 (1970), pp.529-546.

Callister, W.D., Rethwisch, D.G., 2011. Materials science and engineering SI 8th version. ISBN 978-0-470-50586-1, John Wiley Sons 2011.

Chaudhari, G.A., Andhale, S.R.., Patil, N.G., 2012. Experimental evaluation of effect of die angle on hardness and surface finish of cold forward extrusion of aluminum. International Journal of Emerging Technology and Advanced Engineering 2 (7), pp. 334-338.

Cheng, W., Finnie, I., Vardar, Ö., 1991. Measurement of residual stress near the surface using the crack compliance method. Journal of Engineering Materials and Technology 113 (2), pp. 199-204.

Cheng, W., Finnie, I., 1993. Measurement of residual stress distribution near the toe of an attachment welded on a plate using the crack compliance method. Engineering Fracture Mechanics 46 (1), pp. 79-91.

Cohen, D.K., 2012. Texture measurements. PhD Dissertation, Michigan Metrology (2012).

Civin, A., Vlk, M., 2009. Theoretical analysis of ring-core method for residual stress measurement. TechSoft Engineering SVS FEM Conference ANSYS 2009.

DeWald, A.T., Hill, M.R., 2001. Residual stress in a thick steel weld determined using the contour method.

Ekmekci, B., 2004. Theoretical and experimental investigation of residual stresses in electric discharge machining. Dr. Dissertation, January 2004, The Middle East Technical University.

Ekmekci, B., Ekmekci, N., Tekkaya, A.E., Erden, A., 2004. Residual stress measurement with layer removal method. Proceedings of the First Cappadocia International Mechanical Engineering Symposium July 2004, Cappadocia, Turkey.

Ghosh, S., Rana, V.P.S., Kain., V., Mittal, V., Baveja, S.K., 2011. Role of residual stresses induced by industrial fabrication on stress corrosion cracking susceptibility of austenitic stainless steel. Materials and Design 32 (2011), pp. 3823-2831.

Goyal, A., 2017. Investigation of material removal rate and surface roughness during wire electrical discharge machining (WEDM) of Inconel 625 super alloy by cryogenic treated tool electrode. Journal of King Saud University – Science 29 (2017), pp. 528-535.

Hafis, S.M., Ridzuan, M.J.M, Farahana, R.N., Ayob, A., Syahrullail, S., 2013. Paraffinic mineral oil lubrication for cold forward extrusion: Effect of lubricant quantity and friction. Tribology International 60 (2013), pp. 111-115.

Harichard, Chaturvedi, S, Sharma, S. 2012. Optimization of heat treatment process. International Journal of Engineering Science and Technology 4 (3), pp. 998-1004.

Hascalik, A., Caydas, U., 2004. Experimental study of wire electrical discharge machining. Journal of Material Processing Technology 148 (2004), pp. 362-367.

Hauk, V., 1997. Structural and residual stress analysis by non-destructive methods evaluation-application-assessment. Elsevier Science B.V 1997, pp. 1-10.

Heinrichs, J., Jacobson, S., 2014. The influence from shape and size of tool surface defects on the occurrence of galling in cold forming of aluminum. Wear 271 (2011), pp. 2517-2524.

Hill, M.R., Olson, M.D., 2014. Repeatibility of contour method for residual stress measurement. Experimental Mechnics 2014 (54), pp. 1269-1277.

Joun, M.S., Kim, M.C., Yoon, D.J., Choi, H.J, Son, Y.H., 2011. Finite element analysis of central bursting defects occurring in cold forward extrusion. 48 (2008),Proceedings of the ASME 2011 Internatinaol Manufacturing Science and Engineering Conference MSEC 2011, Corvallis, Oregon, USA, pp. 1-6.

Kandil, F.A., Lord, J.D., Fry, A.T., Grant, P.V., 2002. Review of residual stress measurement methods, measurement of residual stress in components. CPM4.5 Characterization and Performance of Materials.

Karabutov, A., Devichensky, A., Ivochkin, A., Lyamshev, M., Pelivanov, I., Rohadgi, U., Solomatin, V., Subudhi, M., 2008. Laser ultrasonic diagnostics of residual stress. Ultrasonics 48 (2008), pp. 631-635.

Koc, M., Culp, J., Altan, T., 2006. Prediction of residual stresses in quenched aluminum blocks and their reduction through cold working processes. Journal of Material Processing Technology 174 (2006), pp. 342-354.

Lange, K., (1985). Handbook of metal forming. ISBN 0872634574, Society of Manufacturing Engineers, McGaw-Hill.

Lee, Y.C., Chen, F.K., 2000. Failure analysis of a cold-extrusion punch to enhance its quality and prolong its life. Journal of Materials Processing Technology 105 (2000), pp. 134-142.

Lin, J., Ma, N., Lei, Y., Murakawa, H., 2016. Measurement of residual stress in arc welded lap joints by cosα X-ray diffraction method. Journal of Materials Processing Technology 243 (2017), pp. 387-394.

Luo, Q., Yang, S., 2017. Uncertainty of the X-ray diffraction (XRD) $\sin^2\psi$ technique in measuring residual stresses of physical vapor deposition (PVD) hard coatings. Coatings 7 (128), pp. 1-16.

Maher, I., Sarhan, A.D.D., Marashi, H., Barzani, M.M., Hamdi, M., 2016. White layer thickness prediction in wire-EDM using using CuZn coated wire electrode – ANFIS modelling. The International Journal of Surface Engineering and coatings, Transactions of IMF 94 (4), pp. 204-210.

Mahmoudi, A.H., Hossain, S., Truman, C.E., Smith, D.J., Pavier, M.J., 2008. A new procedure to measure near yield residual stresses using the deep hole drilling technique. Society of Experimental Mechanics 2009 (49), pp. 595-604.

Mahmoudi, A.H., Saedi, A., 2015. Influence of asymmetrical cuts in measuring residual stresses using contour method. International Journal of Pressure Vessels and Piping 134, pp. 1-10.

Milosevic, I., Winter, G., Grün, F., Kober, M., 2017. Influence of the stress gradient on the fatigue life calculation of a martensitic high strength steel. Frattura ed Integrita Strutturale 42 (2017), pp. 1-8.

Noyan, I.C., Cohen, J.B., 1987. Residual stress measurement by diffraction and interpretation. ISBN 978-0-470-50586-1, Springer-Verlag Berlin Heidelberg New York 1987.

Onuh, S.O., Ekoja, M., Adeyemi, M.B., 2003. Effects of die geometry and extrusion speed on the cold extrusion of aluminium and lead alloys. Journal of Materials Processing Technology 132 (2013), pp. 274-285.

Ossenkemper, S., 2018. Verbundfließpressen in konventionellen Fließpresswerkzeugen.. Dr. –Ing. Dissertation, TU Dortmund.

Pagliaro, P., Prime, M.B., Swenson, H., Zuccarello, B., 2010. Measuring multiple residual stress components using contour method and multiple cuts. Experimental Mechnics 50 (2), pp. 187-194.

Petrosky, H.J., Achenbach, J.D., 1978. Computation of weight function from a stress intensity factor. Engineering Fracture Mechanics 10(2), pp. 257-266.

Plancak, M., 1990. Stress distribution within the specimen in cold forward extrusion of steel . Journal of Materials Processing Technology 24 (1990), pp. 387-394.

Pollard, J.D., Brahimi, S., Watford, A., Jackson, M., Wynne, B.P., 2016. The determination of residual stress in extruded Ti-6Al-4V by contour method and finite element analysis. Proceedings of the 13th World Conference on Titanium, pp. 305-310.

Prime, M.B., Hughes, D.J., Webster P.J., 2001. Weld application of a new method for cross-sectional residual stress mapping. Society for Engineering Mechanics Annual Conference and Exposition, Portland, Oregon.

Prime, M.B., 2001. Cross-sectional mapping of residual stresses by measuring the surface contour after a cut. Journal of Engineering Materials and Technology 123, pp. 162-168.

Prime, M.B., Hill, M.R., 2002. Residual stress, stress relief and inhomogeneity in aluminium plate. Scriptia Materialia 46 (1), pp. 77-82.

Prime, M.B., Newborn, M.A., Balog, J.A., 2003. Quenching and cold-work residual stresses in aluminum hand forgings: Contour measurement and fem prediction. Material Science Forum Vols. 426-432 (2003), pp. 435-440.

Prime, M.B., 2009. The contour method: A new approach in experimental mechanics. Proceedings of the SEM Annual Conference 2009, New Mexico, USA, pp. 156.

Prime, M. B., DeWald, A. T., 2013. The contour method Chapter 5 in Practical Residual Stress Measurement Methods, G. S. Schajer, (ed), Wiley-Blackwell, pp. 109-138.

Prime, M.B., Hill, M.R., DeWald, A.T., Sebring, R.J., Dave, V.R., Cola, M.J., 2003. Residual stress mapping in welds using the contour method. ASM International, 2003, pp. 891-896.

Prime, M.B., 1999. Residual stress measurement by successive extension of a slot: The crack compliance method. Applied Mechanics Reviews 52(2), pp. 75-96.

Prime, M.B., Sebring, R.J., Edwards, J.M., Baumann, J.A., Lederich, R.J., 2004. Contour-method determination of parent-part residual stresses using a partially relaxed fsw test specimen. Proceedings of the 2004 SEM X International Congress and Exposition on Experimental and Applied Mechanics, pp. 144.

Prime, M.B., Sebring, R.J., Edwards, J.M., Hughes, D.J., Webster, P.J., 2004. Laser surface-contouring and spline data-smoothing for residual stress measurement. Society for Experimental Mechanics 44 (2), pp. 176-184.

Prime, M.B., Kastengren, A.L., 2011. The contour method cutting assumption: Error minimization and correction. Experimental and Applied Mechanics 6 (2011), pp. 233-250.

Pyzalla, A., Reimers, W., 1999. Residual stress and texture due to cold and hot extrusion processes. Textures and Microstructures 33, pp. 291-301.

Pyzalla, A., Reimers, W., Royer, A., Liss, K.D., 1999. Microstructure, texture and residual stresses after cold extrusion – application of white high-energy synchrotron radiation. Proceedings of 20th Risoe International Symposium on Materials Science, Risoe National Laboratory, Denmark, pp. 453-458.

Rhouma, B.A., Braham C., Fitzpatrick, M.E., Ledion, J., Sidhom, H., 2001. Effects of surface preparation on pitting resistance, residual stress and stress corrosion cracking in austenitic stainless steels. Journal of Materials Engineering and Performance 10 (5), pp. 507-514.

Rossini, N.S., Dassisti M., Benyounis, K.Y., Olabi, A.G., 2012. Methods of measuring residual stresses in components. Materials and Design 35 (2012), pp. 572-588.

Rudkins, N.T., Modlen, G.F., Webster, P.J., 1994. Residual stresses in cold extrusion and cold drawing: a finite element and neutron diffraction study. Journal of Materials Processing Technology 45 (1994), pp. 287-292.

Schajer, G.S., 2001. Residual stresses: Measurement by destructive testing. Encyclopedia of Materials: Science and Technology ISBN 0-08-0431526, pp. 8152-8158.

Schindler, H.,J., Cheng W., Finnie, I., 1994. Measurement of residual stress distribution in a disk or a solid cylinder using crack compliance method. In Proc. Fourth International Conference Residual Stress, Baltimore, Maryland Society of Experimental Mechanics 19(10), pp. 1266-1274.

Schindler, H.,J., 1995. Determination of residual stress distribution from measured stress intensity factors. International Journal of Fracture 74(2), pp. 23-30.

Schindler, H.,J., Cheng W., Finnie, I., 1997. Experimental determination of stress intensity factors due to residual stresses. Experimental Mechanics 37(3), pp. 272-277.

Shabgard, M., Oliaei, S.N.B., Seyedzavvar, M., Najadebrahimi, A., 2011. Experimental investigation and 3D finite element prediction of the white layer thickness, heat affected zone, and surface roughness in edm process. Journal of Mechanical Science and Technology 25(12), pp. 3173-3183

Shin, S.H., 2005. FEM analysis of plasticity-induced error on measurement of welding residual stress by contour method. Journal of Mechanical Science and Technology 19(10), pp. 1885-1890.

Simsir, C., Duran, D., 2018. A flow stress model for steel in cold forging process range and the associated method for parameter identification. International Journal Advance Manufacturing Technology 2018 (94), pp. 3795 - 3808.

Smith, D.J., Bouchard, P.J., George, D., 2000. Measurement and prediction of residual stresses in thick-section welds. The Journal of Strain Analysis for Engineering Design 35 (4), pp. 287-305.

Soyarslan, C., Tekkaya, A.E., Akyüz, U., 2008. Application of continuum damage mechanics in discontinues crack formation: Forward extrusion chevron predictions. ZAMM Journal of Applied Mathematics and Mechanics 88 (6), pp. 436-453.

Speidel, M.O., 1975. Stress corrosion cracking of aluminium alloy. Metallurgical Transaction A 6A (1975), pp. 631-651.

Sun, Y.L., Roy, M.J., Vasileiou, A.N., Smith, M.C., Francis, J.A., Hosseinzadeh, F., 2017. Evaluation of errors associated with cutting-induced plasticity in residual stress measurements using the contour method. Experimental Mechanics 57 (5), pp. 719-734.

Syahrullail, S., Zubil, B.M., Azwadi, C.S.N., Ridzuan, M.J.M., 2011. Experimental evaluation of palm oil as lubricant in cold forward extrusion process. International Journal of Mechanical Sciences 53 (2011), pp. 549-555.

Tomura, S., Kunieda, M., 2009. Analysis of electromagnetic force in wire-EDM. Precision Engineering 33, pp. 255-262.

Tosun, N., Cogun, C., Pihtili, H., 2003. The effect of cutting parameters on wire crater sizes in wire EDM. Machining Science and Technology 7 (2), pp. 209-219.

Tekkaya, A.E., Gerhardt, J., 1985. Residual stresses in cold-formed workpieces. Annals of the CIRP 34, pp. 225-230.

Tekkaya, A.E., 2000. An improved relationship between Vickers hardness and yield stress for cold formed materials. Residual stresses in cold-formed workpieces. Annals of the CIRP 2000 (49), pp. 205-208.

Traore, Y., Hosseinzadeh, F., Bouchard, P.J., 2014. Plasticity in the contour method of residual stress measurement. Advanced Materials Research 996, pp. 337-342.

Wagener, H.W., Wolf, J., 1994. Coefficient of friction in cold extrusion. Journal of Materials Processing Technology 44 (1994), pp. 283-291.

Waryoba, D.C.R., Mshana, J.S., 1993. Effect of size and stress gradient on fatigue behaviour. International Journal of Pressure Vessels and Piping 60 (1994), pp. 177-182.

Webster, G.A., Ezeilo, A.N., 2001. Residual stress distributions and their influence on fatigue lifetimes. International Journal of Fatigue 23 (2001), pp. 375-383.

Whitehouse, D.J., 2011. Handbook of surface and nanometrology. Taylor Francis, 2nd Edition (2011), pp. 63.

Zhang, Y., Ganguly, S., Edwards, L., Fitzpatrick, M.L., 2004. Cross-sectional mapping of residual stresses in a VPPA weld using contour method. Acta Materialia 52 (2004), pp. 5225-5232.

Zucko, M., Pöhlandt, K., Pyzalla, A., Reimers, W., Kockelmann, H., 1997. Determination of deformation-induced residual stresses in full forward extrusion and comparison to experimental results. Materialwissenschaft und Werkstofftechnik 28 (9), pp. 417-423.

Abaqus 6.12 Abaqus/CAE user`s manual 2012.

Alicona Infinite Focus XL200G5 version a technical spefications EN, June 25, 2014.

ASTM International Designation: E837 – 13a 2014. Standard test method for determining residual stresses by the hole-drilling strain-gage method. ASTM Standards 2014.

BS EN 15305:2008 (2008), Non-destructive testing – Test method for residual stress analysis by x-ray diffraction August (2008). EN 15305:2008.

DIN EN 10084 Standards (2008), Case hardening steels – technical delivery conditions (2008). DIN EN 10084:2008-06.

https://h-and-m-analytical.com/wp/residual-stress-app-note, 2019, 14th of December.

https://www.veqter.co.uk/residual-stress-measurement/deep-hole-drilling, 2019, 14th of December.

MSC Marc 2018.0 Volume A: Theory and user information (2018). U.S. Patent 9361413

MSC Marc 2018.0 Volume B: Element Library (2018). U.S. Patent 9361413

Appendix A

Data analysis Files

Step0

```
function [n]=step0(E)
E=textread('Raw_data.txt')
m=size(E);
n=m(1,1);
  newdata = fopen('data0.txt','wt');
for i=1:1:n
   p=E(i, 1);
   r=E(i, 2);
   s=E(i, 3);
   p=p-ymean;
   r=r-zmean;
   fprintf(newdata,'%f %f %f\n', p, r, s);
end
   fclose(newdata);
end
```

Step1

```
function [g, h]=step1(A)
  A=textread('new_data0.txt');
  m=size(A);
  n=m(1,1);
  newdata = fopen('new_data1.txt','wt');
  for i=1:1:n
     d=A(i,1)^2+A(i,2)^2;
     g=A(i,1);
     h=A(i,2);
     j=A(i,3);
     e=6200^2;
    if (d < e)
        if (j<40.0)
            if (j>-40.0)
        fprintf(newdata,'\r');
        fprintf(newdata,'%f %f %f\n', g, h, j);
            end
        end
    end
  end
       fclose(newdata);
end
```

Step2

```
function [g]=step2(B)
  r=6200.0;
  B=textread('new_data1.txt');
  m=size(B);
  n=m(1,1);
  x =0;
  y =0;
  newdata = fopen('new_data2.txt','wt');
  newdata3 = fopen('new_data3.txt','wt');
while (r>0)
   z=0;
   a=0;
   c=r;
   r=r-50;
   fprintf(newdata,'\r');
    fprintf(newdata,' yaricapi %f ve %f arasinda olan veriler \n', c, r);
  for i=1:1:n
    g=((B(i,1)-x)^2+(B(i,2)-y)^2);
     if (g>(r^2))
         if (g<(c^2))
    z=z+B(i,3);
    a=a+1;
    fprintf(newdata,'\r');
```

```
    fprintf(newdata,'%f %f \n', z, a);
        end
     end
  end
    fprintf(newdata3,'\r');
    b=(z/a);
    fprintf(newdata3,'%f %f %f \n', z, a, b);
end
  fclose(newdata);
  fclose(newdata3);
end
```

Step3

```
function [r]=step3(C)
C=textread('new_data3.txt');
m=size(C);
n=m(1,1);
D=zeros(n,2);
r=6175;
newdata4 = fopen('new_data4.txt','wt');
for i=1:1:n
  D(i,2)=C(i,3);
  D(i,1)=r;
  r=r-50;
   fprintf(newdata4,'\r');
   fprintf(newdata4,'%f %f \n', D(i,1), D(i,2));
end
 fclose(newdata4);
end
```

Step4

```
function [m, k]=step5(H)
 F=textread('new_data4_1A_15_new.txt');
 G=textread('new_data4_1B_15_new.txt');
 m=size(F);
 n=m(1,1);
 k=size(G);
 if n==k(1,1)
    newdata = fopen('new_data5.txt','wt');
 for i=1:1:n
    H(i,2)=(F(i,2)+G(i,2))/2;
    fprintf(newdata,'\r');
    fprintf(newdata,'%f %f \n',F(i,1), H(i,2));
 end
      fclose(newdata);
 end
end
```

Step5

```
function [m, k]=step5(H)
 F=textread('15_A_data4.txt');
 G=textread('15_B_data4.txt');
 m=size(F);
 n=m(1,1);
 k=size(G);
 if n==k(1,1)
    newdata = fopen('data5.txt','wt');
 for i=1:1:n
    H(i,2)=(F(i,2)+G(i,2))/2;
    fprintf(newdata,'\r');
    fprintf(newdata,'%f %f \n',F(i,1), H(i,2));
 end
     fclose(newdata);
 end
end
```

Average

```
function [z, n]=average(A)
A=textread('new_data1.txt')
z=0;
m=size(A);
n=m(1, 1);
  newdata = fopen('average.txt','wt');
  newdata1 = fopen('new_new_data1.txt','wt');
for i=1:1:n
   b=A(i,3);
   z=z+b;
end
   c=z/n;
  for j=1:1:n
   A(j,3)=A(j,3)-c;
   fprintf(newdata1,'%f %f %f\n', A(j,1), A(j,2), A(j,3));
  end
   fprintf(newdata,'%f %f\n', z, n);
   fclose(newdata1);
   fclose(newdata);
end
```

Clamping Apparatus I-II

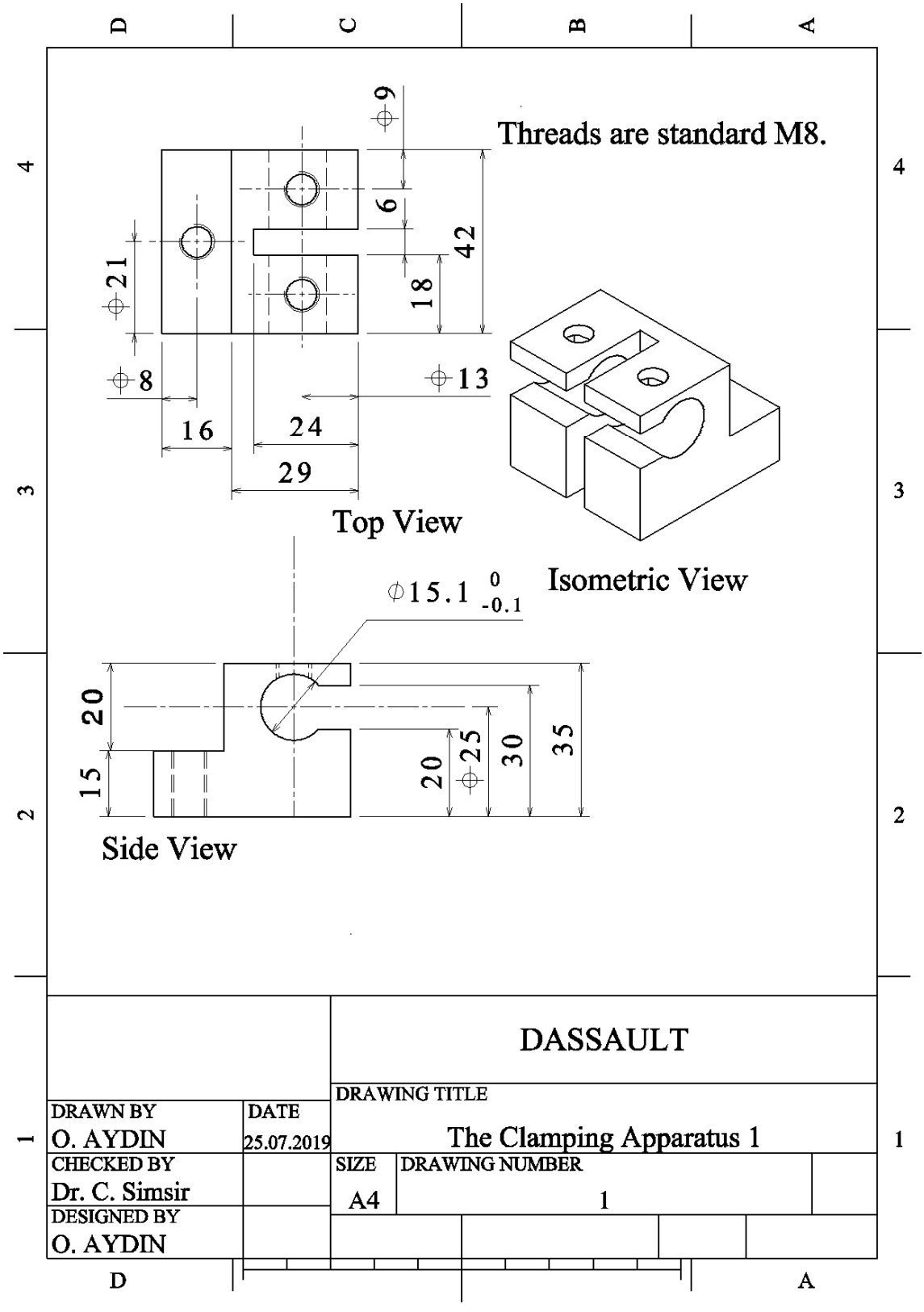

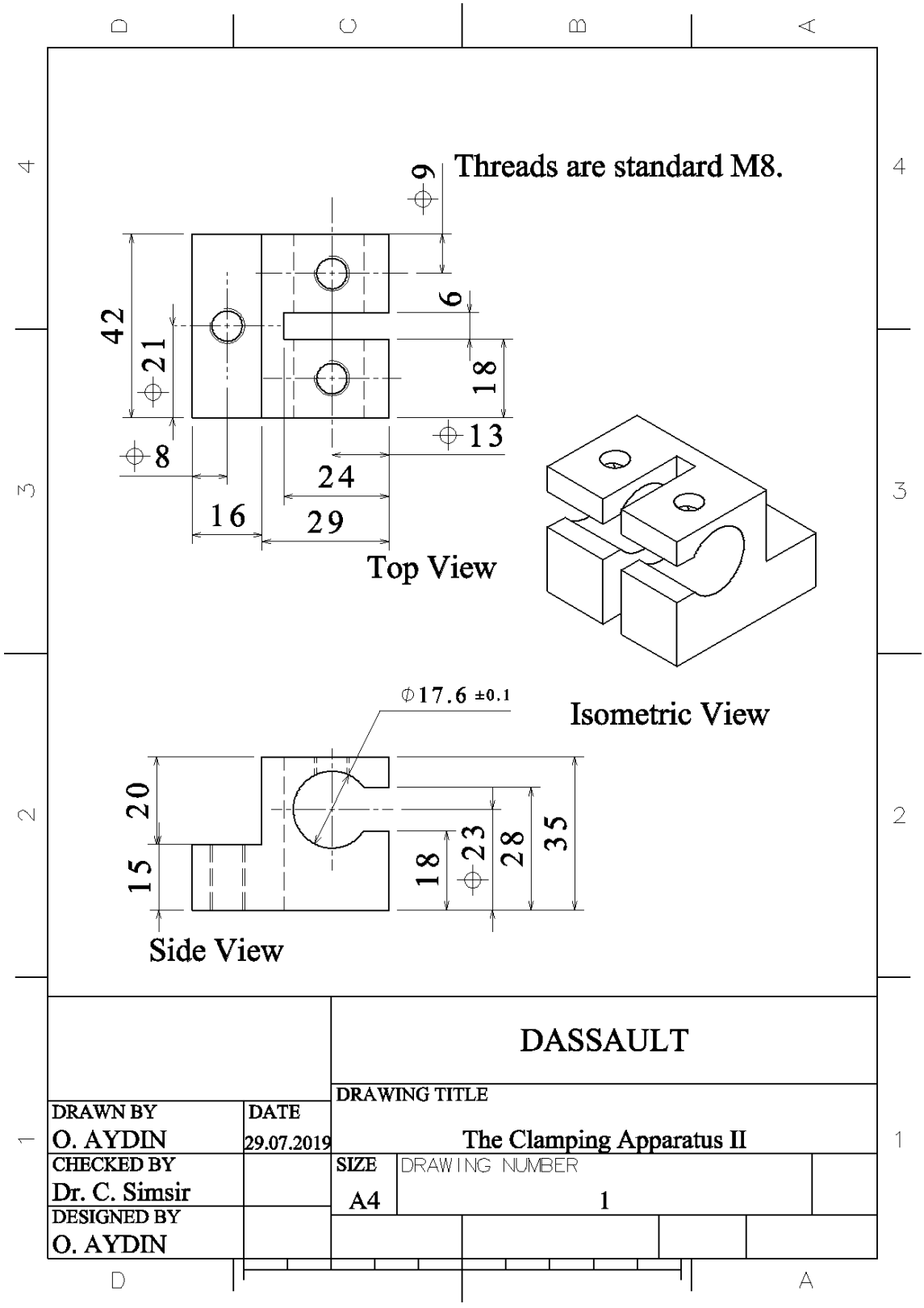
Threads are standard M8.
9
6
42
21
18
13
8
24
16
29
Top View
Isometric View
Φ17.6 ±0.1
20
15
18
23
28
35
Side View
DASSAULT
DRAWING TITLE
The Clamping Apparatus II
DRAWN BY
O. AYDIN
DATE
29.07.2019
CHECKED BY
Dr. C. Simsir
DESIGNED BY
O. AYDIN
SIZE
A4
DRAWING NUMBER
1

Cold Extrusion Dies, φ=0.7, 1.0, 1.4

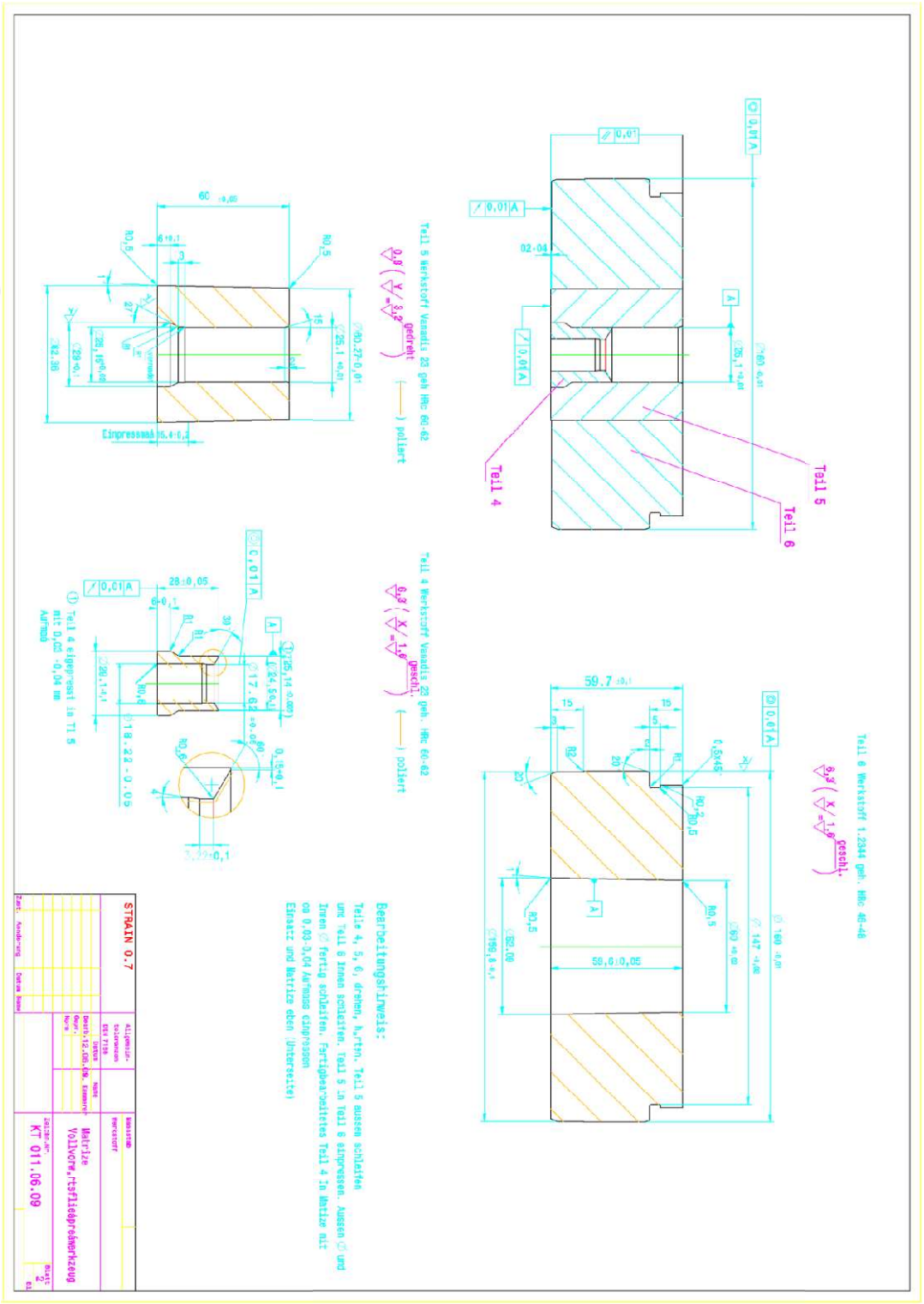

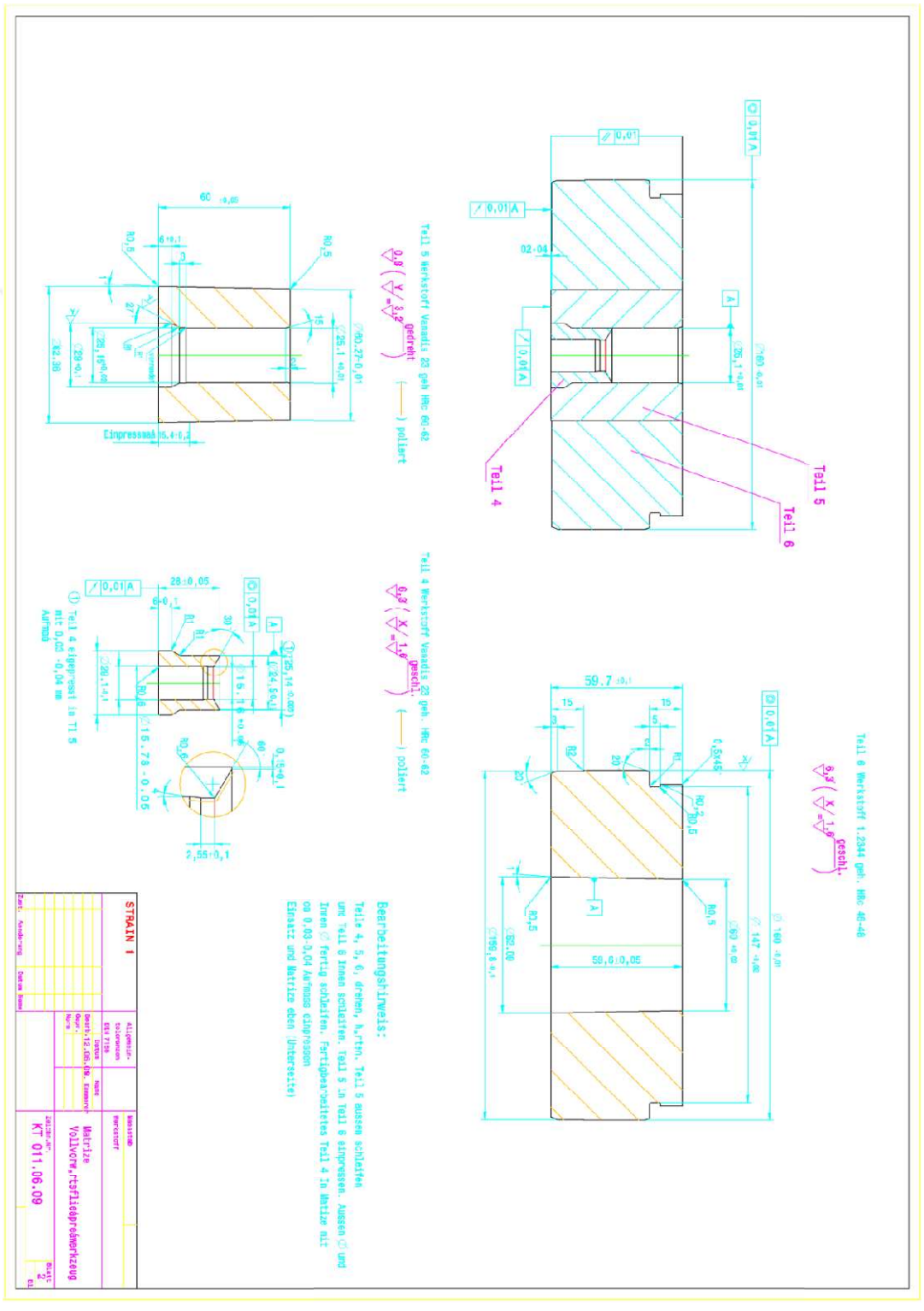
Teil 6 Werkstoff 1.2344 geh. HRc 48-48
Teil 5 Werkstoff Vanadis 23 geh HRc 60-62
Teil 4 Werkstoff Vanadis 23 geh. HRc 60-62
Teil 4
Teil 5
Teil 6
Bearbeitungshinweis:
STRAIN !
Matrize
Vollvers.rtsfließpreßwerkzeug
KT 011.06.09

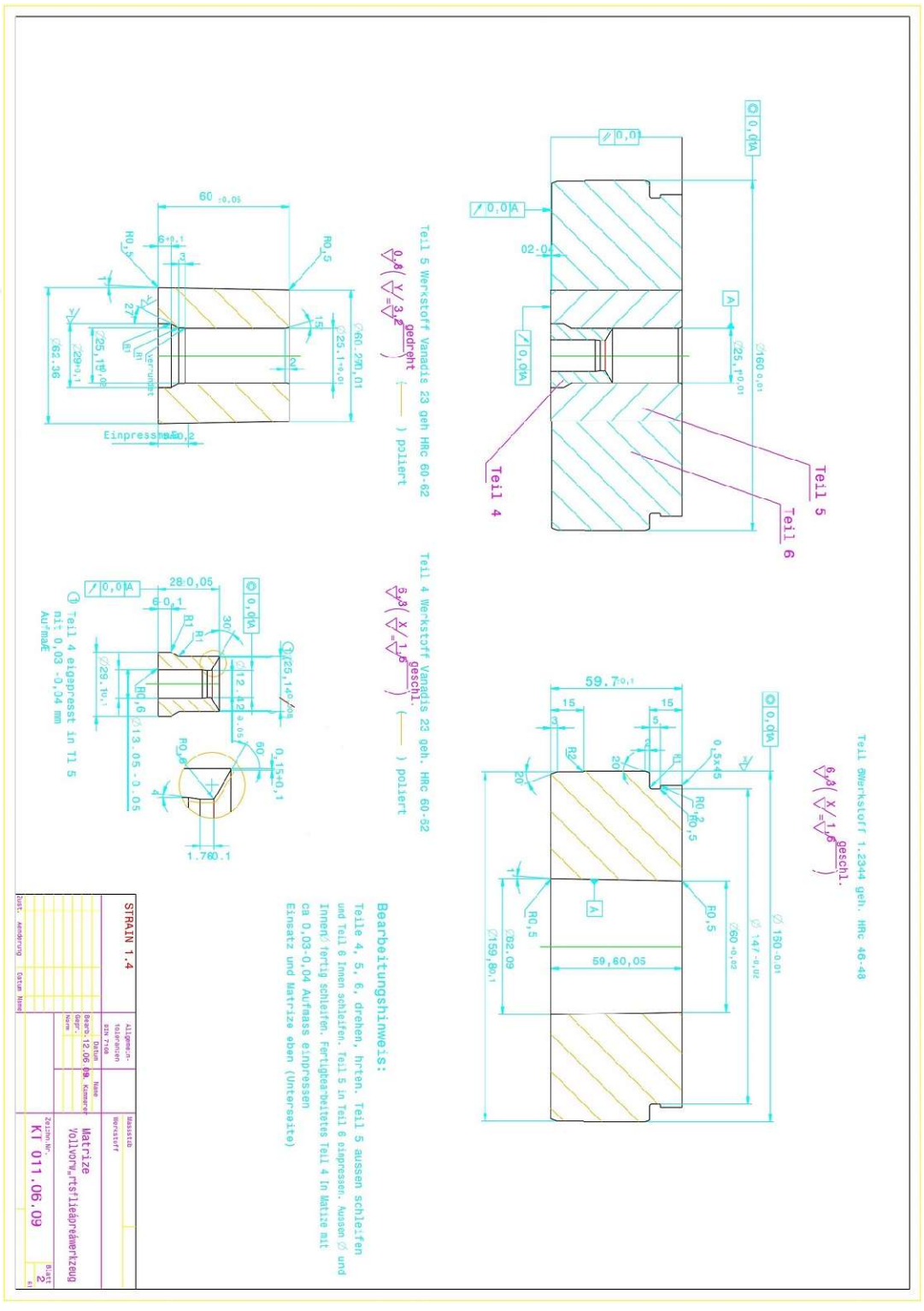
Teil 5
Teil 6
Teil 4
Teil 5 Werkstoff Vanadis 23 geh HRc 60-62
gedreht
poliert
Teil 4 Werkstoff Vanadis 23 geh. HRc 60-62
geschl.
poliert
Teil 6Werkstoff 1.2344 geh. HRc 46-48
geschl.
Bearbeitungshinweis:
Teile 4, 5, 6, drehen, härten. Teil 5 aussen schleifen
und Teil 6 Innen schleifen. Teil 5 in Teil 6 einpressen. Aussen Ø und
Innen fertig schleifen. Fertigbearbeitetes Teil 4 in Matize mit
ca 0,03-0,04 Aufmass einpressen
Einsatz und Matrize oben (Unterseite)
Teil 4 eingepresst in Tl 5
mit 0,03 -0,04 mm
Aufmaß
Einpressmaß
59,60,05
STRAIN 1.4
Matrize
Vollvorw.rtsfließpreßwerkzeug
KT 011.06.09